2017-12-14

Membrane Proteins Take Different Trafficking Pathways to the Primary Cilium

William Joseph Monis
University of Massachusetts Medical School

MEMBRANE PROTEINS TAKE DIFFERENT TRAFFICKING PATHWAYS TO THE PRIMARY CILIUM

A Dissertation Presented

By

William Joseph Monis

Submitted to the Faculty of the
University of Massachusetts Graduate School of Biomedical Sciences, Worcester
in partial fulfillment of the requirements for the degree of

DOCTOR OF PHILOSOPHY

(DECEMBER, 14, 2017)

INTERDISCIPLINARY GRADUATE PROGRAM

MEMBRANE PROTEINS TAKE DIFFERENT TRAFFICKING PATHWAYS TO THE PRIMARY CILIUM

A Dissertation Presented
By

William Joseph Monis

This work was undertaken in the Graduate School of Biomedical Sciences

Interdisciplinary Graduate Program

The signature of the Thesis Advisor signifies
validation of Dissertation content

_____

Gregory J. Pazour, Ph.D., Thesis Advisor

The signatures of the Dissertation Defense Committee signify
completion and approval as to style and content of the Dissertation

_____

Julie A. Jonassen, Ph.D., Member of Committee

_____

Mary Munson, Ph.D., Member of Committee

_____

Silvia Corvera, M.D., Member of Committee

_____

Jagesh V. Shah, Ph.D., External Member of Committee

The signature of the Chair of the Committee signifies that the written dissertation meets
the requirements of the Dissertation Committee

_____

George B. Witman, Ph.D., Chair of Committee

The signature of the Dean of the Graduate School of Biomedical Sciences signifies that
the student has met all graduation requirements of the School

_____

Anthony Carruthers, Ph.D., Dean of the Graduate School of Biomedical Sciences

December 14, 2017

Dedication

For My Mother

“The untold want by life and land ne’er granted,
Now voyager sail thou forth to seek and find.”

- Walt Whitman**,** Leaves of Grass, 1855

Acknowledgments

I thank my thesis advisor Gregory Pazour for his mentorship and for the opportunity to conduct research in his lab. I express my gratitude to all the members of my thesis/dissertation committee for their interest, enthusiasm, and valuable advice that helped me move my thesis project forward. Additionally, I thank all the past and present members of the Pazour Lab along with all my friends at UMass Medical School for their support.

Abstract

Cilia are conserved organelles that extend from the surface of most eukaryotic cells. During development cilia play key roles in force generation and perception of the extracellular environment. Ciliary defects cause a broad class of human diseases called ciliopathies characterized by pleiotropic symptoms including cystic kidneys, retinal degeneration, cardiac malformations and skeletal deformations. Perception of the environment relies on specific proteins being localized to the ciliary membrane compartment. The mechanism for sorting and trafficking membrane proteins to the cilium is poorly understood. To address this question, I developed a fluorescence-based pulse-chase assay to measure the transport kinetics of ciliary membrane proteins. This assay was used to determine the importance of candidate proteins to the delivery of fibrocystin, polycystin-2, and smoothened to cilia. Using this assay, I found that ciliary delivery of fibrocystin and polycystin-2 requires IFT20, GMAP210, and the exocyst while smoothened delivery is largely independent of these proteins. In addition, I determined that polycystin-2, but not smoothened or fibrocystin require the biogenesis of lysosome related organelles complex-1 (BLOC-1) for ciliary delivery. Consistent with a requirement for BLOC-1 in ciliary transport of polycystin-2, BLOC-1 mutant mice have cystic kidney disease. BLOC-1 functions in endosomal sorting and I find that disrupting the recycling endosome also reduced ciliary polycystin-2 and causes its accumulation in the recycling

endosome. This is the first demonstration of a role for BLOC-1 in ciliary biogenesis and highlights the complexity of trafficking pathways to the cilium.

Table of Contents

List of Tables

List of Figures

List of Copyrighted Material

This thesis uses material from the following publication:

Monis, W.J., V. Faundez, and G.J. Pazour. 2017. BLOC-1 is required for selective membrane protein trafficking from endosomes to primary cilia. *J Cell Biol*.

List of Symbols and Abbreviations

AID	Auxin-inducible degron
AP-3	Adaptor protein-3
AQP2	Aquaporin 2
BLOC-1	Biogenesis of lysosome-related organelles complex-1
CTSs	Ciliary targeting sequences
DISC-1	Disrupted in schizophrenia-1
DMEM	Dulbecco modified eagles medium
FBS	Fetal bovine serum
GMAP	Golgi microtubule associated protein
GPCRs	G protein coupled receptors
Gpr161	G protein coupled receptor 161
GPR101	G protein coupled receptor 101
HEK	Human embryonic kidney
IFT	Intraflagellar transport
KIF17	Kinesin family member 17
IMCD3	Inner medullary collecting duct 3
LTA	Lotus tetragonolobus agglutinin
MCHR1	Melanin-concentrating hormone receptor 1
MEK	Mouse embryonic kidney
MyoVb	Myosin Vb
NRK	Normal rat kidney
NSF	N-ethylmaleimide-sensitive factor
PBS	Phosphate buffer saline
PHEM	Pipes, HEPES, EGTA, and magnesium chloride
PKD	Polycystic kidney disease
Pkd2	Polycystin-2
RNAi	Ribonucleic acid interference
SEM	Standard error of the mean
SIM	Structured illumination microscopy
SNAP	Soluble *N*-ethylmaleimide-sensitive factor attachment protein
SNARE	Soluble *N*-ethylmaleimide-sensitive factor attachment protein receptor
SSTR	Somatostatin receptor
TBS	Tris buffer saline
TBST	Tris buffer saline and tween
TIRFM	Total internal reflection fluorescence microscopy
TULP3	Tubby-like protein 3
VAMP	Vesicle-associated membrane protein
5HT	Serotonin receptor
µm	Micrometer
nm	Nanometer

Preface

Chapters II, III, and IV are from the following publication:

Monis, W.J., V. Faundez, and G.J. Pazour. 2017. BLOC-1 is required for selective membrane protein trafficking from endosomes to primary cilia. *J Cell Biol*.

William J. Monis and Dr. Gregory J. Pazour conceived the project and designed experiments.

William J. Monis performed all experimental research and data analysis.

Dr. Victor Faundez contributed advice, mouse tissue, and the original MyoVb C-terminal tail construct.

Figure II-14: Dr. Jovenal San Agustin performed sectioning, hematoxylin and eosin staining, and immunohistochemistry on the young mouse kidneys. William J. Monis performed imaging and quantification.

Chapter I : Introduction

Cilia are conserved organelles that extend from the surface of most eukaryotic cells excluding yeast and higher plants (Pazour and Bloodgood, 2008). Functions of cilia include cell motility and the sensory perception of the extracellular environment. Defects in cilia activity results in genetic diseases called ciliopathies such as cystic kidneys, retinal degeneration, obesity, neurodevelopmental anomalies, heart malformations, and skeletal deformations (Hildebrandt et al., 2011). The sensory function of cilia is mediated through specific membrane protein receptors that localize to the cilium. There is no protein synthesis machinery within cilia meaning that receptors must be translated, sorted, and trafficked from outside of the organelle. The localization of specific receptors at the cilium and the trafficking mechanisms involved are not well understood. Receptors must pass through physical barriers at the cilium in order to enter the organelle and they use unique targeting sequences, trafficking pathways, and protein transport machineries for delivery to the primary cilium.

Primary Cilia Structure and Trafficking Barriers

The single non-motile primary cilium is a sensory organelle that functions by using receptors that are localized in the ciliary membrane. Because cilia extend from the plasma membrane they are not fully enclosed by a membrane layer. The cilium maintains its unique receptor composition due to physical barriers that

are thought to act as a selective gate for membrane protein entry (Czarnecki and Shah, 2012; Reiter et al., 2012; Rosenbaum and Witman, 2002).

The Primary Cilium

Primary cilia are found on the surface of most vertebrate cell types including epithelial and mesenchymal cells. They are derived from centrosomes that are docked at the cell surface. During cell cycle arrest, the centrosome becomes tethered to the plasma membrane and the microtubule axoneme extends from the mother centriole also known as the basal body (Fig. I-1A) (Rosenbaum and Witman, 2002). The axoneme of the primary cilium consists of a core of nine microtubule outer doublets, which is ensheathed in a ciliary membrane that is continuous with the plasma membrane (Fig. I-1A) (Rosenbaum and Witman, 2002).

Photoreceptors Have A Modified Primary Cilium

Photoreceptor cells are sensory neurons and they have a modified type of primary cilia called connecting cilia (Pearring et al., 2013). The function, formation, and structure of the connecting cilium are the same as the primary cilium described above. The connecting cilium bridges the inner segment of the photoreceptor cell to the outer segment (Fig. I-1B). Membrane protein sorting and transport occur within the photoreceptor inner segment. Receptors such as the light detecting opsins traffic to the connecting cilium and then localize in the membrane of the outer segment (Pearring et al., 2013). Photoreceptor outer

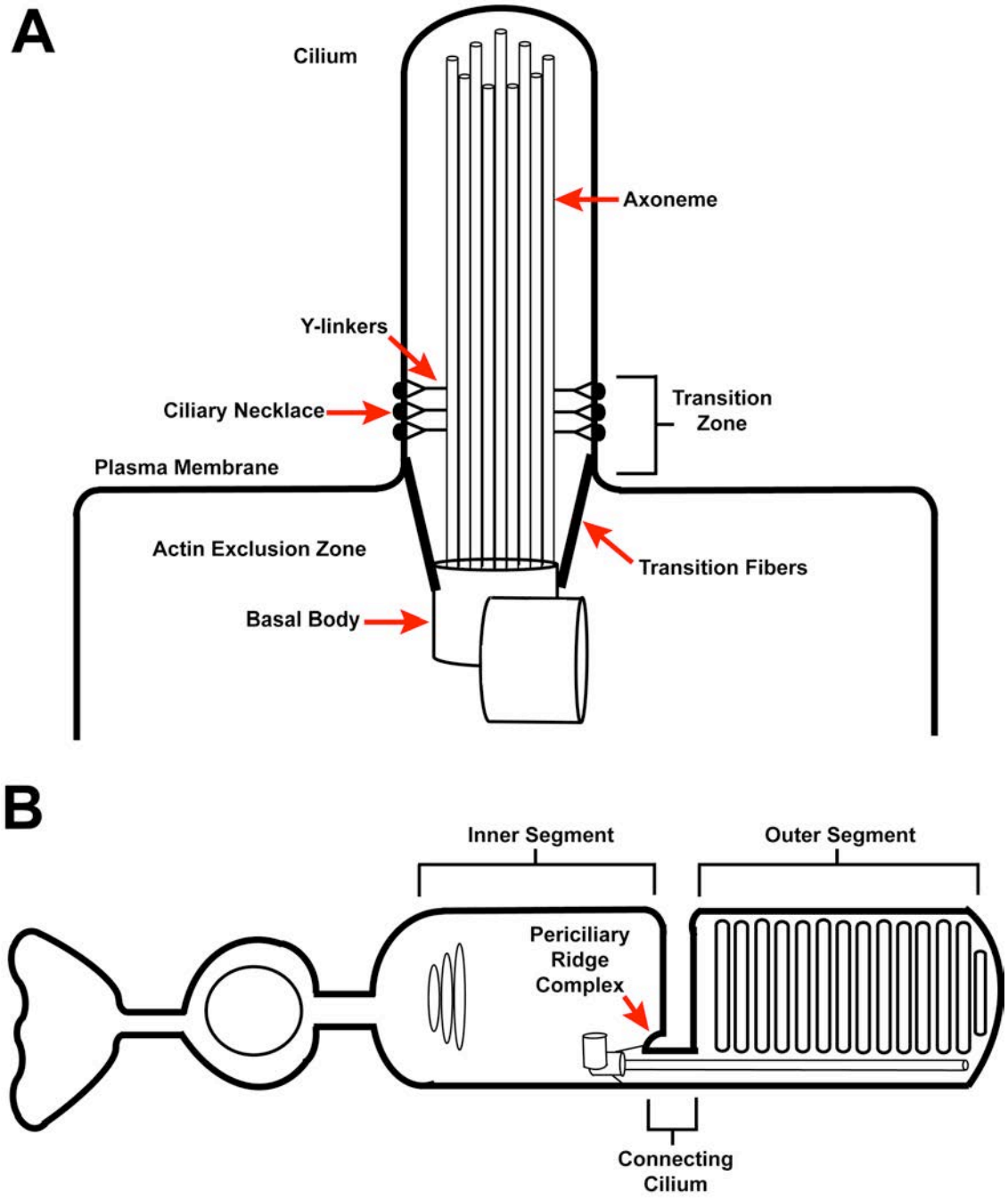

Figure I-1: Structure of the primary cilium.

Figure I-1: Structure of the primary cilium. (**A**) A schematic of a primary cilium extending from the surface of a mammalian epithelial cell. The actin exclusion zone is the region of cytoplasm that is free of actin filaments and it is located at the base of the cilium. Transition fibers tether the centrosome to the cell surface and the microtubule axoneme extends from the basal body. The transition zone is located between the basal body and the more distal ciliary axoneme. Within this ciliary subcompartment are multiple rows of Y-shaped linker structures that project from the microtubule outer doublets and attach to the ciliary membrane. The position of the Y-linkers coincides with the beaded rows of extracellular membrane particles of the ciliary necklace. (**B**) A schematic of a photoreceptor cell showing the connecting cilium bridging the inner and outer segments. Vesicles carrying opsin receptors are trafficked to the periciliary ridge complex at the base of the connecting cilium in the inner segment and then the opsins localize in the membrane of the outer segment.

segments have immense demands for membrane protein transport to maintain its structure. In fish and frogs it is estimated that 50,000 opsin molecules need to be transported per minute into the cilium to maintain the organelle while as many as ~4300 are needed per minute in mice (Besharse and Horst, 1990; Williams, 2002; Young, 1967).

The Ciliary Gate

Vesicle Docking and Fusion Sites

Researchers propose that membrane protein receptors must pass through a series of structural barriers or gates to enter the cilium, one of which being a vesicle-docking site at the ciliary base (Reiter et al., 2012; Rosenbaum and Witman, 2002). Extensive electron microscopic analysis shows no evidence of any vesicles within the cilium implying that receptor-carrying vesicles must dock and fuse outside of cilia to allow the cargo to enter the organelle (Kozminski et al., 1995). In photoreceptors, opsin cargo vesicles dock and fuse at the grooved periciliary ridge complex at the base of the connecting cilium (Fig. I-1B) (Papermaster et al., 1985). The periciliary ridge complex is only found in photoreceptors and is more structurally defined in frogs than in mice (Maerker et al., 2008; Peters et al., 1983). It is thought that this complex is present at the base of all cilia (Nachury et al., 2010) and the actin exclusion zone may be the equivalent in primary cilia of epithelial cells. The actin filament free zone is found in the cytoplasm at the base of the primary cilium and it is thought to allow for

docking of the centrosome with the plasma membrane (Fig. I-1A) (Francis et al., 2011). It is intriguing to speculate that this zone might also serve as a docking site for vesicles carrying membrane protein cargo to primary cilia on epithelial cells.

Vesicle fusion and receptor entry into the cilium has parallels with membrane protein import into the nucleus. The nuclear pore complex is a selective gate that regulates protein entry through the nuclear envelope (Stewart, 2007). Receptor carrying vesicles fuse on the nuclear envelope and then the cargo diffuses across the membrane in the peripheral channels around the nuclear pore complex to enter the nucleus (Ohba et al., 2004; Soullam and Worman, 1995; Wu et al., 2002; Zuleger et al., 2012). The mechanisms membrane proteins use for nuclear import is similar to how vesicles must fuse outside the cilium to allow for receptor entry into the organelle.

Transition Fibers

Another barrier for membrane protein entry into cilia is provided by an array of nine transition fibers that extend from the basal body and tether it to the cell surface (Fig. I-1A). The distance between each transition fiber is 60nm and this area is too small for the passage of cargo carrying vesicles, which have a size between 60-300nm (Anderson, 1972; Deretic and Papermaster, 1991; Oprins et al., 1993; Pearse, 1976). The structure and position of the transition fibers further supports the model that receptor-carrying vesicles must dock and fuse outside of the cilium.

Transition Zone

The transition zone is also thought to act as a barrier for membrane protein import into cilia. This subcompartment of the cilium is located between the basal body and the more distal ciliary axoneme (Fig. I-1A) (Czarnecki and Shah, 2012). The transition zone arises from the basal body and consists of nine outer doublet microtubules along with a propeller array of nine transition fibers. Multiple rows of Y-shaped linker structures project from the microtubule outer doublets and attach to the ciliary membrane (Ringo, 1967). The position of the Y-linkers coincides with the beaded rows of membrane particles located on the extracellular ciliary membrane called the ciliary necklace (Gilula and Satir, 1972). The green algae *Chlamydomonas reinhardtii* has similar beaded rows of membrane particles circling the base of the cilium that is termed the ciliary bracelet, but this structure is not found in other organisms (Dutcher and O'Toole, 2016; Weiss et al., 1977). The termination site of the transition zone is defined by the last row of Y-linker structures that are proximal to the ciliary axoneme (Czarnecki and Shah, 2012). Loss of function *Chlamydomonas reinhardtii* transition zone mutants and knockdown of transition zone proteins in mammalian cells reduces the levels of specific receptors at the cilium suggesting that this ciliary subcompartment maintains the composition of receptors at the organelle (Awata et al., 2014; Chih et al., 2011; Craige et al., 2010; Garcia-Gonzalo et al., 2011). The structural features of the transition fibers, Y-linkers, and ciliary necklace are thought to act as a selective gate for receptor entry into the cilium (Czarnecki and Shah, 2012;

Reiter et al., 2012; Rosenbaum and Witman, 2002). However, the transition zone is distally located from both the vesicle docking sites at the ciliary base and the transition fiber attachment sites on the basal body indicating that vesicle fusion events happen well before the transition zone. This ciliary subcompartment may not be a selective gate for receptor entry, but may instead function to retain receptors within the cilium after delivery. The cell may have evolved the transition zone to compensate for the cilium not being fully enclosed by a membrane bilayer in order to control cilia receptor composition.

Ciliary Targeting Sequences

Membrane proteins use unique sorting signals for targeting to the primary cilium. Some of the ciliary targeting sequences (CTSs) consist of common motifs and these sorting signals are often associated with post-translational modifications. CTSs have been identified in two classes of integral membrane protein receptors: the cystoproteins and the G protein coupled receptors (GPCRs).

Apical and Basolateral Membrane Protein Sorting

The primary cilium extends from the apical cell surface of epithelial cells suggesting that receptor targeting to cilia is analogous to targeting to the apical plasma membrane. Polarized epithelial cells are asymmetric with a basolateral membrane adjacent to neighboring cells and an apical membrane facing the extracellular milieu (Stoops and Caplan, 2014). Proteins rely on unique sorting sequences for delivery to either the basolateral or apical plasma membranes

outside of the cilium. Basolateral sorting signals are found within the primary structure of the protein and include tyrosine or dileucine based motifs (Hunziker and Fumey, 1994; Matter et al., 1992; Stoops and Caplan, 2014). Apical sorting signals are more diverse and can be present in any domain of the protein. Apical targeting motifs can comprise of amino acids, lipids, or carbohydrates (Dunbar et al., 2000; Lisanti et al., 1989; Stoops and Caplan, 2014; Urban et al., 1987). The CTSs discussed below share characteristics of apical sorting signals and this similarity further supports receptor targeting to cilia being comparable to targeting to the apical plasma membrane (Table I-1).

Cystoproteins

Members of the cystoprotein family include polycystin-1, polycystin-2, and fibrocystin (Harris and Torres, 2009; Yokoyama, 2017). Mutations in these receptors are associated with either autosomal dominant or autosomal recessive polycystic kidney disease. Polycystin-1 is an integral membrane protein with a large extracellular N-terminus, eleven transmembrane spanning regions, and an intracellular C-terminus (Harris and Torres, 2009; Hughes et al., 1995). The main signaling function of polycystin-1 is unknown but its topology is that of a receptor or adhesion molecule. Polycystin-1 localizes to the basolateral and apical membranes including the primary cilium (Geng et al., 1996; Scheffers et al., 2000; Yoder et al., 2002). The polycystin-1 CTS was identified by first fusing

Protein	Class	Function	CTS (Key Residues in Bold)	Reference
Polycystin-1	Cystoprotein	Unknown	**KV**H**P**SST	(Ward et al., 2011)
Polycystin-2	Cystoprotein	Cation Channel	MVNSS**RV**Q**P**QQ PGDA	(Geng et al., 2006)
Fibrocystin	Cystoprotein	Unknown	**C**LV**CCWFKKSKT RKIKPE**	(Follit et al., 2010)
Rhodopsin	GPCR	Photon Receptor	SSSQ**V**S**P**A	(Tam et al., 2000)
SSTR3	GPCR	Somatostatin Receptor	**A**PS**CQ** + **A**PA**CQ**	(Berbari et al., 2008a; Jin et al., 2010)
5HT6	GPCR	Serotonin Receptor	**A**TAG**Q**	(Berbari et al., 2008a)
MCHR1	GPCR	Melanin-Concentrating Hormone Receptor	**APASQ**	(Badgandi et al., 2017; Berbari et al., 2008a)
Gpr161	GPCR	Orphan Receptor	(**I**/**V**)**KARK**	(Badgandi et al., 2017; Mukhopadhyay et al., 2013)

Table I-1: Integral membrane protein ciliary targeting sequences.

the last 112 amino acids of the proteins C-terminus with the transmembrane and extracellular domain of the membrane protein CD16.7 (Ward et al., 2011). The CD16.7-polycystin-1 fusion protein localized to cilia suggesting that the C-terminus is sufficient for ciliary trafficking. A conserved KVxP motif found in the CTS of polycystin-2 and rhodopsin was identified in the last 20 amino acid residues of the C-terminus of polycystin-1. Alanine scanning mutagenesis of the KVxP motif and truncation of the 20 amino acid residues prevented CD16.7-polycystin-1 from localizing at the cilium implying that this region is necessary for transport to cilia. However, these polycystin-1 mutants accumulated in the endoplasmic reticulum inferring that their mislocalization to cilia may be due to protein misfolding and not a defect in trafficking. The KVxP motif of polycystin-1 was found in the amino acid sequence KVHPSST (Ward et al., 2011). The full C-terminal tail of membrane protein CD7 was fused to the KVHPSST sequence and it was found to localize at the cilium indicating that it is the CTS of polycystin-1. However, new evidence argues that the KVHPSST motif is not a CTS. Alanine scanning mutagenesis of the KVHPSST sequence in full-length polycystin-1 did not prevent the receptor from localizing at the cilium, which supports that the motif is not the polycystin-1 CTS (Su et al., 2015). This discrepancy could be because the many structural domains in full-length polycystin-1 are needed to interact with multiple proteins to traffic to cilia. Also, full-length polycysin-1 may traffic through a different pathway than smaller fusion proteins. To find the CTS of polycystin-1, truncations of the N- and C-terminus of the full-length protein

were made. Some of these different truncation mutants did not localize at the cilium indicating that polycystin-1 contains multiple CTSs (Su et al., 2015).

Polycystin-2 is a non-selective calcium cation channel with an intracellular N-terminus, six transmembrane spanning regions, and an intracellular C-terminus (Harris and Torres, 2009; Mochizuki et al., 1996). Polycystin-2 localizes at both the cilium and the endoplasmic reticulum (Cai et al., 1999; Pazour et al., 2002b; Yoder et al., 2002). Immunoprecipitation experiments show that polycystin-1 and polycystin-2 interact at their C-terminal ends implying that they may rely on one another for trafficking to the cilium (Cai et al., 1999; Qian et al., 1997). Polycystin-1 does not localize at cilia in polycystin-2 null cells showing that polycystin-1 trafficking to cilia is dependent on polycystin-2 (Su et al., 2015). However, polycystin-2 localizes at cilia in polycystin-1 null cells suggesting that polycystin-2 does not require polycystin-1 for ciliary delivery (Geng et al., 2006). The ability of polycystin-2 to localize to the cilium independently of polycystin-1 supports it having its own CTS. In order to find the CTS of polycystin-2, truncations of the full-length protein were fused to an HA-tag and amino acids 5 – 72 were found to be required for trafficking to cilia, which implies that the sorting sequence is in the N-terminus (Geng et al., 2006). The first 72 amino acids of polycystin-2 were then fused to the N-terminus of the non-ciliary receptor polycystin-2-like-1 and this caused it to localize at the cilium, which supports the sequence as being sufficient for ciliary trafficking. Additional truncations of this 72 amino acid region were fused to the non-ciliary transferrin receptor and a 15

amino acid region was sufficient to localize the receptor at the cilium. A conserved RVxP motif was identified in this refined sequence and alanine-scanning mutagenesis of this motif prevented polycystin-2 from localizing at the cilium inferring that it is necessary for trafficking to cilia (Geng et al., 2006). Some of the truncation and alanine-scanning mutagenesis mutants that did not localize to cilia were found to accumulate in the endoplasmic reticulum. The inability of these mutants to localize at the cilium may not be due to a defect in trafficking but rather the proteins were misfolded and could not exit the endoplasmic reticulum.

The structure of fibrocystin consists of a large extracellular N-terminus, a single transmembrane spanning region, and a short intracellular C-terminus (Harris and Torres, 2009; Onuchic et al., 2002; Ward et al., 2002). The function of fibrocystin is unknown but immunoprecipitation experiments show that it interacts with polycystin-2 implying that the two receptors participate in the same signaling pathway (Wang et al., 2007). Fibrocystin localizes at both the cilium and the endoplasmic reticulum (Follit et al., 2010; Menezes et al., 2004; Wang et al., 2004a; Ward et al., 2003; Zhang et al., 2004). Researchers reasoned that since all of the known CTSs are found on the intracellular side of integral membrane proteins and even though fibrocystin is large, the short C-terminus of the protein might contain the CTS (Follit et al., 2010). This idea was tested by generating two different constructs that comprised of the C-terminus of fibrocystin fused to a reporter protein and observing whether or not they localized at cilia.

The first construct was a fusion between the C-terminal 503 amino acid residues of fibrocystin that includes the proteins transmembrane domain with the extracellular domain of the membrane protein CD8. This construct localized at the cilium meaning the CTS could be in either the transmembrane domain or the intracellular C-terminus. A second fusion was made between the last 193 amino acids of fibrocystin that does not include the membrane-spanning region, to the C-terminus of GFP. This construct was found to localize at cilia indicating that the CTS is in the 193 amino acid C-terminus. Truncations of these residues were fused to GFP and an 18 amino acid region was identified to be sufficient for targeting the reporter protein to the cilium (Follit et al., 2010). However, the researchers could not rule out the possibility of other CTSs being located in the N-terminus of fibrocystin because they did not study the full-length protein. Sequence analysis revealed that there are no conserved motifs in the 18 amino acid region that are present in some other CTSs. Alanine scanning mutagenesis was performed on these 18 amino acids fused to GFP and residues CCC and KTRK were found to be critically required for localizing the reporter protein at the cilium (Follit et al., 2010). Cysteine residues near basic amino acid residues are often palmitoylated which suggests that the three cysteines in the fibrocystin CTS may be lipid modified (Bijlmakers and Marsh, 2003). To test this idea radioactive palmitate was added to mammalian cells expressing either the wildtype CTS of fibrocystin or a CCC mutant fused to a GFP tag and immunoprecipitation assays were performed. The wildtype CTS but not the mutant, incorporated the

radioactive palmitate which supports that the sorting signal is lipid modified. Because a mutation in these cysteine residues prevented the CTS from localizing at the cilium it is thought that the palmitate modification is required for the trafficking of fibrocystin to cilia. To see whether the lipid modification links the CTS of fibrocystin to membranes, centrifugation experiments were performed on membranes from cells expressing the wildtype CTS of fibrocystin or a CCC mutant fused to GFP. The wildtype CTS floated with the membrane fraction to the top of the gradient while the CCC mutant remained at the bottom implying that the palmitoylation of fibrocystin is required for its association with membranes. This experiment also shows that the CTS of fibrocystin can interact with membranes in the absence of its transmembrane domain. Fibrocystin may use the palmitate modifcation to dock to the plasma membrane before fusing and incorporating into the ciliary membrane.

G Protein Coupled Receptors

The activation of GPCRs leads to the initiation of a variety of downstream signaling cascades including the Hedgehog signaling and visual system pathways (Berbari et al., 2009). GPCRs share a similar topology that consists of an extracellular N-terminus, seven transmembrane spanning regions, and an intracellular C-terminus (McIntyre et al., 2016). Rhodopsin is a GPCR that concentrates in the outer segment of photoreceptors and detects light in the first steps of the visual transduction pathway (Burns and Arshavsky, 2005). Mutations in rhodopsin cause retinal degeneration such as retinitis pigmentosa and macular

degeneration (Dryja et al., 1990). These mutations are localized throughout the protein but most of them are concentrated in the C-terminus (Sandberg et al., 1995). Transgenic animals with these mutations show delocalization of rhodopsin to the inner segment plasma membrane suggesting that the C-terminus contains the CTS (Green et al., 2000; Li et al., 1998; Sung et al., 1994). To identify the rhodopsin CTS, a fusion was made between the last 44 amino acids of rhodopsin to the C-terminus of GFP and it was expressed in transgenic frog retinas (Tam et al., 2000). The fusion protein localized to the outer segment meaning that the C-terminus is sufficient for ciliary trafficking. The C-terminus of rhodopsin contains two palimitoylated cysteines that associate with membranes (Moench et al., 1994). To examine whether the lipid modification is required for outer segment transport, the terminal 25 amino acids lacking the palimitoylated cysteines of rhodopsin were fused to GFP. This fusion protein localized to the cytoplasm of the inner segment showing that the palmitate modification and its association with membranes are necessary for trafficking to the cilium. Rhodopsin may require the lipid modification to anchor the C-terminus in an optimal orientation so it can associate with sorting protein machineries. The last 5 residues in rhodopsin contain a single proline that is mutated in some patients with retinitis pigmentosa (Sandberg et al., 1995). A point mutation in this proline caused partial mislocalization of the fusion proteins to the inner segment membranes but only modestly reduced the localization in the outer segment indicating that additional residues are needed for ciliary trafficking. The CTS was further refined by fusing

the last 8 amino acid residues of rhodopsin to the C-terminus of the non-ciliary alpha-adrenergic receptor (Tam et al., 2000). The fusion construct was found exclusively in the outer segment, which supports these 8 amino acid residues as being the CTS. However, the researchers did not study full-length rhodopsin, which indicates that there could be other CTSs within the protein.

Somatostatin and serotonin receptors are GPCRs that control a variety of physiological functions including endocrine signaling and neurotransmission (Barnes and Sharp, 1999; Lahlou et al., 2004). Somatostatin receptor (SSTR) 3 and serotonin receptor (5HT) 6 are the only somatostatin and serotonin receptor subtypes that localize at cilia implying that each have their own CTS (Brailov et al., 2000; Hamon et al., 1999; Handel et al., 1999; Schulz et al., 2000). To find the CTS, different domains of SSTR3 and 5HT6 were swapped with their respective non-ciliary subtypes SSTR5 and 5HT7 (Berbari et al., 2008a). Five residues in the third intracellular loop of SSTR3 and 5HT6 were able to localize the chimera constructs to cilia showing that this region is necessary and sufficient for ciliary trafficking. Sequence analysis identified a conserved AxS/AxQ motif in the third intracellular loop of both SSTR3 and 5HT6. Mutations in the alanine and glutamine residues of this motif caused a reduction of both chimera receptors at the cilium, which indicates that these residues are required for ciliary localization (Berbari et al., 2008a). Another research group fused the third intracellular loop of SSTR3 to the C-terminus of the transmembrane and extracellular domain of the CD8 receptor (Jin et al., 2010). This fusion construct localized at the cilium

confirming that the third intracellular loop of SSTR3 is the CTS. However, this group found that the previously identified alanine and glutamine residues in the conserved motif were not required for the localization of the CD8-SSTR3 fusion construct to cilia. Instead two conserved cysteines that are adjacent to the glutamine are needed for CD8-SSTR3 localization at the cilium suggesting that other structural domains in full-length SSTR3 may be needed for ciliary delivery (Jin et al., 2010). The alanine and glutamine mutations made in the SSTR3/5 chimera may have caused the protein to become misfolded and retained in the endoplasmic reticulum explaining why it did not localize at the cilium.

The AxS/AxQ motif was also used to predict novel ciliary GPCRs and the APASQ sequence was found in the third intracellular loop of melanin-concentrating hormone receptor-1 (MCHR1) (Berbari et al., 2008a). MCHR1 is involved in the regulation of feeding behavior and it localizes at the primary cilium (Berbari et al., 2008a; Pissios et al., 2006). Control or point-mutated versions of the APASQ motif were fused to the C-terminus of the transmembrane and extracellular domain of the CD8 receptor (Badgandi et al., 2017). The control fusion protein but not the mutant localized at the cilium showing that the motif is necessary and sufficient for targeting to cilia. Nevertheless, the researchers did not study full-length MCHR1 meaning there could be other CTSs in the protein sequence.

G protein coupled receptor 161 (Gpr161) is a class A rhodopsin family GPCR that localizes to primary cilia (Mukhopadhyay et al., 2013). It is classified

as an orphan receptor because its ligand is unknown and it is a negative regulator of the Hedgehog signaling pathway (McIntyre et al., 2016; Mukhopadhyay et al., 2013). The sequence of Gpr161 is most closely related to the non-ciliary G protein coupled receptor 101 (GPR101). However, the third intracellular loop and the C-terminus are the most evolutionarily divergent between Gpr161 and GPR101 implying that the CTS of Gpr161 might be in one of these regions (Mukhopadhyay et al., 2013). Deletion of a portion of the third intracellular loop of Gpr161 prevented its localization at cilia supporting this region as necessary for ciliary trafficking. Swapping of the third intracellular loops of GPR101 with Gpr161 resulted in the chimera trafficking to cilia, which shows that this region is sufficient for ciliary localization. Mutagenesis of conserved residues in this region refined the CTS to a five amino acid (I/V)KARK motif that was required for cilia delivery. However, it is possible that the deletion and chimera mutants may have been misfolded and retained in the endoplasmic reticulum inferring that the trafficking defect is indirect. This concern was addressed by fusing either control or point-mutated versions of the (I/V)KARK motif to the C-terminus of the transmembrane and extracellular domain of the CD8 receptor (Badgandi et al., 2017). The control fusion protein but not the mutant localized at the cilium showing that the motif is necessary and sufficient for ciliary targeting. Unfortunately, the researchers did not examine the C-terminus of Gpr161 that was also divergent from the GPR101 sequence suggesting that it may have an additional CTS. The known CTSs of Gpr161,

SSTR3, 5HT6, and MCHR1 are all localized within the third intracellular loop, which may mean that these distinct GPCRs are all using the same trafficking pathway to cilia.

The GPCR smoothened is a positive regulator of the Hedgehog signaling pathway and it localizes at cilia (Alcedo et al., 1996; Corbit et al., 2005; van den Heuvel and Ingham, 1996). A hydrophobic and basic amino acid motif located C-terminal to the seventh transmembrane segment of smoothened is found in other ciliary GPCRs and was thought to be required for trafficking to cilia (Brailov et al., 2000; Corbit et al., 2005; Handel et al., 1999). Missense mutations in this motif impaired smoothened localization at cilia but these mutations may have affected protein folding causing it to be retained in the endoplasmic reticulum (Corbit et al., 2005). Also this motif was not shown to be sufficient for targeting exogenous proteins to the cilium meaning the missense mutation result could be indirect. It is not clear whether the hydrophobic and basic amino acid motif in smoothened is a definitive CTS.

Trafficking Pathways to the Cilium

Membrane proteins are thought to use distinct cellular trafficking pathways for transport to cilia. Receptors are synthesized in the endoplasmic reticulum and then they are delivered to the Golgi apparatus for sorting before being targeted to their final cellular locations (Mellman and Nelson, 2008). Ciliary membrane proteins are proposed to utilize either the lateral, direct, or recycling trafficking

pathways from the Golgi complex to the cilium (Fig. I-2) (Nachury et al., 2010; Weisz and Rodriguez-Boulan, 2009).

Lateral Trafficking Pathway

In the lateral trafficking pathway, receptor-carrying vesicles traffic from the Golgi complex to the plasma membrane where they dock and fuse. The receptors then laterally diffuse across the plasma membrane and incorporate into the ciliary membrane. The agglutinin receptors in *Chlamydomonas reinhardtii* are postulated to use the lateral trafficking pathway for delivery to the cilium. The gametes of opposing *Chlamydomonas reinhardtii* mating types adhere to each other by agglutinin molecules on the surfaces of their cilia during the process of fertilization (Hunnicutt et al., 1990). Agglutinins localize to the plasma membrane outside of the cilium when they are in their basal state. Upon activation they accumulate in the cilium suggesting that they are trafficking from the plasma membrane to the ciliary membrane. To test this idea, an impotent *Chlamydomonas* mutant that can agglutinate but its gametes cannot fuse to form a zygote, was used to induce agglutinin localization to cilia (Hunnicutt et al., 1990). The mutant was deciliated and the proteins at the cell surface were radiolabeled before allowing the cilia to regenerate. The isolated cell body and regenerated cilia fractions both contained a radiolabeled band that ran at the same molecular weight as purified agglutinin, implying that the pre-existing surface labeled cell body agglutinins trafficked to the new ciliary membrane.

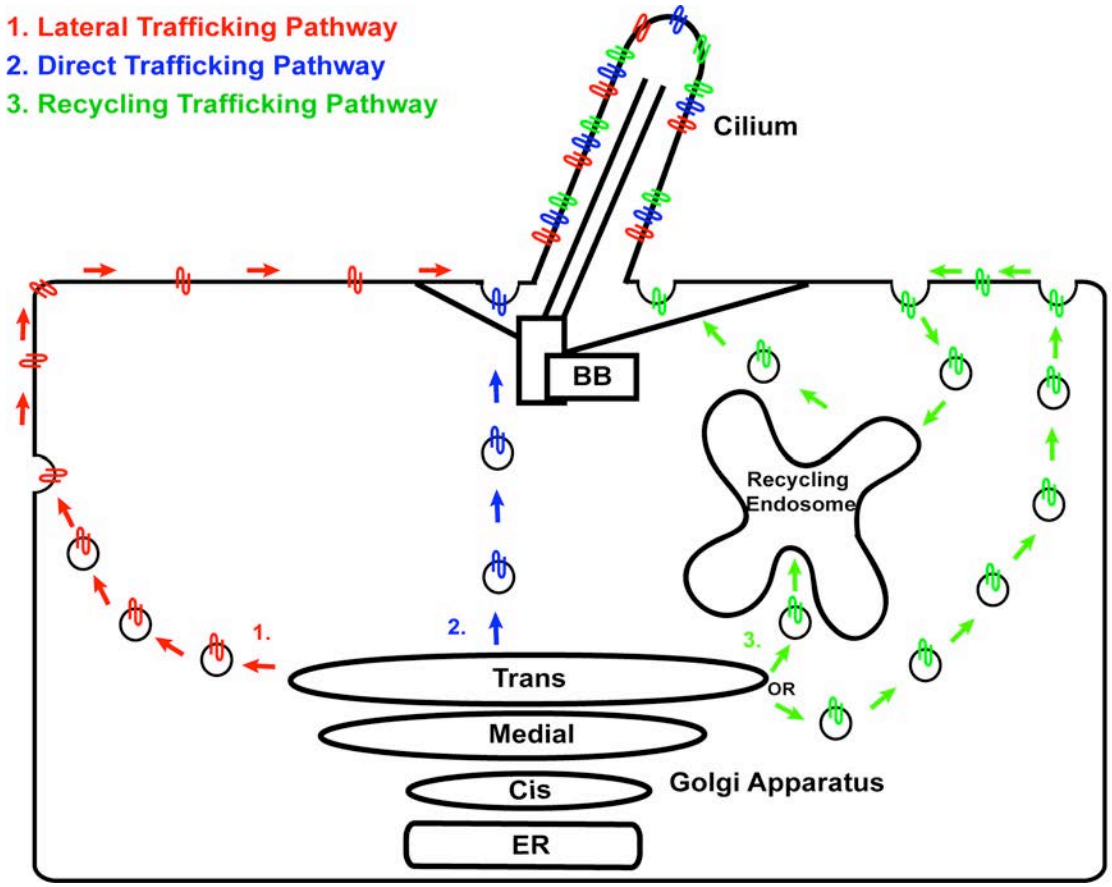

Figure I-2: Membrane protein trafficking pathways from the Golgi apparatus to the cilium.

Figure I-2: Membrane protein trafficking pathways from the Golgi apparatus to the cilium. Membrane proteins are proposed to use distinct ciliary trafficking pathways. Receptors are synthesized in the endoplasmic reticulum and then they are delivered to the Golgi apparatus for sorting before being targeted to the cilium. (**1**) Lateral Trafficking Pathway: Receptor-carrying vesicles traffic from the Golgi complex to the plasma membrane where they dock and fuse. The receptors then laterally diffuse across the plasma membrane and incorporate into the ciliary membrane. (**2**) Direct Trafficking Pathway: Vesicles traffic from the Golgi directly to the base of the cilium outside of the organelle where they then fuse and integrate their receptor cargo into the membrane of the cilium. (**3**) Recycling Trafficking Pathway: Membrane protein carrying vesicles depart from the Golgi complex and are then targeted directly to the endosome recycling system before trafficking to the base of the cilium. Additionally, vesicles can be transported from the Golgi to the plasma membrane where receptors undergo endocytosis to the recycling endosome system and then they are delivered to the ciliary base. BB: basal body; ER: endoplasmic reticulum.

However, the researchers did not use an antibody to confirm that the radiolabeled band they detected was agglutinin meaning that a different protein may be using the lateral trafficking pathway. To address this concern, the agglutinin SAG1 was fused to a HA-tag and was expressed in *Chlamydomonas reinhardtii* (Cao et al., 2015). Immunofluorescence showed basal state SAG1-HA localized on the cell body outside the cilium and cells treated with the agglutinin signaling pathway activator dp-cAMP had increased levels of SAG1-HA at their cilia, indicating that activated SAG1-HA trafficked from the cell body plasma membrane to the cilium. Additional immunoblot analysis of isolated flagella fractions from cells treated with db-CAMP had increased levels of SAG1-HA, which further supports activated agglutinins traversing the plasma membrane to the ciliary membrane. It is possible that inactivated agglutinins are trafficked from the Golgi apparatus directly to the base of the cilium outside the organelle and then diffuse into the surrounding plasma membrane. Upon activation, the agglutinins at the plasma membrane may then diffuse towards the cilium and incorporate into the ciliary membrane. Agglutinins could also be transporting through the endosome system before being delivered to the cilium.

The Hedgehog signaling protein smoothened is also thought to use the lateral trafficking pathway for targeting to the cilium. Smoothened accumulates at cilia when the Hedgehog signaling pathway is activated but the trafficking pathway it is using for ciliary delivery was unknown (Corbit et al., 2005). To answer this question, the localization of smoothened at the cell surface was

examined by expressing a series of extracellular epitope tagged smoothened constructs in mammalian cells (Milenkovic et al., 2009). Immunofluorescence showed smoothened to localize at the plasma membrane outside of the cilium at basal state and cells treated with the Hedgehog signaling activator sonic hedgehog had an accumulation of smoothened at the cilium suggesting that Hedgehog signaling activation causes smoothened present at the plasma membrane to concentrate at the ciliary membrane. However, smoothened could still be trafficking from the cytoplasm to the cilium. A fluorescence based pulse-chase assay was used to determine whether smoothened is trafficking to cilia from either the cell surface or the cytoplasm. Trafficking from the cell surface was observed by labeling smoothened at the plasma membrane with a fluorescent small molecule and then activating the Hedgehog signaling pathway. Smoothened accumulated at the cilium after one hour supporting a rapid transport from the plasma membrane to the cilium. To monitor trafficking from the cytoplasm, smoothened at the cell surface was masked with a non-fluorescent small molecule so that the delivery of smoothened from intracellular pools could be detected at the cilium during Hedgehog signaling activation. Intracellular smoothened was delivered to cilia after a lag phase which is consistent with delayed entry when compared to the rapid trafficking from the cell surface, inferring that smoothened traffics from the cytoplasm to the plasma membrane before delivery to the cilium. Smoothened at basal state may also be trafficking to the base of the cilium outside of the organelle and then diffusing into the plasma

membrane. When Hedgehog signaling is activated, smoothened may diffuse across the plasma membrane towards the cilium and then integrate into the ciliary membrane. Single molecule tracking of smoothened may be required to precisely show lateral trafficking from the plasma membrane to the cilium. It was also proposed that smoothened might be endocytosed at the cell surface before being targeted to cilia (Milenkovic et al., 2009). To perturb endocytosis, dominant negative forms of the GTPase dynamin that mediates endocytotic vesicle session, were expressed in mammalian cells. Immunofluorescence showed no difference in smoothened localization at the cilium in cells expressing dominant negative dynamin when Hedgehog signaling was activated, meaning that dynamin dependent endocytosis is not required for smoothened localization to cilia. There is no quantification of smoothened ciliary localization in this experiment suggesting that there may be a statistical difference that is not apparent by the qualitative analysis. Also, smoothened might be trafficking through other endomembrane organelles such as endosomes before delivery to the cilium.

Direct Trafficking Pathway

The direct trafficking pathway involves vesicles transporting from the Golgi apparatus directly to the base of the cilium outside of the organelle where they then fuse and integrate their receptor cargo into the ciliary membrane. This pathway was first proposed from studies on mastigoneme delivery in the green algae *Ochromonas danica*. Mastigonemes are branching membrane proteins that

laterally project from the surface of cilia and they are involved in propulsion of unicellular organisms (Bouck, 1971). Deciliation and regeneration experiments can be performed on *Ochromonas danica* allowing for the tracking of mastigonemes to newly forming ciliary membranes. *Ochromonas danica* were deciliated and then fixed during different stages of cilia regeneration (Bouck, 1971). Electron microscopy detected mastigonemes on the surface of cilia and at the cell surface near the regenerating cilia base but not on other plasma membrane locations, implying that vesicles carrying mastigoneme cargo are fusing at the base of the cilium outside of the organelle. Mastigonemes were also identified on the Golgi apparatus and in cytoplasmic vesicles near the base of regenerating cilia suggesting that mastigonemes are trafficked directly from the Golgi complex to the base of cilia. It would be intriguing to express fluorescently tagged mastigonemes in *Ochromonas danica* and perform live cell imaging to observe trafficking to regenerating ciliary membranes in real time. This analysis would provide additional evidence on whether mastigonemes are trafficked from the Golgi to the base of the cilium outside the organelle.

Rhodopsin is thought to use the direct trafficking pathway for delivery to the connecting cilium. Observations of frog photoreceptor inner segments found Golgi cisternae and vesicles to be adjacent to the basal body of the connecting cilium inferring that rhodopsin may be trafficking from the Golgi apparatus directly to the base of the cilium (Besharse and Pfenninger, 1980; Kinney and Fisher, 1978). Pulse-chase studies were performed on photoreceptors by injecting

radioactive amino acids into frog retinas and then harvesting the tissue at different time points (Papermaster et al., 1985). Autoradiography showed that most of the heaviest labeled structures in the inner segment cytoplasm were membranous vesicles and Golgi cisternae, implying that the radioactive amino acids incorporated into rhodopsin and it is found in these compartments. To confirm that the radiolabeled structures contained rhodopsin, antibodies specific to rhodopsin were used in parallel localization experiments (Papermaster et al., 1985). Immunohistochemistry detected rhodopsin in the outer segment membrane, the periciliary ridge complex, and the Golgi apparatus but not on the inner segment membrane. This result infers that rhodopsin is trafficking from the Golgi directly to the periciliary ridge complex before integrating into the connecting cilium and localizing at the outer segment membrane. It would be interesting to perform photobleaching experiments on photoreceptors expressing fluorescently labeled rhodopsin in order to follow its transport through the endomembrane system to further confirm that it is using the direct trafficking pathway.

Recycling Trafficking Pathway

In the recycling trafficking pathway, membrane protein carrying vesicles depart from the Golgi complex and are then targeted directly to the endosome recycling system before trafficking to the base of the cilium. Additionally, vesicles can be transported from the Golgi to the plasma membrane where receptors undergo endocytosis to the recycling endosome system and then they are delivered to the

ciliary base. Polycystin-2 ciliary trafficking is dependent on the Biogenesis of lysosome-related organelles complex-1 (BLOC-1) that is involved in transporting receptors from endosomes, implying that polycystin-2 may be using the recycling trafficking pathway for delivery to cilia (Dennis et al., 2016; Monis et al., 2017; Sitaram et al., 2012). To perturb trafficking through recycling endosomes, a dominant negative myosin Vb (MyoVb) C-terminal tail motor that binds Rab11 but lacks motor activity was expressed in mammalian cells (Lapierre et al., 2001; Monis et al., 2017; Volpicelli et al., 2002). Immunofluorescence showed a reduction in the steady state levels of polycystin-2 at the cilium and an accumulation at the recycling endosome in cells expressing dominant negative MyoVb, suggesting that polycystin-2 cannot exit the recycling endosome for delivery to cilia. A pulse-chase assay that measures membrane protein trafficking from the Golgi apparatus to the cilium was then used to examine whether perturbing transport through the recycling endosome affects the delivery of additional receptors to cilia (Monis et al., 2017). Immunofluorescence detected a reduction in the trafficking of polycystin-2 but not fibrocystin or smoothened to cilia in cells expressing dominant negative MyoVb, which supports that polycystin-2 is specifically transported through recycling endosomes to the cilium. To further confirm that polycystin-2 is using the recycling trafficking pathway for ciliary delivery, dominant negative Rab11a that disrupts the recycling endosome system was expressed in mammalian cells (Hehnly and Doxsey, 2014; Monis et al., 2017; Westlake et al., 2011). Immunofluorescence found a reduction in the

steady-state levels of polycystin-2 at the cilium in cells expressing dominant negative Rab11a, which indicates that polycystin-2 is transporting through endosomes to cilia. However, it is unclear whether polycystin-2 is trafficked from the Golgi directly to endsosomes and then to the cilium or if it is endocytosed at the plasma membrane to the recycling endosome system before being delivered to cilia.

Proteins Implicated in Ciliary Trafficking

The protein machineries required for the sorting, transporting, tethering, and fusion of receptor cargo vesicles at the base of the cilium are not well understood. The process of intraflagellar transport (IFT) is required for cilia formation and maintenance, suggesting that it may be involved in membrane protein trafficking to the cilium. The IFT system consists of an adaptor protein complex made up of IFT complex A, IFT complex B, and the BBSome, and the molecular motors kinesin-2 and dynein-2 (Nachury et al., 2007; Rosenbaum and Witman, 2002). Small GTPases have also been implicated in cilia formation and receptor targeting to cilia. Additionally the exocyst complex and the soluble *N*-ethylmaleimide-sensitive factor attachment protein receptors (SNAREs) are thought to regulate the tethering and fusing of vesicles to the ciliary base. Furthermore, the BLOC-1 complex was recently proposed to coordinate receptor transport from endosomes to the primary cilium. Each of these systems will be discussed below in regard to their role in ciliary membrane protein trafficking.

IFT Complex A and B

Currently twenty-two proteins are known to comprise IFT complex A and B (Rosenbaum and Witman, 2002). All of these IFT particle proteins, with the exception of IFT20, predominantly localize at the cilium and at the centrosome region at the ciliary base. Loss of function IFT complex A animals have cystic kidneys and Hedgehog signaling related developmental defects, and cells that are null for IFT complex A subunits form short bulgy cilia, implying that IFT Complex A is required for cilium formation (Fu et al., 2016; Jonassen et al., 2012; Liem et al., 2012; Zhu et al., 2017). Knockout or RNAi knockdown of IFT complex A subunits in mammalian cells reduced the localization of GPCRs, including smoothened and Gpr161, at the cilium showing that IFT complex A is involved in membrane protein trafficking to cilia (Caparros-Martin et al., 2015; Fu et al., 2016; Hirano et al., 2017; Liem et al., 2012). However, some of these experiments report the percentage of receptor positive cilia and it is unclear whether the area of the cilium was accounted for in these measurements. Cells that are null for IFT complex A subunits form short cilia meaning that mutants have a smaller ciliary area for receptor localization compared to the controls. A qualitative comparison of receptor localization in control and short cilia might infer a defect in ciliary trafficking, while a quantitative measurement accounting for the area of the cilium may suggest no difference in trafficking.

Tubby-like protein 3 (TULP3) is proposed to regulate the function of IFT complex A in ciliary receptor targeting. Tandem affinity purification and mass

spectrometry analysis found TULP3 to interact with IFT complex A and it also localizes at cilia, suggesting that it may have a role in cilium formation (Mukhopadhyay et al., 2010). RNAi knockdown of TULP3 in mammalian cells had no effect on cilia assembly indicating that it is not required for cilia formation and that it might be involved in ciliary receptor trafficking. Additional TULP3 knockdown experiments found reduced localization of GPCRs including SSTR3 and MCHR1, and cystoproteins such as fibrocystin and polycystin-2, at the cilium inferring that TULP3 is required for selective membrane protein trafficking to cilia (Badgandi et al., 2017; Mukhopadhyay et al., 2010). TULP3 ciliary localization is dependent on IFT Complex A and because it is involved in receptor trafficking, TULP3 was proposed to be an adaptor that delivers receptors to the ciliary base where it then coordinates with IFT complex A to incorporate the cargo into the cilium (Badgandi et al., 2017; Mukhopadhyay et al., 2010). Proximity biotinylation and cross linking assays demonstrated that TULP3 is in close proximity with multiple CTSs including that of Gpr161 and fibrocystin, which supports its function as an adaptor that directs receptor cargoes to the cilium.

IFT complex B is also thought to be involved in ciliary membrane protein trafficking. Most IFT complex B null animal models do not form a cilium and this causes embryonic lethality, which shows that the majority of IFT complex B subunits are critically required for cilia assembly (Berbari et al., 2011; Follit et al., 2006). Knockdown of IFT complex B subunits IFT57 or IFT172 in mammalian cells, to levels where there was enough protein to allow cilia to form, reduced

localization of the GPCR dopamine receptor-1 at the cilium and expression of these subunits rescued its localization, inferring that IFT complex B is required for dopamine receptor-1 transport to cilia (Leaf and Von Zastrow, 2015). Immunoprecipitation assays also found dopamine receptor-1 to interact with IFT57, which proposes that dopamine receptor-1 may coordinate with IFT complex B at the base of the cilium for entry into the organelle. The researchers did not examine whether IFT57 or IFT172 are required for the trafficking of other ciliary receptors meaning that these subunits may be involved in delivering additional membrane proteins to the cilium.

IFT complex B subunits IFT25 and IFT27 have been postulated to regulate the export of membrane proteins from cilia. Unlike other IFT complex B particle proteins, IFT25 and IFT27 are both dispensable for cilium formation and null animals die at birth due to Hedgehog signaling related developmental defects (Eguether et al., 2014; Keady et al., 2012). Given the phenotype of the null animals, investigators examined the localization of the ciliary Hedgehog signaling receptors patched-1 and smoothened in mutant cells (Eguether et al., 2014; Keady et al., 2012). Immunofluorescence of IFT25 or IFT27 null mammalian cells showed an accumulation of patched-1 and smoothened at cilia, implying that IFT25 and IFT27 are involved in removal of these receptors from the cilium. It would be interesting to determine whether IFT25 and IFT27 are required for the removal of other receptors from cilia.

Golgi-IFT Complex

The IFT complex B subunit IFT20 is the only known IFT protein that localizes at both the cilium and the Golgi apparatus, suggesting that it plays a role in membrane protein trafficking to cilia (Follit et al., 2006). The pool of IFT20 at the Golgi is designated the Golgi-IFT complex because it is considered to be separate from the pool of IFT particles at the cilium. Immunofluorescence showed IFT20 to co-localize with markers for the –*cis* and –*medial* but not the –*trans* Golgi cisternae, implying that IFT20 localizes specifically to the –*cis* and –*medial* Golgi compartments. IFT20 may sort receptors that are transporting from the –*cis* and –*medial* cisternae to the –*trans* Golgi. Live cell imaging of IFT20 fused to a GFP tag identified punctae movement from the Golgi complex to the cilium, inferring that IFT20 is marking vesicles that are trafficking between the two organelles and that it may function as an adaptor for ciliary receptor transport. However, these experiments do not demonstrate whether IFT20 is functionally required for ciliary membrane protein trafficking. To address this concern, knockdown of IFT20 in mammalian cells reduced the steady-state levels of the cystoprotein polycystin-2 at the cilium, which supports the involvement of IFT20 in polycystin-2 trafficking to cilia (Follit et al., 2006; Monis et al., 2017). Additional pulse-chase assays, that measure receptor trafficking from the Golgi complex to cilia, were performed on IFT20 knockdown cells (Monis et al., 2017). Immunofluorescence detected a reduction in the trafficking of

polycystin-2 and fibrocystin, but not smoothened to cilia demonstrating that IFT20 regulates the delivery of specific membrane proteins to the cilium.

IFT20 is thought to by anchored to the Golgi complex through its interaction with the vesicle tethering golgin Golgi microtubule associated protein 210 (GMAP210), which implies that GMAP210 may also be involved in ciliary receptor targeting (Follit et al., 2008). Immunoprecipitation and mass spectrometry analysis found GMAP210 to interact with IFT20 but not other IFT complex B subunits indicating that the interaction between IFT20 and GMAP210 is independent of IFT complex B. Also, immunofluorescence demonstrated that IFT20 and GMAP210 co-localize at the Golgi apparatus, classifying GMAP210 as a member of the Golgi-IFT complex. Cells that are null for GMAP210 do not have IFT20 localized at the Golgi and expression of exogenous GMAP210 rescues IFT20 localization, which infers that GMAP210 anchors IFT20 to the Golgi cisternae. IFT20 may require GMAP210 to anchor it to Golgi membranes so that it can sort receptors destined for the cilium. GMAP210 tethers vesicles that are trafficked from the endoplasmic reticulum to the Golgi complex meaning that it may capture receptor-carrying vesicles en route to cilia (Drin et al., 2007; Drin et al., 2008; Wong and Munro, 2014). Null GMAP210 animals die after birth due to heart and lung defects but assemble normal length cilia suggesting that GMAP210 is not required for cilia formation but rather receptor targeting. To determine whether GMAP210 is functionally involved in ciliary membrane protein trafficking, immunofluorescence of GMAP210 null cells identified a reduction in

the steady-state levels of polycystin-2 at the cilium and expression of exogenous GMAP210 rescued receptor localization indicating that it is necessary for polycystin-2 delivery to cilia (Follit et al., 2008). Additional, pulse-chase trafficking assays performed on GMAP210 knockdown cells found a reduction in the trafficking of polycystin-2 and fibrocystin, but not smoothened to cilia demonstrating that GMAP210 coordinates the transport of specific receptors to the cilium (Monis et al., 2017). It would be exciting to identify new proteins that interact with GMAP210 and determine whether they have a role in ciliary receptor targeting.

Since IFT20 is involved in trafficking receptors to the primary cilia of epithelial cells, it was proposed that it would also be required for rhodopsin transport to photoreceptor outer segments. Immunoprecipitation experiments found IFT20 to interact with the C-terminal tail of rhodopsin indicating that it might coordinate rhodopsin delivery to the connecting cilium (Keady et al., 2011). Floxed allele deletion of IFT20 in mouse photoreceptors caused degradation of the outer segment and rhodopsin to mislocalize implying that IFT20 is required for rhodopsin trafficking to outer segments (Crouse et al., 2014; Keady et al., 2011). To discern whether rhodopsin is trafficking from the Golgi apparatus to the cilium, IFT20 or IFT complex A subunit IFT140 were deleted in mouse photoreceptors and then rhodopsin localization was examined (Crouse et al., 2014). Interestingly, deletion of IFT20 caused rhodopsin to accumulate at the Golgi complex whereas deletion of IFT140 resulted in rhodopsin concentrating in

the inner segement plasma membrane, indicating that IFT20 is sorting rhodopsin at the Golgi complex for delivery to the base of the connecting cilium (Crouse et al., 2014; Keady et al., 2011). It would be interesting to delete GMAP210 in photoreceptors and see whether rhodopsin accumulates at the Golgi complex. This result would support a role for GMAP210 in transporting rhodopsin from the Golgi to outer segments.

BBSome

The BBSome is part of the IFT machinery and consists of eight proteins (BBS1, BBS2, BBS4, BBS5, BBS7, BBS8, BBS9 and BBIP10). Some patients diagnosed with the ciliopathy Bardet-Biedl syndrome have mutations in these subunits with symptoms including obesity, kidney malformations, retinal degeneration, and polydactyly (Hildebrandt et al., 2011; Nachury et al., 2007). The BBSome localizes at the cilium but it is dispensable for cilia formation, suggesting that it may coordinate ciliary receptor targeting (Berbari et al., 2008b; Nachury et al., 2007). Electron microscopy analysis identified the BBSome to cover the surfaces of liposomes *in vitro* implying that it may be a vesicle coat structure but it did not have the ability to deform membranes, which is a characteristic of a protein coat (Jin et al., 2010). The current consensus is that the BBSome is not a vesicular protein coat but rather an adaptor complex that regulates ciliary trafficking (Eguether et al., 2014; Lechtreck et al., 2009). Immunoprecipitation experiments found BBSome subunits to interact with the CTS of SSTR3, which supports its function as an adaptor involved in ciliary membrane protein trafficking (Jin et al.,

2010). Knockout of BBSome subunits BBS2 or BBS4 in neurons reduced the localization of the GPCRs SSTR3 and MCHR1 at cilia and expression of these subunits rescued receptor localization at the cilium, suggesting that BBSome is necessary for the trafficking of SSTR3 and MCHR1 to cilia (Berbari et al., 2008b).

However, the hypothesis that the BBSome is necessary for trafficking receptors to cilia has been called into question by recent findings that support the involvement of the BBSome in the removal of membrane protein receptors from the cilium. Live cell imaging of BBS2 or BBS4 knockdown cells showed an accumulation of GPCRs including SSTR3 at cilia and subsequent ectocytosis from the ciliary tip, supporting that membrane proteins that are not retrieved from cilia are released into ectosomes and explains why previous studies observed an apparent reduction in receptors at the cilium in BBSome mutants (Nager et al., 2017). In addition other researchers found that knockout of BBSome subunits in mammalian cells show an accumulation of GPCRs including smoothened and dopamine receptor-1 at the cilium, which further supports the role of the BBSome in ciliary receptor retrieval (Domire et al., 2011; Eguether et al., 2014; Seo et al., 2011). The function of the BBSome in ciliary receptor export has been observed in additional model systems as well. The *Chlamydomonas reinhardtii* BBS4 mutant accumulates the membrane protein phospholipase D at their cilia and expression of the wild type subunit reduced the levels of the receptor at the cilium suggesting that the BBSome is required for the export of phospholipase D from cilia (Lechtreck et al., 2013; Lechtreck et al., 2009). *Caenorhabditis elegans*

BBSome mutants accumulate the cystoprotein polycystin-2 at cilia (Xu et al., 2015). This evidence supports that the function of the BBSome in ciliary receptor removal is evolutionarily conserved. It is thought that BBSome coordinates with the IFT particle for the retrograde removal of receptors from cilia and it may work with the rest of the IFT particle in removing specific membrane proteins from the tips of cilia by the process of ectocytosis as an alternative to retrograde export (Eguether et al., 2014; Lechtreck et al., 2009; Nager et al., 2017).

Molecular Motors

Kinesin-2 and dynein-2 motors transport the IFT particle along the ciliary axoneme, but not much information is known about the molecular motors that deliver receptor carrying vesicles to cilia (Rosenbaum and Witman, 2002). Intracellular transport relies upon molecular motor proteins that carry vesicular cargo directionally along cytoskeleton tracks, with myosins on actin and kinesins and dyneins on microtubules (Hartman and Spudich, 2012; Vale, 2003). The molecular motor kinesin family member 17 (KIF17) transports vesicles carrying non-ciliary receptors in vertebrate neurons and it also localizes at cilia but it is dispensable for vertebrate cilia formation, indicating that KIF17 may be involved in ciliary receptor trafficking (Setou et al., 2000; Signor et al., 1999; Zhao et al., 2012). Expression of dominant negative KIF17 in mammalian cells showed a reduction in the localization of receptors including dopamine receptor-1 at cilia, implying that KIF17 is transporting vesicles containing receptor cargo to the cilium (Jenkins et al., 2006; Leaf and Von Zastrow, 2015). However,

overexpression of dominant negative KIF17 may have an indirect effect on intracellular protein trafficking. Knockout or knockdown of KIF17 will show whether the motor is involved in ciliary receptor targeting and subsequent rescue experiments will support KIF17 as being necessary for membrane protein trafficking to cilia.

The molecular motor myosin VI is thought to be involved in removing membrane protein receptors from the tips of cilia through the process of ectosome shedding (Nager et al., 2017). Ciliary proteomic profiling of cells that are defective in exporting receptors from cilia identified the actin regulator myosin VI suggesting that it may be involved in removing membrane proteins from the cilium (Mick et al., 2015). Live cell imaging of myosin VI knockdown cells showed a reduction in the ectocytosis of vesicles containing the GPCR neuropeptide Y receptor 2 from the tips of cilia, indicating that myosin VI regulates the export of membrane proteins from the cilium. Ciliary membrane shedding has also been documented in photoreceptors, *Caenorhabditis elegans*, and *Chlamydomonas reinhardtii* implying that the process is conserved but it is not known whether this function is for turning over ciliary receptors or if it is a form of extracellular signaling (Besharse et al., 1977; Nager et al., 2017; Wang et al., 2014; Wood et al., 2013).

Small GTPases

Small G proteins regulate receptor transport through the cellular secretory pathway and are proposed to coordinate the delivery of membrane proteins to

cilia. Small G proteins are GTPases that cycle between GTP and GDP bound states, the GTP bound catalytically active state binds effector proteins and the GDP bound or nucleotide free form is the inactive state (Gillingham and Munro, 2007). Members of the Arf, Arl, and Rab subfamilies of the Ras superfamily of small G proteins have been implicated in ciliary receptor trafficking.

Arf Small GTPases

Functions of Arf small GTPases include the recruitment of coat proteins to assist in sorting vesicle cargo, recruiting and activating trafficking enzymes, and interacting with the cellular cytoskeleton (D'Souza-Schorey and Chavrier, 2006; Donaldson and Jackson, 2011). Arf4 has been suggested to play an essential role in membrane protein trafficking to cilia but this function has been recently called into question. Arf4 localizes at the Golgi apparatus and immunoprecipitation assays found Arf4 to interact with the GPCR rhodopsin, implying that it may coordinate the delivery of rhodopsin from the Golgi complex to photoreceptor outer segments (D'Souza-Schorey and Chavrier, 2006; Donaldson and Jackson, 2011; Mazelova et al., 2009a). Antibody perturbation of Arf4 in Golgi budding *in vitro* assays identified a reduction in the formation of rhodopsin transport carriers, indicating that Arf4 regulates the budding of vesicles carrying rhodopsin cargo at Golgi cisternae (Deretic et al., 2005; Mazelova et al., 2009a). The researchers then examined Arf4 *in vivo* by expressing dominant negative Arf4 in frog photoreceptors, which resulted in retinal degeneration and rhodopsin mislocalization further supporting the model that Arf4 regulates

rhodopsin transport to outer segments (Mazelova et al., 2009a). Nonetheless, overexpression of dominant negative Arf4 may have compromised the integrity of the Golgi apparatus causing the retinal degeneration and rhodopsin mislocalization result to be indirect.

Arf4 was also proposed to regulate the trafficking of the cystoproteins polycystin-1 and fibrocystin to cilia. Immunoprecipitation assays identified Arf4 to interact with polycystin-1 and knockdown of Arf4 in mammalian cells reduced the localization of polycystin-1 at the cilium, indicating that Arf4 is involved in the transport of this receptor to cilia (Ward et al., 2011). Arf4 was also found to interact with fibrocystin and pulse-chase trafficking assays performed on Arf4 knockdown cells showed a delay in fibrocystin trafficking to cilia, inferring that Arf4 is not critically required for the ciliary targeting of fibrocystin (Follit et al., 2014). The delay in fibrocystin delivery to the cilium may be due to a general cellular trafficking defect that is not specific to cilia.

If Arf4 plays a role in the trafficking of rhodopsin, polycystin-1, and fibrocystin to cilia, than loss of Arf4 *in vivo* would result in a retinal degeneration and a cystic kidney phenotype. To address this question, an Arf4 floxed mouse was generated because Arf4 null mice are embryonic lethal (Follit et al., 2014; Pearring et al., 2017). Deletion of Arf4 in photoreceptors did not cause retinal degeneration and rhodopsin was not mislocalized, supporting that Arf4 is not required for rhodopsin transport to outer segments. Deletion of Arf4 in the kidney did not result in cyst formation and cilia assembly was unaffected, implying that

fibrocystin and polycystin-1 delivery to cilia is Arf4 independent (Pearring et al., 2017). Interestingly, loss of Arf4 in the pancreas causes non-cilia related exocrine pancreas degeneration (Pearring et al., 2017). The *in vivo* mouse model demonstrates that Arf4 is not required for membrane protein trafficking to cilia but it is involved in endomembrane trafficking in the pancreas.

Arl Small GTPases

Arl small GTPases are structurally similar to Arfs but play a broader role in protein trafficking, and the Arls that are involved in ciliary trafficking include Arl13b, Arl3, and Arl6 (D'Souza-Schorey and Chavrier, 2006; Donaldson and Jackson, 2011). Arl13b is a palmitoylated peripheral membrane protein that localizes at cilia and some patients diagnosed with the ciliopathy Joubert syndrome have mutations in Arl13b with symptoms including hindbrain abnormalities (Cantagrel et al., 2008; Cevik et al., 2010; Duldulao et al., 2009; Sun et al., 2004). Loss of function Arl13b animals have Hedgehog signaling related developmental defects, cystic kidneys, and short cilia indicating that Arl13b is required for formation of the cilium (Caspary et al., 2007; Seixas et al., 2016). A *Caenorhabditis elegan* Arl13b mutant was found to accumulate polycystin-2 at its cilia, which suggests that Arl13b may be involved in receptor export from the cilium (Cevik et al., 2010). However, this mutant is not a null but rather it contains an in frame deletion that encodes a truncated form of Arl13b with an intact GTPase domain, meaning it is not clear whether the accumulation

of polycystin-2 at the cilium is a direct affect of the Arl13b mutation (Cevik et al., 2010; Li et al., 2010).

Arl3 localizes at cilia and loss of function Arl3 animals have a pleiotropic phenotype consisting of cysts in the kidney, liver, and pancreas and photoreceptor degeneration, inferring that it is required for ciliary formation (Cuvillier et al., 2000; Grayson et al., 2002; Hanke-Gogokhia et al., 2016; Schrick et al., 2006; Zhou et al., 2006). Immunohistochemistry of Arl3 null mouse photoreceptors identified mislocalization of rhodopsin, which indicates that Arl3 is required for rhodopsin trafficking to outer segments (Schrick et al., 2006). Nevertheless, floxed deletions of Arl3 in mouse photoreceptors found no defect in the localization of rhodopsin to outer segments suggesting that rhodopsin transport is Arl3 independent (Hanke-Gogokhia et al., 2016). The discrepancy in rhodopsin localization may be because Arl3 was not completely deleted in the floxed photoreceptors.

It is also thought that Arl3 is required for trafficking the cystoproteins polycystin-1 and polycystin-2 to cilia. Immunoprecipiration assays showed Arl3 to interact with polycystin-1 and knockdown of Arl3 in mammalian cells identified a reduction in the localization of polycystin-1 and polycystin-2 at the cilium, proposing that Arl3 coordinates the trafficking of these receptors to cilia (Kim et al., 2014). Some of the proteins that control the enzymatic activity of Arl3 were recently identified and they may direct ciliary protein trafficking. Crystallography and biochemical analysis demonstrated that the membrane-associated protein

retinitis pigmentosa 2 is the GTPase-activating protein for Arl3 and Arl13b is the guanine nucleotide exchange factor (Gotthardt et al., 2015; Veltel et al., 2008). Retinitis pigmentosa 2 also localizes at cilia and it is intriguing to speculate that it may work with Arl13b to regulate Arl3 activity in transporting rhodopsin, polycystin-1, and polycystin-2 to cilia (Evans et al., 2010; Hurd et al., 2011).

The BBSome is the major effector of Arl6 and this small GTPase recruits this complex to lipid membranes for entry into the cilium (Jin et al., 2010). Some patients diagnosed with Bardet-Biedl syndrome have mutations in Arl6 and it also localizes at the cilium but it is not required for cilium formation, indicating that it may have a potential role in ciliary protein trafficking (Jin et al., 2010; Khan et al., 2013; Nachury et al., 2007; Zhang et al., 2011). Expression of dominant negative Arl6 in mammalian cells reduced the localization of polycystin-1 at cilia supporting the involvement of Arl6 in targeting polycystin-1 to cilia (Su et al., 2014). However, overexpression of dominant negative Arl6 may have an indirect effect on intracellular protein trafficking. Knockout or knockdown of Arl6 will show whether the small GTPase is regulating the delivery of receptors to the cilium and subsequent rescue experiments will support Arl6 as being necessary for ciliary membrane protein transport.

Arl6 has also been implicated in the removal of receptors from cilia. Immunofluorescence of Arl6 null mammalian cells show an accumulation of GPCRs including smoothened and SSTR3 at their cilia, implying that Arl6 coordinates the retrograde export of membrane proteins from the cilium

(Eguether et al., 2014; Liew et al., 2014; Nager et al., 2017; Zhang et al., 2011). Additional live cell imaging of Arl6 null mammalian cells identified an increase in the release of ecotosomes carrying SSTR3 from the tips of cilia suggesting that specific receptors are ectocytosed from cilia tips when ciliary retrograde removal is compromised (Nager et al., 2017). SSTR3 may be ectocytosed as a means of receptor disposal or it might be used in extracellular signaling.

Rab Small GTPases

Rab small GTPases regulate membrane compartment identity and control different stages of cellular trafficking such as vesicle formation, transport, and tethering; the Rabs that are involved in ciliary trafficking include Rab8, Rab23, and Rab29 (Stenmark, 2009; Zerial and McBride, 2001). Rab8 localizes at the cilium but Rab8 null animals do not have any visible ciliopathies such as cystic kidneys or retinal degeneration, and they form normal length cilia implying that it is not required for cilium assembly (Nachury et al., 2007; Sato et al., 2014; Sato et al., 2007; Yoshimura et al., 2007). Nonetheless Rab8 is proposed to regulate rhodopsin transport to photoreceptor outer segments. Sucrose density gradients performed on frog retinal homogenates detected Rab8 in the Golgi membrane fraction inferring that it may bind to rhodopsin carrying post Golgi vesicles (Deretic et al., 1995). Additionally, frogs expressing dominant negative Rab8 had retinal degeneration and an accumulation of rhodopsin adjacent to the periciliary ridge complex at the base of the connecting cilium supporting Rab8 in transporting rhodopsin from the Golgi complex to outer segments (Moritz et al.,

2001). However, the retinal degeneration and the rhodopsin mislocalization phenotypes may be an indirect effect of the overexpression of dominant negative Rab8.

Rab8 is also thought to control the transport of fibrocystin to cilia. Immunoprecipitation assays found Rab8 to interact with fibrocystin and expression of dominant negative Rab8 in mammalian cells reduced the steady state levels of fibrocystin at the cilium, indicating that Rab8 regulates fibrocystin ciliary trafficking (Follit et al., 2010). It is possible that the fibrocystin localization result is not direct because overexpression of dominant negative Rab8 may have off target effects. Rab8 knockdown and rescue experiments would identify whether it is necessary for delivering fibrocystin to the cilium.

Rab8 is part of a small G protein cascade that involves Rab11 recruiting the GTPase Rabin8 to the base of cilium to activate Rab8 and it is postulated that this pathway regulates ciliary protein trafficking (Lu et al., 2015; Nachury et al., 2007; Westlake et al., 2011). The proteins in this cascade interact with subunits of the transport protein particle II vesicle tethering complex that localizes at the base of cilia, indicating they may work together to coordinate ciliary receptor targeting (Schou et al., 2014; Westlake et al., 2011).

Rab23 is a negative regulator of Hedgehog signaling and some patients diagnosed with the ciliopathy Carpenter syndrome have mutations in Rab23 with symptoms including polydactyly (Alessandri et al., 2010; Eggenschwiler et al., 2006; Eggenschwiler et al., 2001; Jenkins et al., 2007). Loss of function Rab23

animals have an open neural tube phenotype suggesting that Rab23 plays a role in determining neural cell fate (Eggenschwiler et al., 2001). The Hedgehog signaling related developmental defects in patients and animals implies that Rab23 may be required for the trafficking of Hedgehog signaling receptors to cilia. Fluorescence recovery after photobleaching experiments performed on Rab23 knockdown or dominant negative Rab23 expressing mammalian cells identified faster recovery kinetics of smoothened at the cilium indicating that Rab23 regulates smoothened ciliary delivery but it is unclear why perturbing Rab23 would cause an increase in trafficking to the cilium (Boehlke et al., 2010). It is possible that Rab23 acts as a suppressor for smoothened entry into the cilium, which may be one of its functions as a negative regulator of Hedgehog signaling. Rab23 is also involved in the delivery of other GPCRs to the cilium. Knockdown of Rab23 in mammalian cells showed a reduction in the localization of dopamine receptor-1 and SSTR3 at cilia supporting Rab23 as being required for the ciliary transport of these receptors (Leaf and Von Zastrow, 2015).

The localization of Rab23 at cilia is debated and this discrepancy could be due to how fluorescent or epitope tags were fused onto the protein (Boehlke et al., 2010; Leaf and Von Zastrow, 2015; Yoshimura et al., 2007). Rabs associate with membranes through the use of lipidated cysteines located at the end of their C-terminus, meaning that a tag fused to this region may hinder the Rabs interactions with membranes and cause it not to localize at the cilium (Stenmark and Olkkonen, 2001).

Rab29 localizes at the base of cilia and it is required for cilia formation, indicating that Rab29 is involved in ciliary protein transport (Onnis et al., 2015). Immunoprecipitation assays found Rab29 to interact with IFT20 and knockdown of Rab29 in mammalian cells showed a reduction in the localization of smoothened at the cilium, which implies that it is required for smoothened delivery to cilia (Onnis et al., 2015). Rab29 may not be coordinating with IFT20 for smoothened ciliary targeting because smoothened transport to cilia is IFT20 independent (Monis et al., 2017). However, Rab29 and IFT20 may function together to traffic other receptors to the cilium.

Exocyst

The exocyst is a multi-subunit complex that tethers vesicles to membrane target sites prior to membrane fusion and it consists of eight protein subunits (Sec3/Exoc1, Sec5/Exoc2, Sec6/Exoc3, Sec8/Exoc4, Sec10/Exoc5, Sec15/Exoc6, Exo70/Exoc7, and Exo84/Exoc8) that are conserved from yeast to mammals (Heider et al., 2016; Heider and Munson, 2012; Kee et al., 1997; Luo et al., 2014; TerBush et al., 1996). A patient diagnosed with the ciliopathy Joubert syndrome has a mutation in exocyst subunit Exo84/Exoc8 and loss of function exocyst animals have a pleiotropic phenotype including cystic kidneys, retinal degeneration, and short cilia implying the exocyst plays a role in ciliary protein targeting (Dixon-Salazar et al., 2012; Fogelgren et al., 2015; Friedrich et al., 1997; Lobo et al., 2017; Seixas et al., 2016). Immunofluorescence of mammalian polarized epithelial cells found exocyst components along the sites

of secretion on the lateral membrane and at the ciliary base on the apical membrane and subunits of the exocyst are located at the base of the connecting cilium in photoreceptors suggesting that the complex tethers receptor carrying vesicles to the base of cilia (Grindstaff et al., 1998; Mazelova et al., 2009b; Monis et al., 2017; Rogers et al., 2004; Seixas et al., 2016; Zuo et al., 2009). Electron microscopy and immunofluorescence detected some exocyst subunits in the cilium but it is likely that these components are independent of the complete complex because there are no membrane bound vesicles in cilia, which means that exocyst mediated vesicle tethering must occur outside of the organelle (Fogelgren et al., 2011; Seixas et al., 2016; Zuo et al., 2009).

The exocyst is proposed to regulate the transport of specific receptors to cilia. Deletion of the exocyst subunit Sec10/Exoc5 in either zebra fish or mouse photoreceptors showed rhodopsin mislocalization implying that the exocyst is required for rhodopsin trafficking to outer segements (Lobo et al., 2017). Immunoprecipitation assays using mammalian epithelial cell lysates found subunits of the exocyst to interact with IFT20 and polycystin-2 which indicates that the exocyst may work with IFT20 at the ciliary base to deliver polycystin-2 to cilia (Fogelgren et al., 2011; Monis et al., 2017; Seixas et al., 2016). Additional, pulse-chase trafficking assays performed on Exo70/Exoc7 or Sec8/Exoc4 knockdown cells identified a reduction in the trafficking of polycystin-2 and fibrocystin, but not smoothened to cilia demonstrating that exocyst coordinates the transport of specific receptors to the cilium (Monis et al., 2017). It would be

exciting to find other receptors that are dependent on the exocyst for ciliary receptor targeting.

SNAREs

After a membrane vesicle is tethered to a membrane target site, the SNARE proteins then initiate and regulate the fusion between these two compartments. SNAREs are localized on both vesicle and target membranes and the SNARE proteins on the opposing membranes fuse to form a four-helix bundle that positions the membranes in close proximity to initiate the merger (Jahn and Scheller, 2006). The SNARE four-helix bundle is then dissolved by N-ethylmaleimide-sensitive factors (NSFs) allowing for the SNAREs to be recycled for continued fusion events (Jahn and Scheller, 2006). SNARE proteins have been extensively studied in cellular trafficking processes but little information is known about the SNAREs involved in ciliary protein trafficking. Immunohistochemistry of frog photoreceptors found the SNAREs syntaxin-3 and soluble NSF attachment protein (SNAP)-25 to localize at the base of the connecting cilium adjacent to the periciliary ridge complex implying that these SNAREs may regulate the fusion of receptor carrying vesicles at cilia (Mazelova et al., 2009a). Additionally, structured illumination microscopy of mammalian cells identified SNAP-29 at the ciliary base and knockdown of this SNARE reduced cilia assembly indicating that it is required for cilium formation probably by regulating membrane fusion events at the base of cilia (Lu et al., 2015). The only SNARE that is known to be involved in ciliary receptor transport is vesicle-

associated membrane protein (VAMP)-3. Knockdown of VAMP-3 in mammalian cells formed short cilia and caused a reduction in the localization of smoothened at the cilium, which supports VAMP-3 as being a regulator of smoothened ciliary delivery (Finetti et al., 2015). It is not known whether VAMP-3 localizes at the base of cilia. Smoothened may be coordinating with VAMP-3 during fusion events at the plasma membrane instead of the ciliary base because it is thought to use the lateral trafficking pathway.

BLOC-1

BLOC-1 regulates protein transport from endosomes to lysosome-related organelles such as platelet-dense granules and melanosomes, and this complex consists of eight protein subunits (pallidin, dysbindin, muted, snapin, cappuccino, BLOS1, BLOS2, and BLOS3) (Ciciotte et al., 2003; Delevoye et al., 2016; Dennis et al., 2016; Falcon-Perez et al., 2002; Li et al., 2003; Moriyama and Bonifacino, 2002; Mullin et al., 2011; Sitaram et al., 2012; Starcevic and Dell'Angelica, 2004). Some patients diagnosed with Hermansky-Pudlak syndrome have mutations in these BLOC-1 subunits with symptoms including severe hypopigmentation and platelet aggregation defects (Morgan et al., 2006). Additionally, the BLOC-1 subunit dysbindin is a schizophrenia susceptibility gene and this complex is involved in membrane protein targeting to synaptic vesicles, trafficking dopamine receptors to the cell surface, and dopamine and glutamate release (Hartwig et al., 2017; Iizuka et al., 2007; Ji et al., 2009; Kumamoto et al., 2006; Larimore et al., 2011; Marley and von Zastrow, 2010a; Newell-Litwa et al., 2009; Numakawa

et al., 2004). BLOC-1 also coordinates membrane protein delivery to primary cilia. Immunofluorescence identified pallidin and BLOS2 to localize at the centrosome region at the base of the cilium and knockdown of dysbindin in mammalian cells caused a reduction in cilia assembly indicating that BLOC-1 is required for cilia formation (Monis et al., 2017; Wang et al., 2004b). Immunoprecipitation assays found BLOC-1 subunits to interact with IFT20, the exocyst, and polycystin-2 suggesting that this complex may work with IFT20 and the exocyst in trafficking polycystin-2 to cilia (Gokhale et al., 2012; Monis et al., 2017). To address this question, pulse-chase trafficking assays were performed on either pallidin or dysbindin knockdown mammalian cells and demonstrated a reduction in the trafficking of polycystin-2 but not fibrocystin or smoothened to cilia, which supports the involvement of BLOC-1 in polycystin-2 ciliary targeting (Monis et al., 2017). This model was further supported by the finding that BLOC-1 loss of function animals have cystic kidneys and short cilia (Monis et al., 2017). It would be intriguing to identify other ciliary receptors that are dependent on BLOC-1 for their transport to cilia.

Conclusion

Primary cilia perceive the extracellular environment through the utilization of membrane protein receptors that localize to the ciliary membrane and how these receptors are delivered to the cilium is only beginning to be understood. More detailed experimentation is required to elucidate the function of the selective

gating at the cilium, the receptor targeting sequences and trafficking pathways, and the protein machineries that are involved in ciliary receptor transport.

Chapter II : BLOC-1 is required for selective membrane protein trafficking from endosomes to primary cilia

Introduction

Many vertebrate cells possess a single nonmotile primary cilium that extends from the cell surface. These cilia perceive the extracellular environment by localizing specific receptors to the ciliary membrane. To date, more than 25 different receptors have been found to be ciliary localized (Hilgendorf et al., 2016). These include the important cystoproteins polycystin-1, polycystin-2, and fibrocystin, which are defective in polycystic kidney disease (PKD) and the hedgehog receptors patched-1 and smoothened (Corbit et al., 2005; Follit et al., 2010; Harris and Torres, 2009; Pazour et al., 2002b; Rohatgi et al., 2007; Yoder et al., 2002). Heritable mutations in genes that encode proteins essential for the structure or function of primary cilia cause a broad class of human diseases called the ciliopathies (Sattar and Gleeson, 2011). The ciliopathies include a wide variety of developmental and degenerative diseases that reflect the important and diverse roles that cilia play in organ development and tissue homeostasis.

Cilia have no protein synthesis capability, and thus all components are synthesized in the cytoplasm and trafficked into the organelle (Nachury et al., 2010). Nonmembrane proteins are thought to be transported from a pool at the base of the cilium into the cilium by intraflagellar transport (IFT). The IFT system consists of kinesin-2 and dynein-2 motors, and a large adaptor complex made up of IFT complex A, IFT complex B, and the BBSome (Nachury et al., 2007;

Rosenbaum and Witman, 2002). The involvement of IFT in the trafficking of membrane proteins has not been fully addressed.

The IFT complex B subunit IFT20 is localized at both the primary cilium and the Golgi apparatus, where it is in a complex with the golgin protein GMAP210 (Follit et al., 2008; Follit et al., 2006). Finding IFT20 at the Golgi complex suggested that IFT20 might be involved in trafficking of membrane proteins from the Golgi apparatus to the primary cilium. Complete loss of IFT20 blocked ciliary assembly precluding analysis of membrane protein trafficking to the organelle. However, cells with a partial loss of IFT20 (which could still ciliate) had reduced ciliary polycystin-2, consistent with a role for IFT20 in transport of this membrane protein (Follit et al., 2006). The golgin GMAP210, which anchors IFT20 to the Golgi membrane, is not required for ciliary assembly, but cells lacking it have reduced ciliary polycystin-2 suggesting that the Golgi pool of IFT20 is important for sorting ciliary membrane proteins (Follit et al., 2008). Photoreceptor outer segments, which are cilia, have very high demands for membrane protein transport to maintain the structure. In mouse it is estimated that ~4300 opsin molecules need to be transported per minute into the cilium to maintain the organelle while as many as 50,000 are needed per minute in fish and frogs (Besharse and Horst, 1990; Williams, 2002; Young, 1967). Loss of IFT20 or other IFT proteins leads to opsin mislocalization and photoreceptor degeneration (Crouse et al., 2014; Keady et al., 2011). Interestingly, acute deletion of IFT20 causes opsin accumulation at the Golgi complex, whereas

acute deletion of IFT140 causes opsin accumulation in the inner segment plasma membrane (Crouse et al., 2014; Keady et al., 2011). These data are consistent with a model in which IFT20 is important for sorting or trafficking of membrane proteins from the Golgi apparatus to the base of the cilium, where they engage the rest of the IFT system (Follit et al., 2006).

It is not clear that all membrane proteins are trafficked to the cilium by the same route. Early work on opsin transport in frogs and mastigoneme transport in *Ochromonas danica* suggested that these proteins traffic in vesicles directly from the Golgi apparatus to the base of the cilium, where the vesicles dock to the plasma membrane just outside of the cilium before the proteins are transported into the organelle (Bouck, 1971; Deretic et al., 1995; Papermaster et al., 1985). More recent work on smoothened transport suggests that this protein is trafficked to the plasma membrane and laterally moves into the cilium (Milenkovic et al., 2009). Agglutinin transport in *Chlamydomonas reinhardtii* uses a similar mechanism (Cao et al., 2015; Hunnicutt et al., 1990). A third pathway where proteins are first transported to the plasma membrane followed by endocytosis and delivery to the base of the cilium by the recycling pathway has been proposed, but no proteins are known to take this route (Nachury et al., 2010; Weisz and Rodriguez-Boulan, 2009).

The finding of opsin transport defects when IFT20 is perturbed suggests a role for IFT20-GMAP210 in the direct trafficking pathway from the Golgi complex to the base of the cilium. However, the role of IFT20 in trafficking additional

membrane proteins from the Golgi complex and/or through other organelles has not been tested. To assess their importance in trafficking of ciliary membrane proteins, we use a fluorescence-based pulse-chase assay to measure the dynamics of smoothened, polycystin-2 and fibrocystin delivery to the cilium after perturbing the IFT20-GMAP210 complex. We find that this complex is important for fibrocystin and polycystin-2 trafficking but has a minimal role in smoothened delivery.

To understand how IFT20 functions to traffic membrane proteins to cilia, we examined interactome data (Rual et al., 2005; Wang et al., 2011) and found connections between IFT20 and the exocyst and the biogenesis of lysosome-related organelles complex-1 (BLOC-1). Using our fluorescence-based pulse-chase assay, we find minimal roles for these complexes in smoothened transport, while the exocyst is important for both fibrocystin and polycystin-2 delivery. Interestingly, BLOC-1 is required only for the delivery of polycystin-2. Consistent with this, we find that loss of function BLOC-1 mouse models have a mild cystic kidney phenotype. Given the role of BLOC-1 in recycling endosome trafficking, we used a dominant negative MyoVb construct to perturb trafficking through the recycling endosome (Lapierre et al., 2001; Volpicelli et al., 2002). The construct blocks polycystin-2 trafficking to cilia but does not affect fibrocystin or smoothened delivery to cilia. Polycystin-2 trafficking is also perturbed by expression of a Rab11a dominant-negative mutation that disrupts the recycling endosome. Our studies uncover a new endosomal BLOC-1-dependent pathway

for delivery of membrane proteins to cilia and demonstrate that membrane proteins use different routes for delivery to the primary cilium.

Results

Fibrocystin and polycystin-2 are dependent on IFT20 and GMAP210 for ciliary trafficking, while smoothened delivery to cilia is largely independent of this complex.

We previously showed that IFT20 and GMAP210 are important for localization of polycystin-2 to cilia but their involvement in trafficking of other ciliary membrane proteins is not known. To extend our understanding of IFT20-GMAP210 in ciliary trafficking, we used a pulse-chase assay to compare polycystin-2 to two other ciliary membrane proteins when IFT20 or GMAP210 was perturbed. The proteins fibrocystin and smoothened were chosen because of their diverse structures and because of their importance to human disease. Fibrocystin is a single-pass transmembrane protein mutated in human autosomal recessive PKD, smoothened is a seven transmembrane receptor involved in hedgehog signaling and polycystin-2 is multispan membrane protein mutated in human autosomal dominant PKD (Alcedo et al., 1996; Mochizuki et al., 1996; van den Heuvel and Ingham, 1996; Ward et al., 2002; Ward et al., 2003).

Our pulse-chase assay is based on the SNAP tag, which can be derivatised with a variety of modified benzylguanines (Follit and Pazour, 2013; Follit et al., 2014). This allows one to first block all existing protein with a non-fluorescent derivative and then follow newly synthesized protein with a

fluorescent derivative (Sun et al., 2011). The fibrocystin construct consisted of the extracellular domain of CD8 fused to fibrocystin just N-terminal to the transmembrane domain with a SNAP tag placed just before the stop codon. The polycystin-2 construct consists of the first 703 amino acids fused to SNAP and GFP at the C-terminal end. Similarly, full length smoothened was tagged with SNAP and GFP at the C-terminal end (Fig. II-1, Aa, Ba, Ca). The SNAP tag is used to quantify newly synthesized protein, while the CD8 epitope tag (included in the extracellular domain of CD8) and GFP are used to monitor total protein levels at steady-state. Each of these chimeric proteins is robustly localized to cilia (Fig. II-1, Ab, Bb, Cb). IMCD3 Flp-In cell lines that uniformly expressed each of the proteins were then infected with lenti-viral shRNA constructs to knockdown the levels of proteins of interest. Reduction of protein was verified by immunoblot, and the amount remaining was typically about ~10-20% of the controls (Figs. II-2, II-3, II-8, II-9, II-10, and II-11).

The assay starts with blocking all the SNAP-tag binding sites with a cell permeable nonfluorescent benzylguanine. This substrate is then washed out of the media, and the cells are allowed to synthesize new protein for 1.5 hrs. The cells are then treated with cycloheximide to inhibit further protein synthesis and shifted to 19˚C to prevent the Golgi apparatus from releasing proteins. This causes an accumulation of newly synthesized protein at the Golgi apparatus (Ang et al., 2004). While still keeping the cells in cycloheximide, the cells are shifted back to 37˚C, allowing newly synthesized protein to be released from the

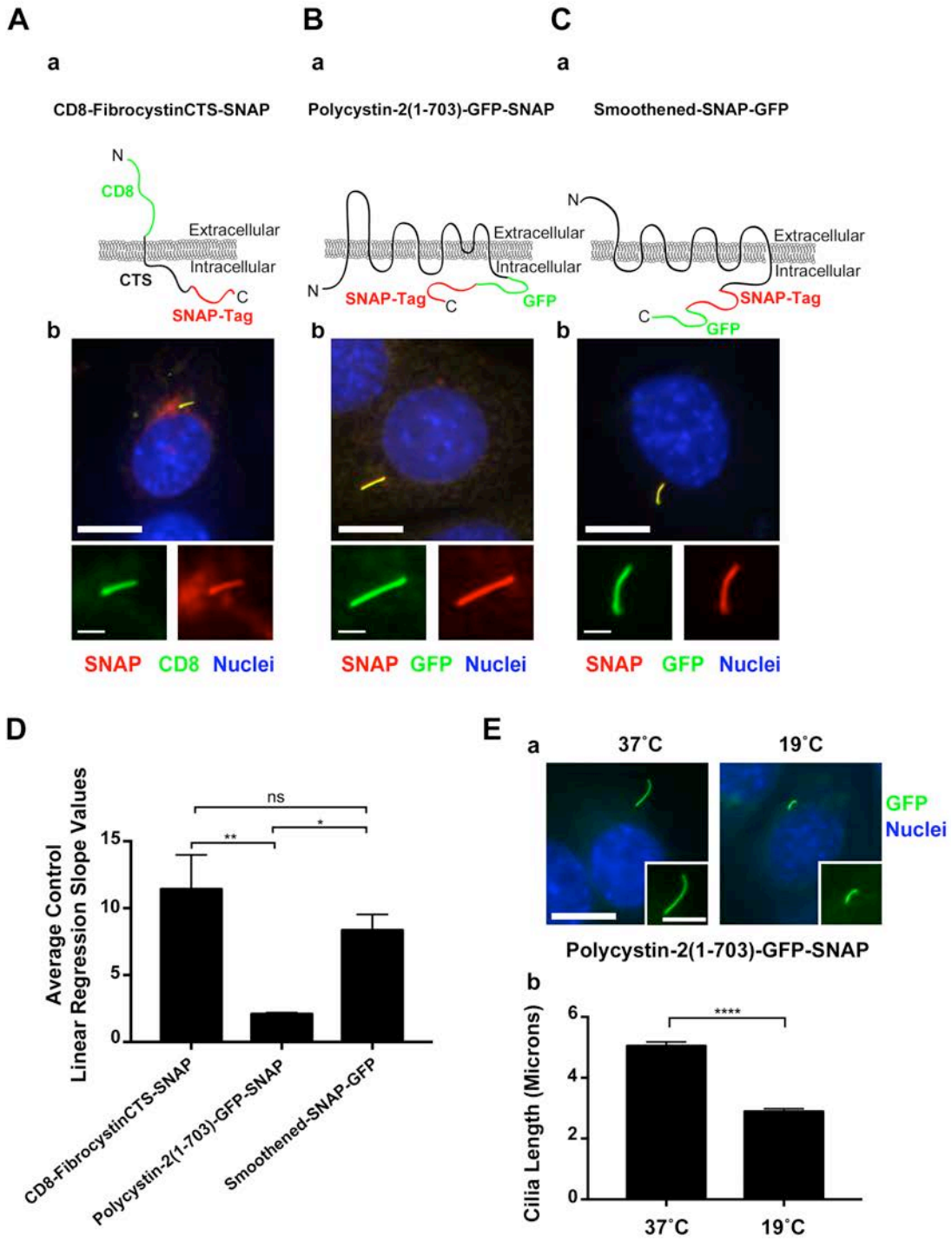

Figure II-1: Ciliary membrane protein constructs, trafficking rates, and cilia length after temperature shift to 19˚C.

Figure II-1. Ciliary membrane protein constructs, trafficking rates, and cilia length after temperature shift to 19˚C.

(**A**) HsCD8-MmFibrocystinCTS-SNAP (WJM8). (**Aa**) This construct contains part of the extracellular domain, the single transmembrane domain, and entire ciliary targeting sequence of MmFibrocystin. The extracellular N-terminal HsCD8 tag is used as an epitope marker and to maintain proper membrane protein topology. (**Ab**) IMCD3 Flp-In cells expressing ciliary localized CD8-FibrocystinCTS-SNAP stained with SNAP TMR STAR (red), CD8 antibody (green) and nuclei detected with DAPI (blue). Scale bar is 10 μm. Insets are 235% enlargements of the cilia. (**B**) HsPolycystin-2(1-703)-GFP-SNAP (WJM15). (**Ba**) This construct is truncated after amino acid 703 and is missing the ER-retention signal on its C-terminal end. (**Bb**) IMCD3 Flp-In cells expressing ciliary localized Polycystin-2(1-703)-GFP-SNAP stained with SNAP TMR STAR (red), GFP (green) and nuclei detected with DAPI (blue). Scale bar is 10 μm. (**C**) MmSmoothened-SNAP-GFP (WJM6). (**Ca**) This construct contains the full-length amino acid sequence of MmSmoothened. (**Cb**) IMCD3 Flp-In cells expressing ciliary localized Smoothened-SNAP-GFP stained with SNAP TMR STAR (red), GFP (green) and nuclei detected with DAPI (blue). Scale bar is 10 μm. (**D**) Mean control linear regression slope values for CD8-FibrocystinCTS-SNAP, Polycystin-2(1-703)-GFP-SNAP, and Smoothened-SNAP-GFP from Figure II-4 (n = 6 control slope values per membrane protein). The data was analyzed with One-way ANOVA and Tukey's multiple comparison test. * $p < 0.05$, ** $p < 0.01$, and ns = non-significant. (**E**) 19˚C causes cilia to shorten. (**Ea**) Polycystin-2-GFP-SNAP IMCD

Flp-In cells incubated at either 37˚C or for two hours at 19˚C. GFP (green) and nuclei detected with DAPI (blue). Scale bar is 10 μm. Insets are 150% enlargements of the cilia. (**Eb**) Cilia incubated at 19˚C are shorter compared with control (n = 100 cilia). The data was analyzed with unpaired student t-test. **** $p < 0.0001$. Error bars represent standard error of the mean.

Golgi complex and trafficked to the cilium. The cells were then fixed at indicated time points after temperature shift back to 37˚C, and the amount of newly synthesized and total tagged proteins in the cilium was measured.

For each experiment, we quantified the effectiveness of the shRNA knockdown by charge-coupled device detection of chemiluminescence and displayed results normalized to the untransfected control sample using gamma tubulin or IFT27 as a loading control. For each trafficking experiment, we measured cilia length, ciliary SNAP fluorescence, and either ciliary GFP fluorescence or CD8 immunofluorescence at 0, 1, 2, 4, and 6 hours after shift from 19˚C to 37˚C. The data was then plotted with respect to time, and the trafficking rate determined from the slope of the curve derived from the SNAP fluorescence. All experiments are plotted and displayed similarly, with the control cell displayed in blue, the non-silencing shRNA in green, and the two shRNAs targeting the gene of interest in red and black.

Under control conditions, the proteins showed different kinetics of delivery to the cilium (Figs. II-1, D and II-2 Ae, Af, Be, Bf, Ce, Cf). In all cases, newly synthesized protein could be detected in cilia within 1 hr of temperature shift. Rates of delivery of fibrocystin and smoothened were similar to each other but substantially higher than polycystin-2 (Fig. II-1, D). Fibrocystin typically reached a plateau within 2 to 4 hours after temperature shift while smoothened and polycystin-2 were still increasing at the 6 hr time point. We were unable to follow

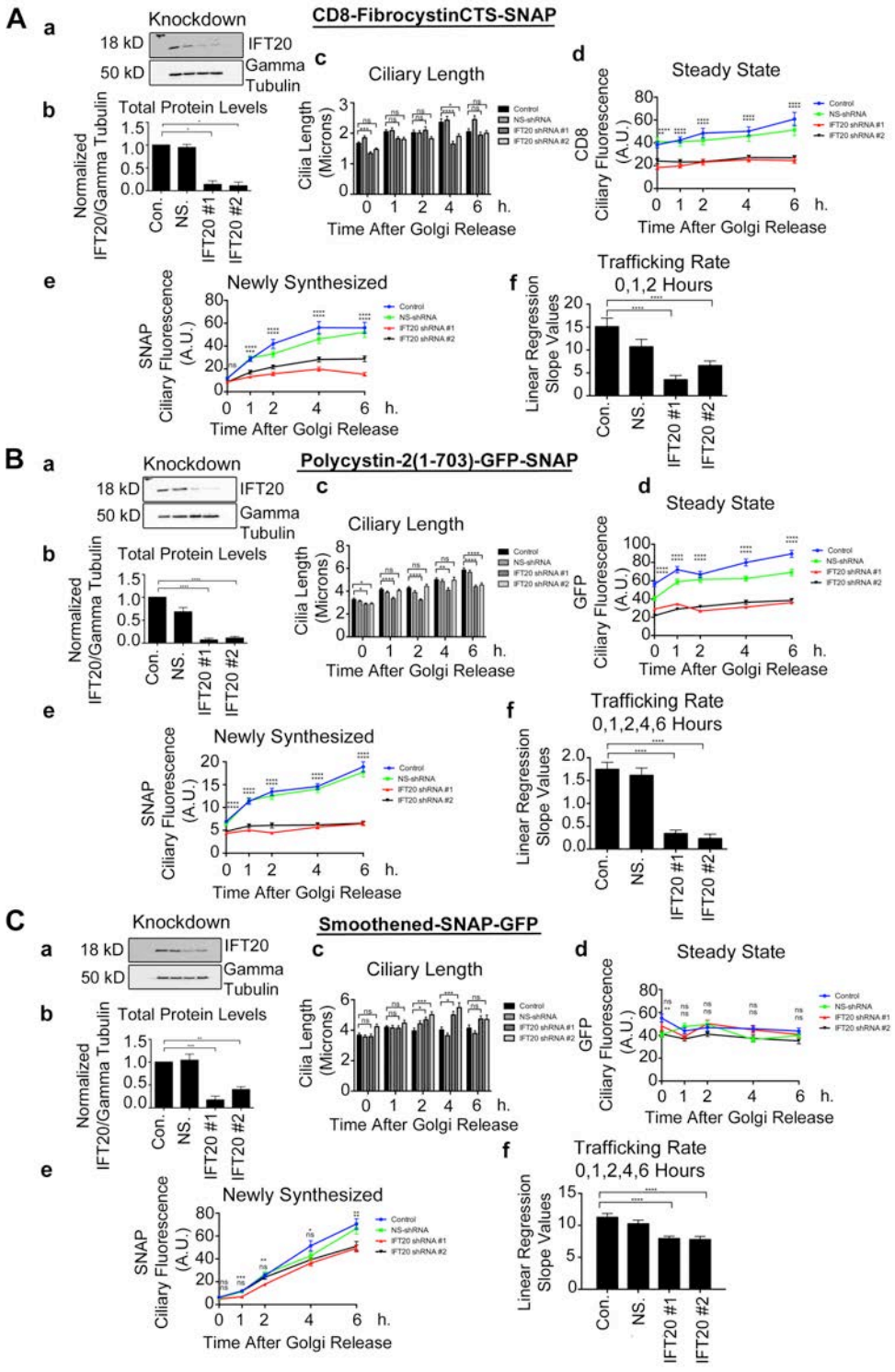

Figure II-2: IFT20 knockdown affects fibrocystin and polycystin-2 ciliary trafficking but only modestly affects smoothened trafficking to the cilium.

Figure II-2. IFT20 knockdown affects fibrocystin and polycystin-2 ciliary trafficking but only modestly affects smoothened trafficking to the cilium.

(A) Quantification of CD8-FibrocystinCTS-SNAP, (**B**) Polycystin-2(1-703)-GFP-SNAP, and (**C**) Smoothened-SNAP-GFP trafficking from the Golgi apparatus to the primary cilium during lenti-shRNA knockdown of IFT20. (**Aa, Ba, Ca**) Selected immunoblot images of IFT20 knockdown and gamma tubulin loading control. (**Ab, Bb, Cb**) Quantification of knockdown. Mean protein levels plotted from three independent experiments for each condition (Control, NS-shRNA, shRNA#1, and shRNA#2) and normalized to their corresponding gamma tubulin loading control. shRNA mediated knockdown of IFT20 results in >90% reduction of total protein abundance. (**Ac, Bc, Cc**) Mean cilia length, (**Ad, Bd, Cd**) Mean CD8 or GFP ciliary fluorescence, and (**Ae, Be, Ce**) Mean SNAP ciliary fluorescence plotted from three independent experiments in which 30 cilia were quantified for each condition (Control, NS-shRNA, shRNA#1, and shRNA#2) at each time point (n = 90 total cilia per time point). CD8 or GFP and SNAP pixel intensity measurements were taken at individual time points starting at the time of temperature shift from 19°C to 37°C (0 Hours). The data was analyzed with One-way ANOVA and Bonferroni multiple comparisons test. The control condition was compared with shRNA#1 and shRNA#2 conditions to determine statistical significance. (**Af, Bf, Cf**) Linear regression analysis of selected time points of newly synthesized membrane protein delivery to the cilium was completed. Slope values between control and experimental shRNA groups were compared with one another to determine statistical significance. * $p < 0.05$, ** $p <$

0.01, *** $p < 0.001$, **** $p < 0.0001$ and ns = non-significant. Error bars represent standard error of the mean.

cells for longer time, as the cells became unhealthy because of the cycloheximide treatment.

Initially we examined the functions of IFT20 and GMAP210 on the transport of our three model ciliary membrane proteins. As we observed previously, only a small amount of IFT20 is needed to support ciliary assembly, as knockdown to ~20% of normal had minimal effect on cilia length (Fig. II-2, Ac, Bc, Cc). Knockdown of GMAP210 had no effect on cilia length (Fig. II-3, Ac, Bc, Cc). In all experiments, we noted that ciliary length increased after shift to 37˚C. This is likely due to recovery from ciliary shortening that occurs when cells are placed at 19˚C (Fig. II-1, E). The knockdown of IFT20 and GMAP210 reduced the steady state levels of ciliary fibrocystin and polycystin-2 and also reduced the rate of delivery of these proteins to cilia (Figs. II-2, Ad, Bd, Ae, Be, Af, Bf; and II-3, Ad, Bd, Ae, Be; and II-4, D and E). In contrast, the steady state levels of ciliary smoothened and its rate of delivery to cilia was not greatly affected by the reduction in either IFT20 or GMAP210 (Figs. II-2, Cd, Ce, Cf; and II-3, Cd and Ce; and II-4, F). The differences in rates of delivery of the three model proteins and the fact that IFT20 and GMAP210 are not needed for the delivery of smoothened support a model where proteins can take different pathways to the cilium.

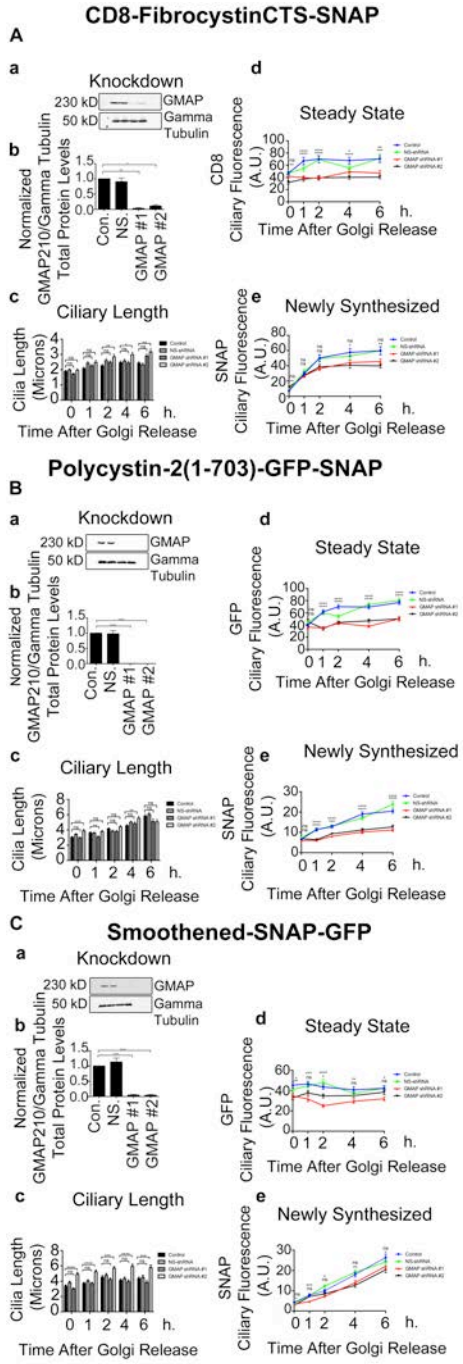

Figure II-3: GMAP210 knockdown strongly affects fibrocystin and polycystin-2 ciliary trafficking but only modestly affects smoothened trafficking to the primary cilium.

Figure II-3. GMAP210 knockdown strongly affects fibrocystin and polycystin-2 ciliary trafficking but only modestly affects smoothened trafficking to the primary cilium.

(**A**) Quantification of CD8-FibrocystinCTS-SNAP, (**B**) Polycystin-2(1-703)-GFP-SNAP, and (**C**) Smoothened-SNAP-GFP trafficking from the Golgi apparatus to the primary cilium during lenti-shRNA knockdown of GMAP210. (**Aa, Ba, Ca**) Selected immuno blot images of GMAP210 knockdown and gamma tubulin loading control. (**Ab, Bb, Cb**) Quantification of knockdown. Mean protein levels plotted from three independent experiments for each condition (Control, NS-shRNA, shRNA#1, and shRNA#2) and normalized to their corresponding gamma tubulin loading control. shRNA mediated knockdown of GMAP210 results in >90% reduction of total protein abundance. (**Ac, Bc, Cc**) Mean cilia length, (**Ad, Bd, Cd**) mean CD8 or GFP ciliary fluorescence, and (**Ae, Be, Ce**) mean SNAP ciliary fluorescence plotted from three independent experiments in which 30 cilia were quantified for each condition (Control, NS-shRNA, shRNA#1, and shRNA#2) at each time point (n = 90 total cilia per time point). CD8 or GFP and SNAP pixel intensity measurements were taken at individual time points starting at the time of temperature shift from 19°C to 37°C (0 Hours). The data was analyzed with One-way ANOVA and Bonferroni multiple comparisons test. The control condition was compared with shRNA#1 and shRNA#2 conditions to determine statistical significance. * $p < 0.05$, ** $p < 0.01$, *** $p < 0.001$, **** $p < 0.0001$ and ns = non-significant. Error bars represent standard error of the mean.

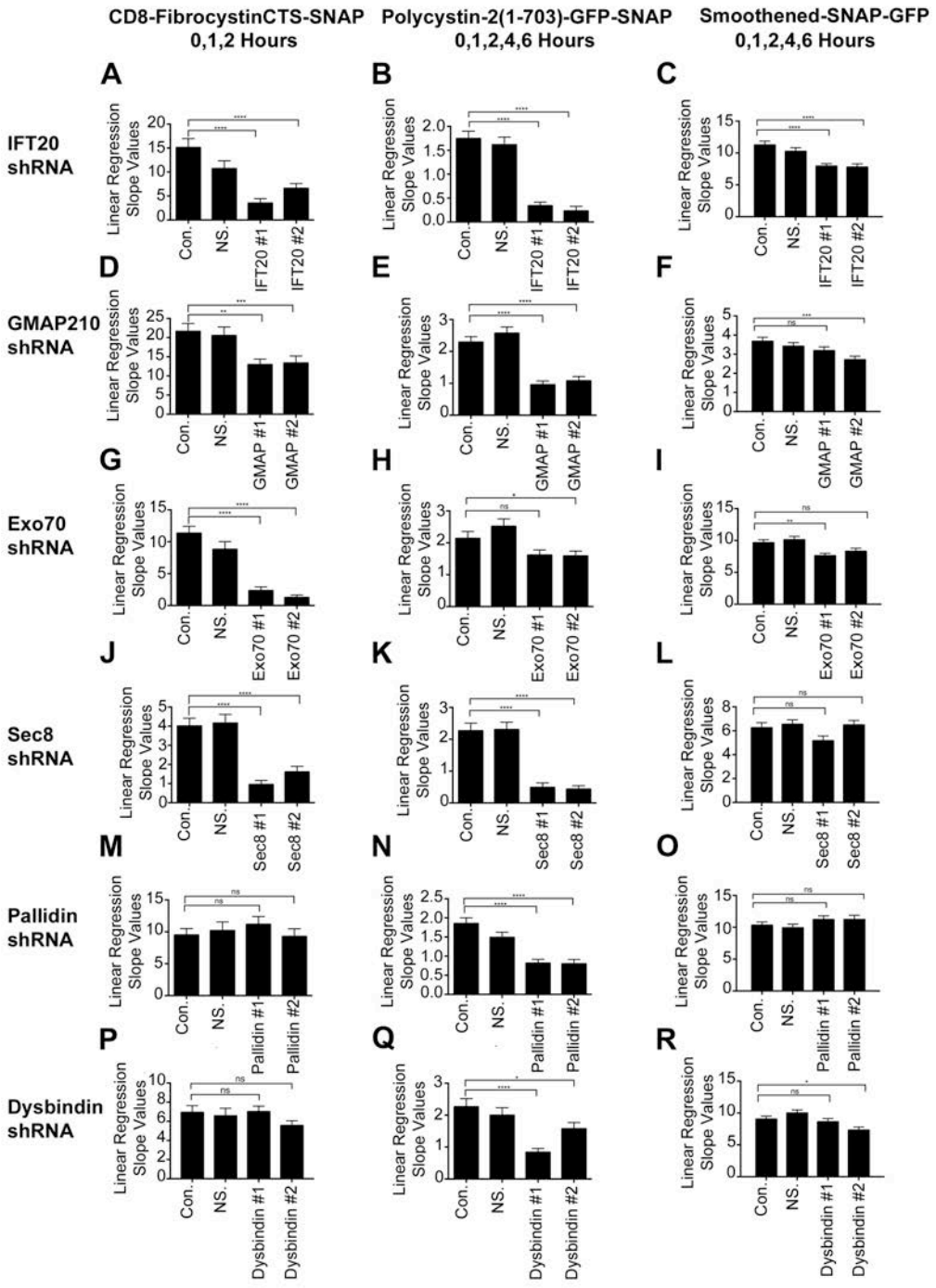

Figure II-4: Fibrocystin, polycystin-2, and smoothened trafficking rates to the primary cilium.

Figure II-4. Fibrocystin, polycystin-2, and smoothened trafficking rates to the primary cilium.

(**A – C**) Linear regression slope value analysis of newly synthesized CD8-FibrocystinCTS-SNAP, Polycystin-2-GFP-SNAP, or Smoothened-SNAP-GFP trafficking from the Golgi apparatus to the primary cilium when either IFT20, (**D – F**) GMAP210, (**G – I**) Exo70, (**J – L**) Sec8, (**M – O**) Pallidin or (**P – R**) Dysbindin are knocked down using lenti-shRNAs. Linear regression analysis of newly synthesized membrane protein delivery to the cilium was performed on selected time points: (0, 1, 2 Hours for CD8-FibrocystinCTS-SNAP; 0, 1, 2, 4, 6 Hours for Polycystin-2-GFP-SNAP; and 0, 1, 2, 4, 6 Hours for Smoothened-SNAP-GFP). The time points were chosen by determining which data points remained linear before (or if) reaching a plateau in the control groups (see Figs. II-2, II-3, II-8, II-9, II-10, and II-11). The slope values obtained from this analysis represent the trafficking rates of newly synthesized membrane protein delivery to the cilium. Slope values between control and experimental shRNA groups were compared with one another to determine statistical significance. shRNAs of interest are listed vertically on the left side and their corresponding membrane proteins are listed horizontally. Error bars represent standard error of the mean. * $p < 0.05$, ** $p < 0.01$, *** $p < 0.001$, **** $p < 0.0001$ and ns = non-significant. The IFT20 shRNA linear regression analysis (**A – C**) from Fig. II-2 is shown again for completion**.**

IFT20 interacts with the BLOC-1 subunit pallidin and the exocyst subunits Exo70 and Sec8.

To gain insight into the mechanism of how IFT20 and GMAP210 direct proteins to the ciliary membrane, we examined large-scale yeast-two hybrid screens for new IFT20-interacting proteins (Rual et al., 2005; Wang et al., 2011). From this, we identified the exocyst subunit Exo70, the BLOC-1 subunit pallidin, and a KxDL motif containing protein named KXD1 as candidate IFT20-binding proteins (Rual et al., 2005; Wang et al., 2011). To determine if these bind to IFT20, the coding sequences were cloned with N-terminal Flag tags, expressed in IMCD3 cells, and immunoprecipitated with anti-Flag resin (Fig. II-5, A). Flag-GFP and Flag-IFT54 were used as negative and positive controls (Follit et al., 2009). As expected, Flag-GFP did not pull down IFT20, but Flag-IFT54 showed a strong interaction with IFT20 (Fig. II-5, Ab). Flag-Pallidin brought down endogenous IFT20, while no binding of IFT20 was observed with Flag-KXD1 and Flag-Exo70 (Fig. II-5, Ab). Interestingly, Flag-Pallidin also precipitated endogenous polycystin-2 (Fig. II-5, Ab). Endogenous Exo70 was brought down by Flag-Pallidin (Fig. II-5, Ab). This is consistent with work showing BLOC-1 interacting with the exocyst components Sec6 and Sec8 (Gokhale et al., 2012). Flag-KXD1 pulled down Exo70 (Fig. II-5, Ab), which may be explained by KXD1 interacting with BLOC-1 (Hayes et al., 2011; Yang et al., 2012).

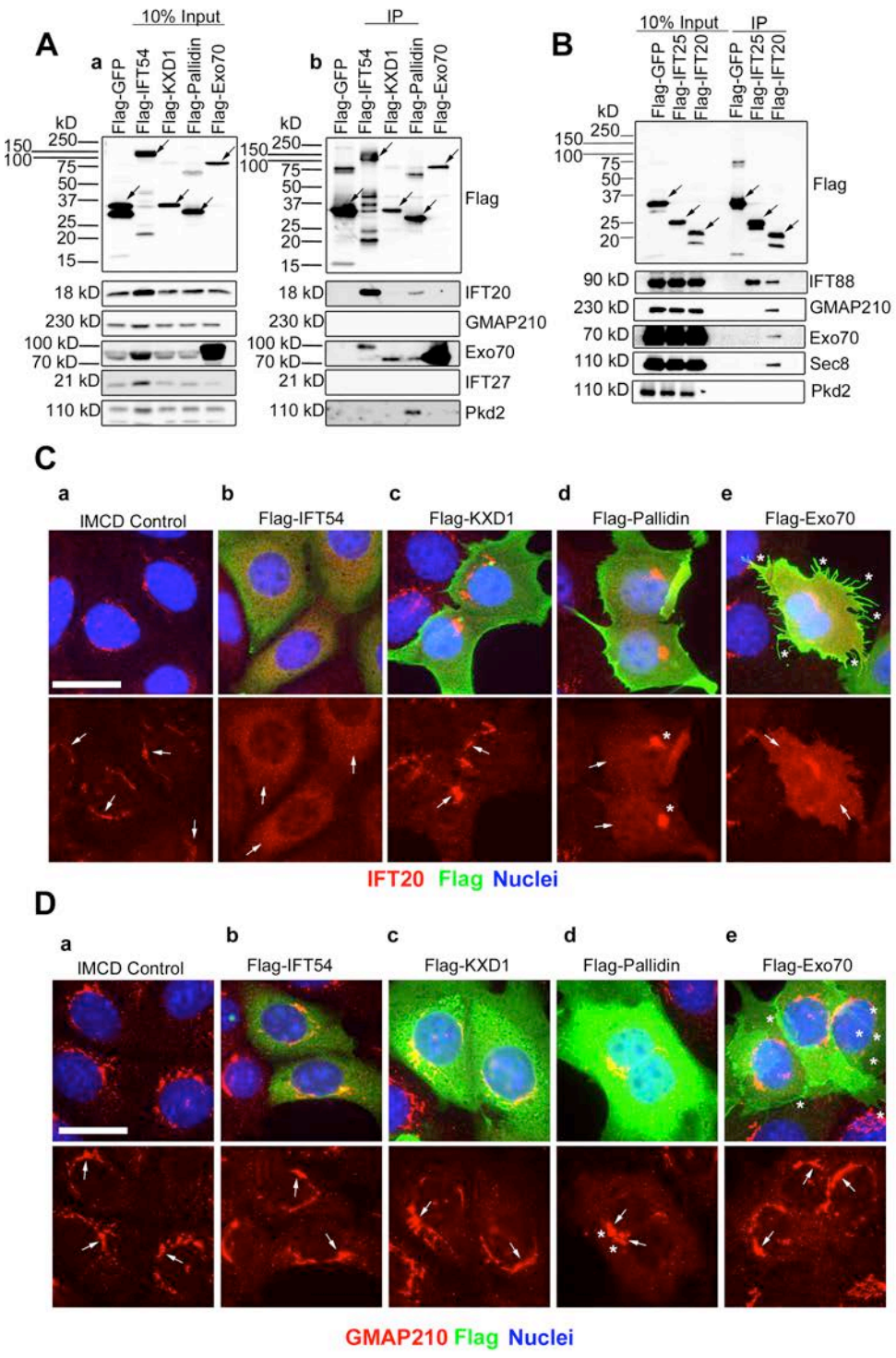

Figure II-5: IFT20 interacts with the BLOC-1 subunit pallidin and the exocyst subunits Exo70 and Sec8.

Figure II-5. IFT20 interacts with the BLOC-1 subunit pallidin and the exocyst subunits Exo70 and Sec8.

(**A**) Flag-GFP (negative IFT20 binding control), Flag-IFT54 (positive IFT20 binding control), Flag-KXD1, Flag-Pallidin, and Flag-Exo70 were expressed in mouse IMCD3 cells. The cells were lysed, immunoprecipitated with Flag antibody and analyzed by immunoblotting. (**Aa**) The left group is the starting material before immunoprecipitation (10% input) and (**Ab**) the right group is the precipitated material (IP). Flag-tagged proteins are marked with arrows on the Flag Western blot. Antibodies used for the Western blots are listed on the right side. (**B**) Flag-GFP (negative binding control), Flag-IFT25 (positive binding control for IFT complex B protein IFT88) and Flag-IFT20, were expressed in mouse IMCD3 cells. The cells were lysed, immunoprecipitated with Flag antibody and analyzed by immunoblotting. The left group is the starting material before immunoprecipitation (10% input) and the right group is the precipitated material (IP). Proteins are marked with arrows. Antibodies used for the Western blots are listed on the right side. (**C**) Selected images of IMCD3 cells expressing the Flag-fusion proteins that are listed horizontally at the top of the figure. Flag-fusion proteins were detected with Flag antibody staining (green), endogenous IFT20 antibody staining (red), and nuclei detected with DAPI (blue). (**Ca**) IFT20 is localized at the Golgi membranes in IMCD3 control cells (arrows). (**Cb**) Increased pixel intensity of IFT20 in the cytoplasm (arrows) and complete loss of IFT20 from the perinuclear Golgi pool in Flag-IFT54 expressing cells. (**Cc**) Flag-KXD1 expressing cells show IFT20 localization at the Golgi membranes (arrows)

and no IFT20 displacement into the cytoplasm. (**Cd**) Compacted Golgi membranes (asterisks) and increased pixel intensity of IFT20 in the cytoplasm (arrows) and partial displacement from the Golgi membranes in Flag-Pallidin expressing cells. (**Ce**) Up-regulated filopodia (asterisks) formation and increased IFT20 pixel intensity (arrows), with partial IFT20 displacement from Golgi membranes in cells expressing Flag-Exo70. Scale bar is 10 μm. (**D**) Selected images of IMCD3 cells expressing the Flag-fusion proteins that are listed horizontally at the top of the figure. Flag-fusion proteins were detected with Flag antibody staining (green), endogenous GMAP210 antibody staining (red), and nuclei detected with DAPI (blue). (**Da**) GMAP210 is localized at the Golgi membranes in IMCD3 control cells, (**Db**) Flag-IFT54 expressing cells, and (**Dc**) Flag-KXD1 expressing cells (arrows). (**Dd**) Compacted Golgi membranes (asterisks) and GMAP210 is localized at the Golgi membranes (arrows) in Flag-Pallidin expressing cells. (**De**) Up-regulated filopodia (asterisks) formation and GMAP210 is localized at the Golgi membranes (arrows) in cells expressing Flag-Exo70. Scale bar is 10 μm.

Because no interaction was observed between Flag-Exo70 and endogenous IFT20, we tested to see if Flag-IFT20 could precipitate endogenous Exo70 or Sec8 exocyst subunits (Fig. II-5, B). Flag-GFP and Flag-IFT25 were negative controls and neither interacted with either of the exocyst components. As positive controls, Flag-IFT20, and Flag-IFT25 interacted as expected with IFT88 and Flag-IFT20 with GMAP210 (Fig. II-5, B) (Follit et al., 2008; Follit et al., 2009; Keady et al., 2011). Importantly, Flag-IFT20 also brought down endogenous Exo70 and Sec8 (Fig. II-5, B). The reason for the discrepancy between the two immunoprecipitations is unknown but not uncommon in these types of studies. However, our finding of an interaction between IFT20 and both Exo70 and Sec8 is consistent with prior work showing that the Sec10 subunit of the exocyst could co-precipitate IFT20 and IFT88 (Fogelgren et al., 2011).

Previously we showed that overexpressing the IFT20-binding proteins IFT54 or GMAP210 displaces IFT20 from the Golgi membranes. Importantly, overexpressing other IFT proteins that do not directly bind IFT20 did not have any effect on the distribution of IFT20 in cells (Follit et al., 2009). As a further test for evidence of interaction with IFT20, we overexpressed Flag-KXD1, Flag-Pallidin, Flag-Exo70, and, as a positive control, Flag-IFT54 (Fig. II-5, C). Flag-IFT54 overexpression completely displaced IFT20 from the Golgi stacks (Fig. II-5, Cb). High expression of Flag-KXD1 did not displace IFT20 from the Golgi (Fig. II-5, Cc), consistent with a failure to interact in the immunoprecipitation assay. Flag-Pallidin overexpression resulted in partial displacement of IFT20 into the

cytoplasm and for unknown reasons caused the Golgi apparatus to compact (Fig. II-5, Cd). Flag-Exo70 overexpression also caused displacement of IFT20 from the Golgi and induced filopodia formation, similar to what has been described (Zuo et al., 2006) (Fig. II-5, Ce and De). To ensure that this result was not due to disruption of the Golgi complex by overexpression of our test proteins, we stained with the Golgi marker GMAP210. GMAP210 was not displaced by overexpression of any of the proteins, and Golgi structure was normal except for the compaction observed when Flag-Pallidin was expressed (Fig. II-5, D). Together the immunoprecipitation and displacement results provide strong evidence that IFT20 interacts with the BLOC-1 subunit pallidin and the exocyst subunit Exo70.

The localization of pallidin at the basal body is partially dependent on IFT20.

Because IFT20 binds Exo70 and pallidin, we determined whether their cellular localization is dependent on IFT20. To do this, wild type and *Ift20*$^{-/-}$ mouse embryonic kidney (MEK) cells (Jonassen et al., 2008) were transfected with Flag-Pallidin or stained for endogenous Exo70 (Fig. II-6). In wild type cells, Flag-Pallidin partially localizes at the basal body (Fig. II-6, Aa). This is consistent with prior work showing other BLOC-1 subunits localizing to the centrosome (Wang et al., 2004b). Interestingly, there is a significant decrease in the amount of basal

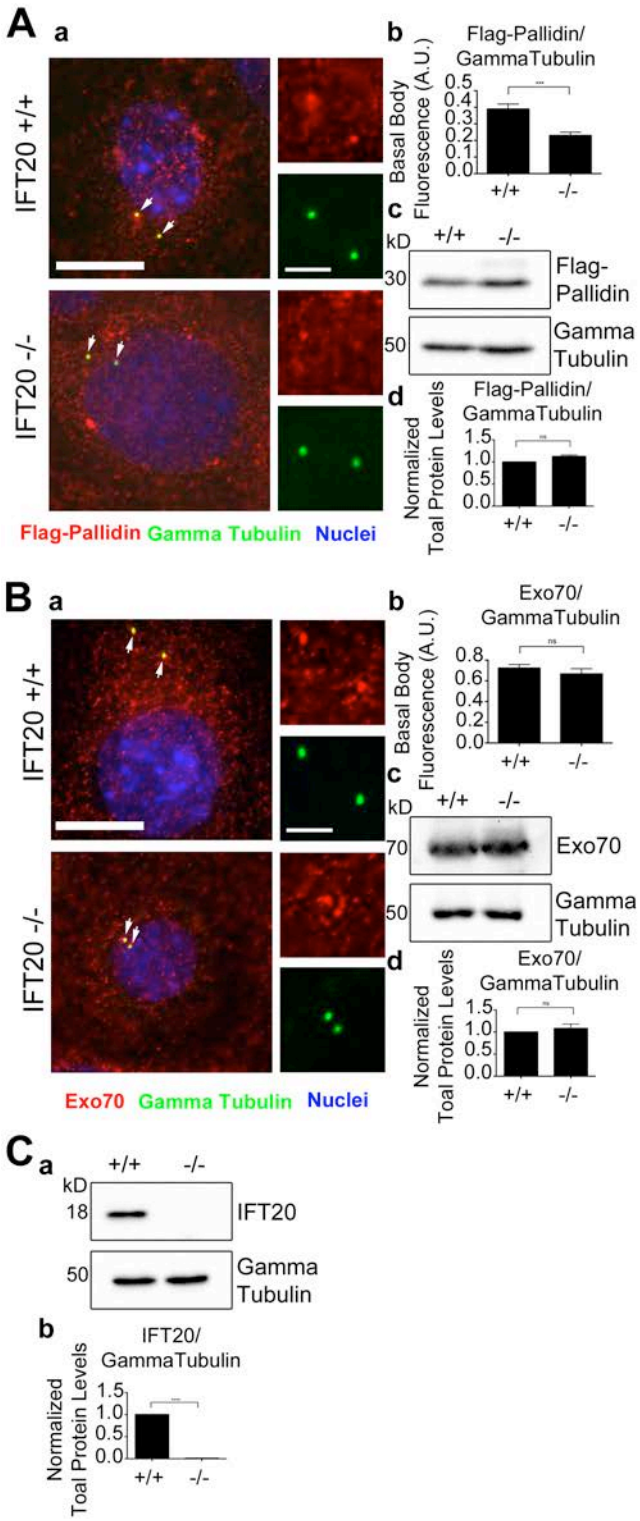

Figure II-6: Localization of pallidin at the basal body is dependent on IFT20.

Figure II-6. Localization of pallidin at the basal body is dependent on IFT20. (**A**) Wild type and *Ift20*$^{-/-}$ MEK cells expressing Flag-Pallidin. (**Aa**) Flag antibody staining (red), gamma tubulin antibody staining (green), and nuclei detected with DAPI (blue). Flag-pallidin localizes at the basal body (arrows). (**Ab**) Mean steady-state levels of Flag-Pallidin at the basal body are decreased in the *Ift20* null cells. (**Ac**) Selected immunoblot images of total Flag-Pallidin and gamma tubulin loading control protein levels. (**Ad**) No difference in the mean total protein levels of Flag-Pallidin in the *Ift20*$^{-/-}$ MEK cells compared to the control. (**B**) Endogenous Exo70 levels at the basal body in wild type and *Ift20*$^{-/-}$ MEK cells. (**Ba**) MEK cells stained for endogenous Exo70 (red), gamma tubulin (green), and nuclei detected with DAPI (blue). Endogenous Exo70 localizes at the basal body (arrows). (**Bb**) No difference in the mean steady-state levels of Exo70 at the basal body in the *Ift20*$^{-/-}$ cells compared to the control. (**Bc**) Selected immunoblot images of total endogenous Exo70 and gamma tubulin loading control protein levels. (**Bd**) No difference in the mean total protein levels of Exo70 in the *Ift20*$^{-/-}$ cells compared to the control. (**C**) Total protein levels of endogenous IFT20 in wild type and *Ift20*$^{-/-}$ MEK cells. (**Ca**) Selected immunoblot images of total endogenous IFT20 and gamma tubulin loading control. (**Cb**) Mean immunoblot pixel intensity quantification showing no IFT20 protein present in the *Ift20*$^{-/-}$ MEK cells. n = 50 basal bodies per experimental group. Error bars are standard error of the mean. The data was analyzed with unpaired student t-test. *** $p < 0.001$, **** $p < 0.0001$

and ns = non-significant. Scale bars are 10 μm. Insets are 190% enlargements of the centrosome regions.

body-localized Flag-Pallidin in the *Ift20*$^{-/-}$ MEKs, while there is no difference in the total Flag-Pallidin levels in the cell (Fig. II-6, A). Endogenous Exo70 partially localizes at the basal body, but there was no difference between control and *Ift20*$^{-/-}$ cells (Fig. II-6, B).

There does not appear to be any effect on IFT20 localization when either pallidin or Exo70 is knocked down (Fig. II-7), indicating that IFT20 localization is not dependent on either protein.

The exocyst complex is involved in the ciliary trafficking of fibrocystin and polycystin-2.

Previous work had demonstrated a role for exocyst subunit Sec10 in ciliary assembly (Zuo et al., 2009). Because we had found that IFT20 was able to precipitate the exocyst subunits Exo70 and Sec8, we tested the exocyst's role in trafficking of our model ciliary proteins by knocking down these subunits (Figs. II-4, G – L; and II-8; and II-9). Knockdown of Exo70 to about ~20% of normal had modest effects on ciliary length (Fig. II-8, Ac, Bc, Cc) while a knockdown of Sec8 to ~20% of controls decreased ciliary length to ~40% of normal (Fig. II-9, Ac, Bc, Cc). Knockdown of these exocyst subunits reduced the steady-state levels of ciliary fibrocystin and polycystin-2 (Figs. II-8, Ad, Bd; and II-9, Ad, Bd) and reduced the rate of delivery of these proteins to cilia (Figs. II-4, G, H, J, K; and II-8, Ae, Be; and II-9, Ae, Be).

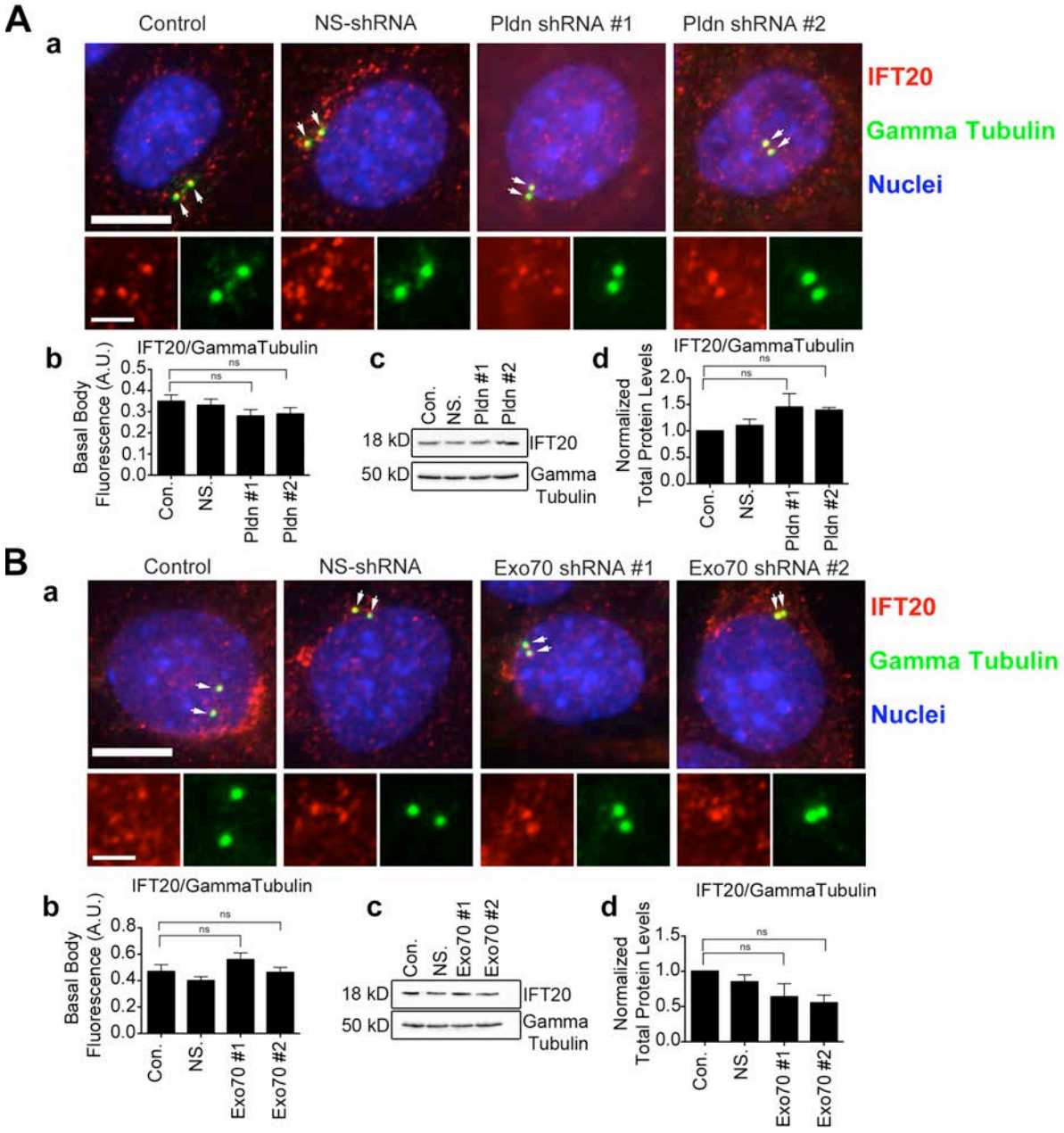

Figure II-7: IFT20 localization at the basal body is not affected by the knockdown of either pallidin or Exo70.

Figure II-7. IFT20 localization at the basal body is not affected by the knockdown of either pallidin or Exo70.

(**A**) Endogenous IFT20 levels at the basal body in CD8-FibrocystinCTS-SNAP Flp-In IMCD3 cells expressing either non-silencing or pallidin lenti-shRNAs. (**Aa**) Selected images showing IFT20 localization at the basal body (arrows). IFT20 antibody staining (red), gamma tubulin antibody staining (green), and nuclei are detected with DAPI (blue). Scale bar is 10 μm. Insets are 185% enlargements of the centrosome regions. (**Ab**) No difference in the mean steady-state levels of IFT20 at the basal body in the pallidin knockdown cells compared to the control. (**Ac**) Selected immunoblot images of total endogenous IFT20 and gamma tubulin loading control protein levels. (**Ad**) No difference in the mean total protein levels of IFT20 in the pallidin knockdown cells compared to the control. (**B**) Endogenous IFT20 levels at the basal body in CD8-FibrocystinCTS-SNAP Flp-In IMCD3 cells expressing either non-silencing or Exo70 lenti-shRNAs. (**Ba**) Selected images showing IFT20 localization at the basal body (arrows). IFT20 antibody staining (red), gamma tubulin antibody staining (green), and nuclei are detected with DAPI (blue). Scale bar is 10 μm. Insets are 185% enlargements of the centrosome regions. (**Bb**) No difference in the mean steady-state levels of IFT20 at the basal body in the Exo70 knockdown cells compared to the control. (**Bc**) Selected immunoblot images of total endogenous IFT20 and gamma tubulin loading control protein levels. (**Bd**) No difference in the mean total protein levels of IFT20 in the Exo70 knockdown cells compared to the control. n = 50 basal bodies per experimental group. Error bars are standard error of the mean. The

data was analyzed with One-way ANOVA and Bonferroni multiple comparisons test. * $p < 0.05$, ** $p < 0.01$, *** $p < 0.001$, **** $p < 0.0001$ and ns = non-significant.

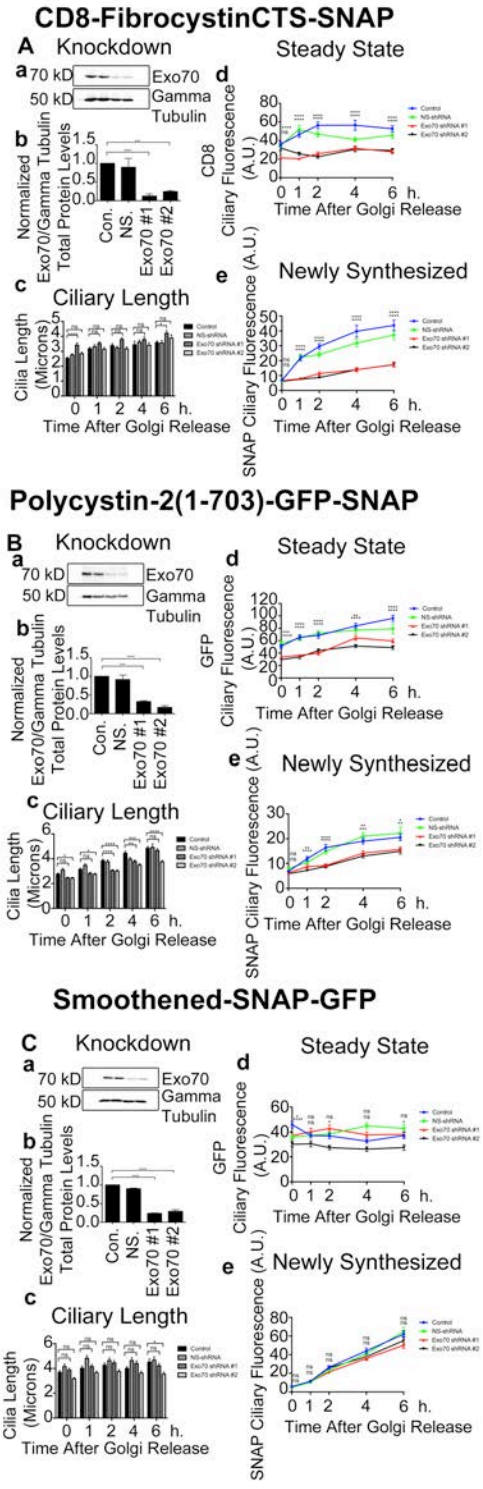

Figure II-8: Exo70 knockdown affects fibrocystin, polycystin-2 but not smoothened trafficking to the primary cilium.

Figure II-8. Exo70 knockdown affects fibrocystin, polycystin-2 but not smoothened trafficking to the primary cilium.

(**A**) Quantification of CD8-FibrocystinCTS-SNAP, (**B**) Polycstin-2(1-703)-GFP-SNAP, and (**C**) Smoothened-SNAP-GFP trafficking from the Golgi apparatus to the primary cilium during lenti-shRNA knockdown of either Exo70 or Sec8. (**Aa, Ba, Ca**) Selected immunoblot images of Exo70 knockdown and gamma tubulin loading control. (**Ab, Bb, Cb**) Quantification of knockdown. Mean protein levels plotted from three independent experiments for each condition (Control, NS-shRNA, shRNA#1, and shRNA#2) and normalized to their corresponding gamma tubulin loading control. shRNA mediated knockdown of Exo70 results in 80-90% reduction of total protein abundance. (**Ac, Bc, Cc**) Mean cilia length, (**Ad, Bd, Cd**) mean CD8 or GFP ciliary fluorescence, and (**Ae, Be, Ce**) mean SNAP ciliary fluorescence plotted from three independent experiments in which 30 cilia were quantified for each condition (Control, NS-shRNA, shRNA#1, and shRNA#2) at each time point (n = 90 total cilia per time point). CD8 or GFP and SNAP pixel intensity measurements were taken at individual time points starting at the time of temperature shift from 19°C to 37°C (0 Hours). The data was analyzed with One-way ANOVA and Bonferroni multiple comparisons test. The control condition was compared to shRNA#1 and shRNA#2 conditions to determine statistical significance. * $p < 0.05$, ** $p < 0.01$, *** $p < 0.001$, **** $p < 0.0001$ and ns = non-significant. Error bars represent standard error of the mean.

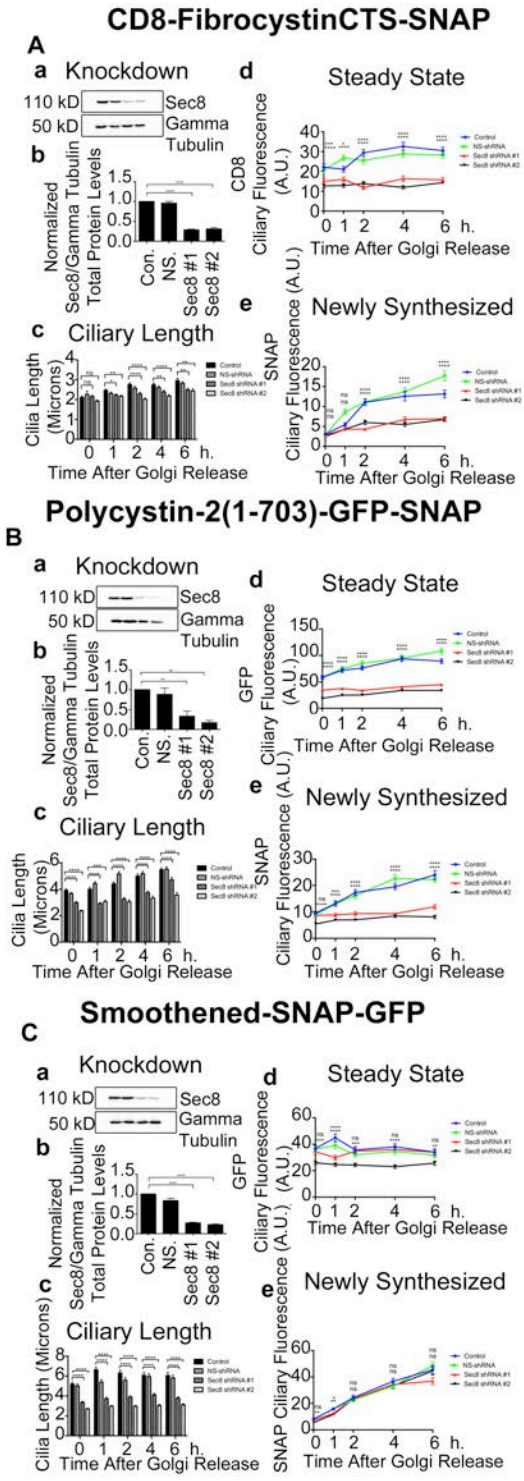

Figure II-9: Sec8 knockdown affects fibrocystin, polycystin-2 but not smoothened trafficking to the primary cilium.

Figure II-9. Sec8 knockdown affects fibrocystin, polycystin-2 but not smoothened trafficking to the primary cilium.

(**A**) Quantification of CD8-FibrocystinCTS-SNAP, (**B**) Polycstin-2(1-703)-GFP-SNAP, and (**C**) Smoothened-SNAP-GFP trafficking from the Golgi apparatus to the primary cilium during lenti-shRNA knockdown of Sec8. (**Aa, Ba, Ca**) Selected immunoblot images of Sec8 knockdown and gamma tubulin loading control. (**Ab, Bb, Cb**) Quantification of knockdown. Mean protein levels plotted from three independent experiments for each condition (Control, NS-shRNA, shRNA#1, and shRNA#2) and normalized to their corresponding gamma tubulin loading control. shRNA mediated knockdown of Sec8 results in 80-90% reduction of total protein abundance. (**Ac, Bc, Cc**) Mean cilia length, (**Ad, Bd, Cd**) mean CD8 or GFP ciliary fluorescence, and (**Ae, Be, Ce**) mean SNAP ciliary fluorescence plotted from three independent experiments in which 30 cilia were quantified for each condition (Control, NS-shRNA, shRNA#1, and shRNA#2) at each time point (n = 90 total cilia per time point). CD8 or GFP and SNAP pixel intensity measurements were taken at individual time points starting at the time of temperature shift from 19°C to 37°C (0 Hours). The data was analyzed with One-way ANOVA and Bonferroni multiple comparisons test. The control condition was compared to shRNA#1 and shRNA#2 conditions to determine statistical significance. * $p < 0.05$, ** $p < 0.01$, *** $p < 0.001$, **** $p < 0.0001$ and ns = non-significant. Error bars represent standard error of the mean.

The reduction of Exo70 or Sec8 did not affect the rate of delivery of newly synthesized smoothened to the cilium (Figs. II-4, I and L; and II-8, Ce; and II-9, Ce) and the steady-state level of ciliary smoothened was only modestly or not affected (Figs. II-8, Cd; and II-9, Cd). This further strengthens the idea that distinct membrane proteins are using different trafficking pathways and specific molecular machineries for ciliary delivery.

BLOC-1 is important for the trafficking of polycystin-2 to primary cilia.

BLOC-1 has not been previously implicated in ciliary trafficking but our finding that pallidin bound IFT20 and polycystin-2 suggests involvement. To test this idea, we assayed ciliary transport after knocking down pallidin and another BLOC-1 subunit dysbindin. Knockdown of pallidin to ~10-15% of normal had no effect on ciliary length (Fig. II-10, Ac, Bc, Cc). Knockdown of dysbindin to ~10% of normal affects ciliary assembly (Fig. II-11, Ac, Bc, Cc). Knockdown of either dysbindin or pallidin had no effect on steady-state levels or rates of delivery of fibrocystin and smoothened to cilia (Figs. II-4, M, O, P, R; and II-10, Ad, Cd, Ae, Ce; and II-11, Ad, Cd, Ae, Ce). In contrast, knockdown of either dysbindin or pallidin reduced the rates of delivery of polycystin-2 to cilia and dysbindin knockdown decreased steady-state levels of ciliary polycystin-2 (Figs. II-4, N and Q; and II-10, Be; and II-11, Bd and Be). The amount of reduction in steady-state ciliary polycystin-2 varied between the two dysbindin shRNAs, but correlated with the more effective knockdown causing a larger decrease in ciliary polycystin-2

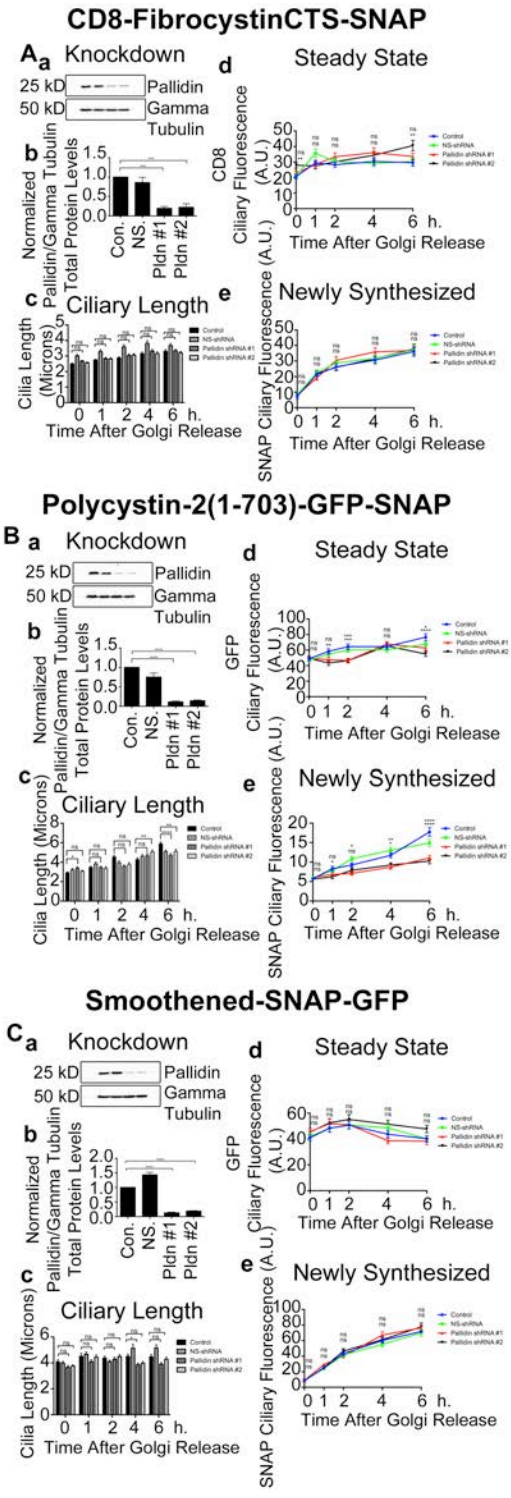

Figure II-10: Pallidin knockdown affects polycystin-2 but not fibrocystin or smoothened trafficking to the primary cilium.

Figure II-10. Pallidin knockdown affects polycystin-2 but not fibrocystin or smoothened trafficking to the primary cilium.

(**A**) Quantification of CD8-FibrocystinCTS-SNAP, (**B**) Polycstin-2(1-703)-GFP-SNAP, and **(C**) Smoothened-SNAP-GFP trafficking from the Golgi apparatus to the primary cilium during lenti-shRNA knockdown of pallidin. (**Aa, Ba, Ca**) Selected immunoblot images of pallidin knockdown and gamma tubulin loading control. (**Ab, Bb, Cb**) Quantification of knockdown. Mean protein levels plotted from three independent experiments for each condition (Control, NS-shRNA, shRNA#1, and shRNA#2) and normalized to their corresponding gamma tubulin loading control. shRNA mediated knockdown of pallidin results in >90% reduction of total protein abundance. (**Ac, Bc, Cc**) Mean cilia length, (**Ad, Bd, Cd**) mean CD8 or GFP ciliary fluorescence, and (**Ae, Be, Ce**) mean SNAP ciliary fluorescence plotted from three independent experiments in which 30 cilia were quantified for each condition (Control, NS-shRNA, shRNA#1, and shRNA#2) at each time point (n = 90 total cilia per time point). CD8 or GFP and SNAP pixel intensity measurements were taken at individual time points starting at the time of temperature shift from 19°C to 37°C (0 Hours). The data was analyzed with One-way ANOVA and Bonferroni multiple comparisons test. The control condition was compared to shRNA#1 and shRNA#2 conditions to determine statistical significance. * $p < 0.05$, ** $p < 0.01$, *** $p < 0.001$, **** $p < 0.0001$ and ns = non-significant. Error bars represent standard error of the mean.

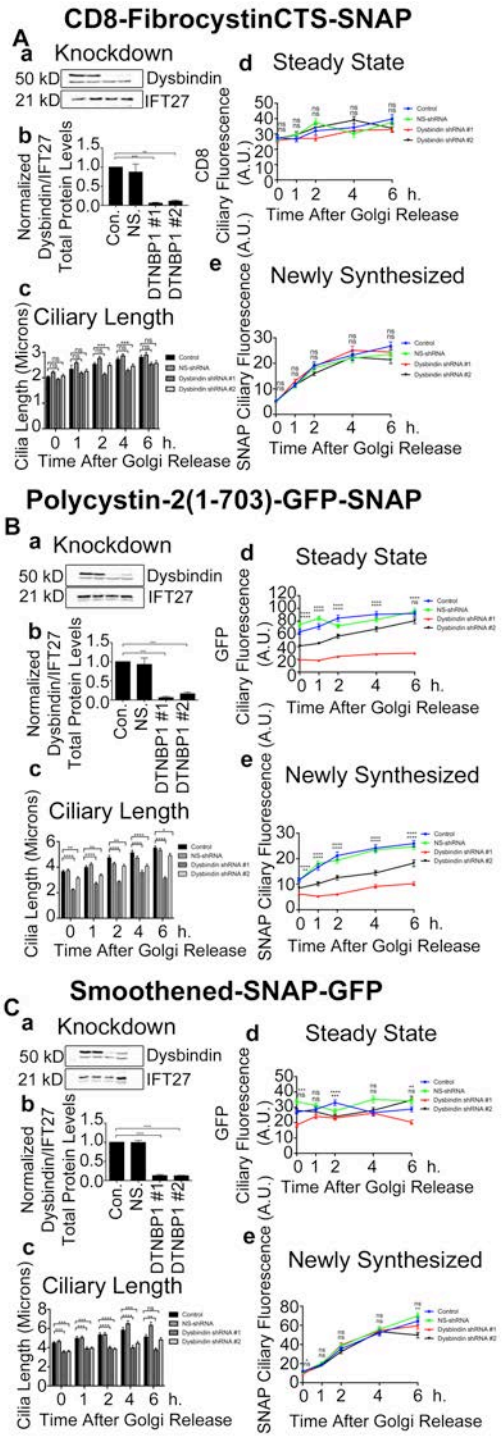

Figure II-11: Dysbindin knockdown affects polycystin-2 but not fibrocystin or smoothened trafficking to the primary cilium.

Figure II-11. Dysbindin knockdown affects polycystin-2 but not fibrocystin or smoothened trafficking to the primary cilium.

(**A**) Quantification of CD8-FibrocystinCTS-SNAP, (**B**) Polycstin-2(1-703)-GFP-SNAP, and **(C**) Smoothened-SNAP-GFP trafficking from the Golgi apparatus to the primary cilium during lenti-shRNA knockdown of dysbindin. (**Aa, Ba, Ca**) Selected immunoblot images of dysbindin knockdown and IFT27 loading control. (**Ab, Bb, Cb**) Quantification of knockdown. Mean protein levels plotted from three independent experiments for each condition (Control, NS-shRNA, shRNA#1, and shRNA#2) and normalized to their corresponding IFT27 loading control. shRNA mediated knockdown of dysbindin results in >90% reduction of total protein abundance. (**Ac, Bc, Cc**) Mean cilia length, (**Ad, Bd, Cd**) mean CD8 or GFP ciliary fluorescence, and (**Ae, Be, Ce**) mean SNAP ciliary fluorescence plotted from three independent experiments in which 30 cilia were quantified for each condition (Control, NS-shRNA, shRNA#1, and shRNA#2) at each time point (n = 90 total cilia per time point). CD8 or GFP and SNAP pixel intensity measurements were taken at individual time points starting at the time of temperature shift from 19°C to 37°C (0 Hours). The data was analyzed with One-way ANOVA and Bonferroni multiple comparisons test. The control condition was compared to shRNA#1 and shRNA#2 conditions to determine statistical significance. * $p < 0.05$, ** $p < 0.01$, *** $p < 0.001$, **** $p < 0.0001$ and ns = non-significant. Error bars represent standard error of the mean.

levels (Figs. II-4 Q; and II-11, Ba, Bb, Bd, Be). Our protein interaction data and pulse-chase trafficking data gives strong evidence that BLOC-1 is specifically involved in polycystin-2 delivery to cilia. This emphasizes that polycystin-2 is taking a specific pathway to the cilium that is dependent on BLOC-1 machinery.

Perturbation of the exocyst or BLOC-1 complexes decreases endogenous polycystin-2 levels at the primary cilium.

To further verify our finding that the exocyst complex and BLOC-1 are involved in trafficking polycystin-2 to the primary cilium, we performed knockdowns in MEK cells and measured endogenous polycystin-2 ciliary levels. MEK cells were chosen because they have more polycystin-2 in their cilia than IMCD3 cells, and because they are mouse cells, the shRNAs developed previously are effective in them.

Similar to what we observed in IMCD3 cells, Exo70 knockdown had little to no effect on ciliary assembly in MEK cells, but Sec8 knockdown decreased ciliary length (Fig. II-12, Bd and Cd). Importantly, knockdown of either Exo70 or Sec8 resulted in decreased steady-state ciliary levels of polycystin-2 (Fig. II-12, Ba, Bb, Bc) confirming our results with an exogenous chimeric protein. Additionally, the knockdown of Sec8 but not Exo70 reduced the ciliary levels of Arl13b at the cilium (Fig. II-12 Ca, Cb, Cc). Arl13b is a peripheral membrane protein anchored to the cilium by palmitoylated cysteines (Cevik et al., 2010; Li et al., 2010; Sun et al., 2004). It is not clear why the two subunits have different

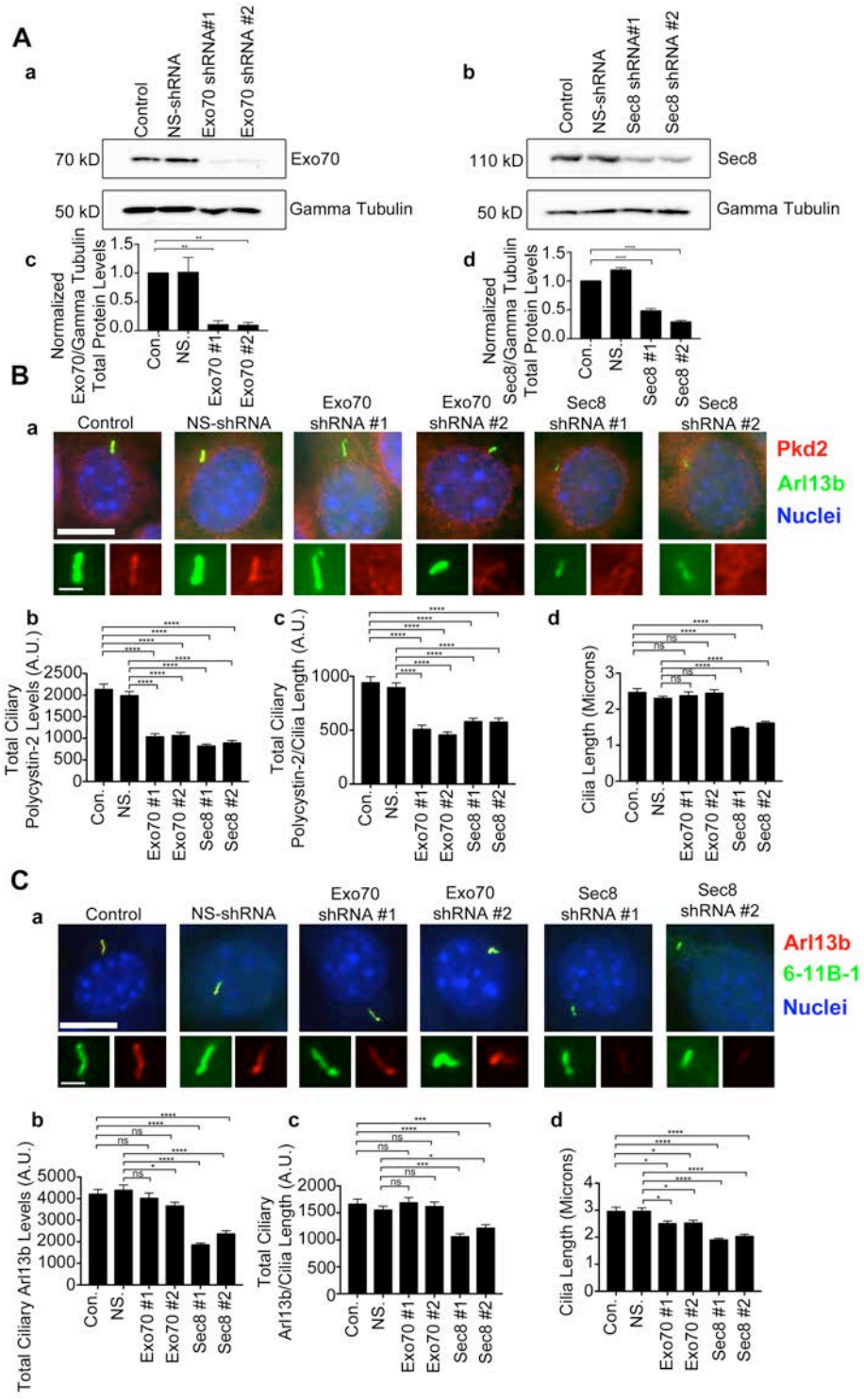

Figure II-12: Exo70 and Sec8 knockdown decreases endogenous ciliary polycystin-2 levels.

Figure II-12. Exo70 and Sec8 knockdown decreases endogenous ciliary polycystin-2 levels.

(**A**) Immunoblot and quantification of total protein levels of MEK cells expressing either Exo70 or Sec8 lenti-shRNAs. (**Aa**) Selected immunoblot images showing Exo70 knockdown and (**Ab**) Sec8 knockdown with gamma tubulin loading control. (**Ac**) Quantification of Exo70 mean protein levels and (**Ad**) Sec8 mean protein levels for each condition (Control, NS-shRNA, shRNA#1, and shRNA#2) that are normalized to their corresponding gamma tubulin loading control. shRNA mediated knockdown of either Exo70 or Sec8 results in >80% reduction of total protein abundance. (**B**) Immunostaining and quantification of ciliary polycystin-2 and cilia length in MEK cells expressing either Exo70 or Sec8 lenti-shRNA. (**Ba**) Selected images of polycystin-2 (Pkd2) antibody staining (red), Arl13b staining (green), and nuclei are detected with DAPI (blue) Scale bar is 10 μm. Insets are 240% enlargements of the cilia. (**Bb**) Mean total ciliary polycystin-2 (**Bc**) and ciliary polycystin-2 per micron is reduced in cells expressing Exo70 or Sec8 lenti-shRNAs. (Bd) Mean cilia length is reduced in cells expressing Sec8 shRNAs. (**C**) Immunostaining and quantification of ciliary Arl13b and cilia length in MEK cells expressing either Exo70 or Sec8 lenti-shRNA. (**Ca**) Selected images of Arl13b antibody staining (red), acetylated tubulin (6-11B-1) antibody staining (green), and nuclei are detected with DAPI (blue) Scale bar is 10 μm. Insets are 240% enlargements of the cilia. (**Cb**) Mean steady-state ciliary Arl13b and (**Cc**) ciliary Arl13b per micron is reduced in cells expressing Sec8 lenti-shRNAs. (**Cd**) Mean ciliary assembly is reduced in cells expressing Sec8 shRNAs. n = 107 cilia per

experimental group. Error bars are standard error of the mean. Data was analyzed with One-way ANOVA and Bonferroni multiple comparisons test. * $p < 0.05$, ** $p < 0.01$, *** $p < 0.001$, **** $p < 0.0001$ and ns = non-significant.

effects on ciliary Arl13b levels, but Sec8 is a core exocyst subunit, while Exo70 is a peripheral membrane-docking subunit (He et al., 2007; TerBush et al., 1996; TerBush and Novick, 1995; Wu et al., 2010). It is possible that core subunits are more important for delivery of Arl13b or that higher levels of Sec8 are needed than Exo70 and the Exo70 levels were not reduced below the critical level.

To confirm the results obtained with the exogenous chimeric protein, we examined the involvement of BLOC-1 in trafficking of endogenous polycystin-2 to primary cilia. Again, MEK cells were used because of their high levels of ciliary polycystin-2. In these cells, knockdown reduced pallidin and dysbindin to ~10-15% of normal (Fig. II-13, Ac and Ad). The dysbindin knockdown caused a decrease in cilia length and reduced the steady-state level of ciliary polycystin-2 (Fig. II-13 B). Similar to what we saw in IMCD3 cells, the pallidin knockdown did not affect cilia length or the levels of ciliary polycystin-2 (Fig. II-13 B). This continues to strengthen the evidence that the exocyst complex and BLOC-1 are involved in the trafficking of polycystin-2 to cilia.

Dtnbp1$^{sdy/sdy}$ and *Pldn*$^{pa/pa}$ mice possess a cystic kidney phenotype.

The sandy (*Dtnbp1*$^{sdy/sdy}$) and pallid mice (*Pldn*$^{pa/pa}$) are loss-of-function models of dysbindin and pallidin (Huang et al., 1999; Li et al., 2003). Given that our data suggest BLOC-1 is involved in the trafficking of polycystin-2 to primary cilia, we hypothesized that the *Dtnbp1*$^{sdy/sdy}$ and *Pldn*$^{pa/pa}$ mice will have cystic kidneys. Hematoxylin and eosin staining of 5 week old *Dtnbp1*$^{sdy/sdy}$ and 8 week old

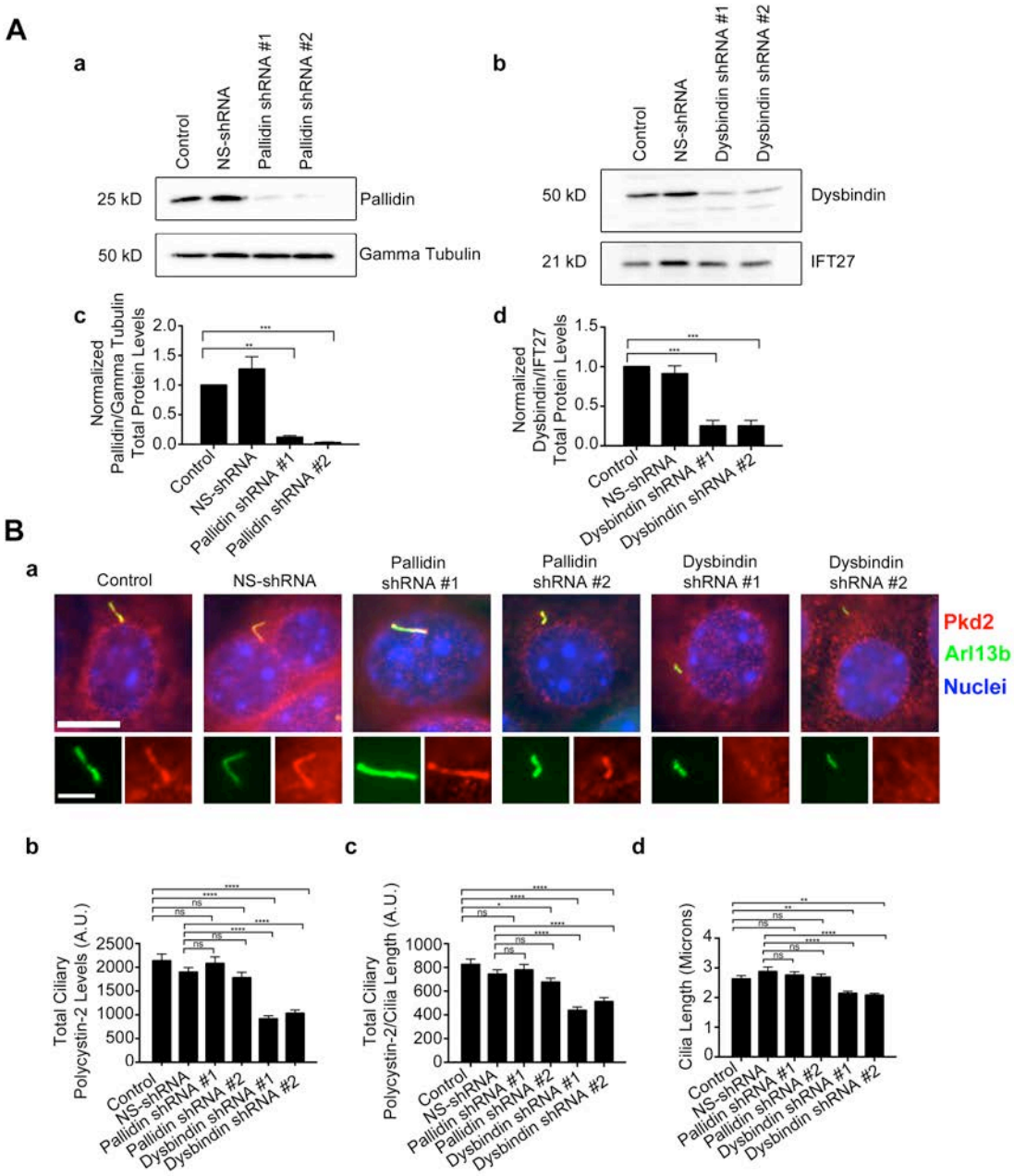

Figure II-13: Dysbindin knockdown decreases endogenous ciliary polycystin-2 levels.

Figure II-13. Dysbindin knockdown decreases endogenous ciliary polycystin-2 levels.

(**A**) Immunoblot and quantification of total protein levels of MEK cells expressing either pallidin or dysbindin lenti-shRNAs. (**Aa**) Selected immunoblot images showing pallidin knockdown and (**Ab**) dysbindin knockdown with either gamma tubulin or IFT27 loading control. (**Ac**) Mean quantification of pallidin and (**Ad**) dysbindin knockdown under each condition (Control, NS-shRNA, shRNA#1, and shRNA#2). Intensity was normalized to their corresponding gamma tubulin or IFT27 loading control. shRNA mediated knockdown of either pallidin or dysbindin results in >90% reduction of total protein abundance. (**B**) Immunostaining and quantification of ciliary polycystin-2 and cilia length in MEK cells expressing either pallidin or dysbindin lenti-shRNAs. (**Ba**) Selected images of polycystin-2 (Pkd2) antibody staining (red), Arl13b antibody staining (green), and nuclei are detected with DAPI (blue) Scale bar is 10 μm. Insets are 170% enlargements of the cilia. (**Bb**) Mean steady-state ciliary polycystin-2 is decreased and (**Bc**) mean ciliary polycystin-2 per micron is reduced in cells expressing dysbindin lenti-shRNAs. (**Bd**) Mean cilia length is reduced in cells expressing dysbindin shRNAs. n = 107 cilia per experimental group. Error bars are standard error of the mean. The data was analyzed with One-way ANOVA and Bonferroni multiple comparisons test. * $p < 0.05$, ** $p < 0.01$, *** $p < 0.001$, **** $p < 0.0001$ and ns = non-significant.

Pldn$^{pa/pa}$ kidneys showed no prominent cyst formation, but the collecting ducts in the papilla were slightly distended in both mouse models (Fig. II-14, A, Ba, Bb). Proximal tubule circumference was also slightly increased in the *Dtnbp1*$^{sdy/sdy}$ mice, and both the *Dtnbp1*$^{sdy/sdy}$ and *Pldn*$^{pa/pa}$ mice had a slight increase in the mean number of proximal tubule nuclei per cross section (Fig. II-14, C). Additionally, the *Dtnbp1*$^{sdy/sdy}$ and *Pldn*$^{pa/pa}$ mice had a moderate decrease in ciliary length, and *Dtnbp1*$^{sdy/sdy}$ mice showed a modest decrease in the percentage of cilia per basal body (Fig. II-14, Bc and Bd).

Given that the first cohort of *Dtnbp1*$^{sdy/sdy}$ and *Pldn*$^{pa/pa}$ mice were relatively young, we aged a second cohort for 12 months to see whether they would present a more severe cystic kidney phenotype. These animals suffer from lung fibrosis, and very few animals survive to one year of age (McGarry et al., 2002). However, we were able to collect three *Dtnbp1*$^{sdy/sdy}$ and one *Pldn*$^{pa/pa}$ animals at this age. None of the animals showed prominent cysts, but the collecting ducts were obviously distended (Fig. II-15, A). Quantification showed a significant increase in the *Dtnbp1*$^{sdy/sdy}$ collecting duct diameter measured in the kidney cortex, at the junction between the outer and inner medulla, and in the inner medulla at the tip of the papilla (Fig. II-15, B). The *Pldn*$^{pa/pa}$ also showed increased diameter of collecting ducts, but only one animal was examined. Proximal tubules were also dilated in the two models. In both models, the circumferences were slightly larger, and the number of nuclei per cross section was increased (Fig. II-15, D and E).

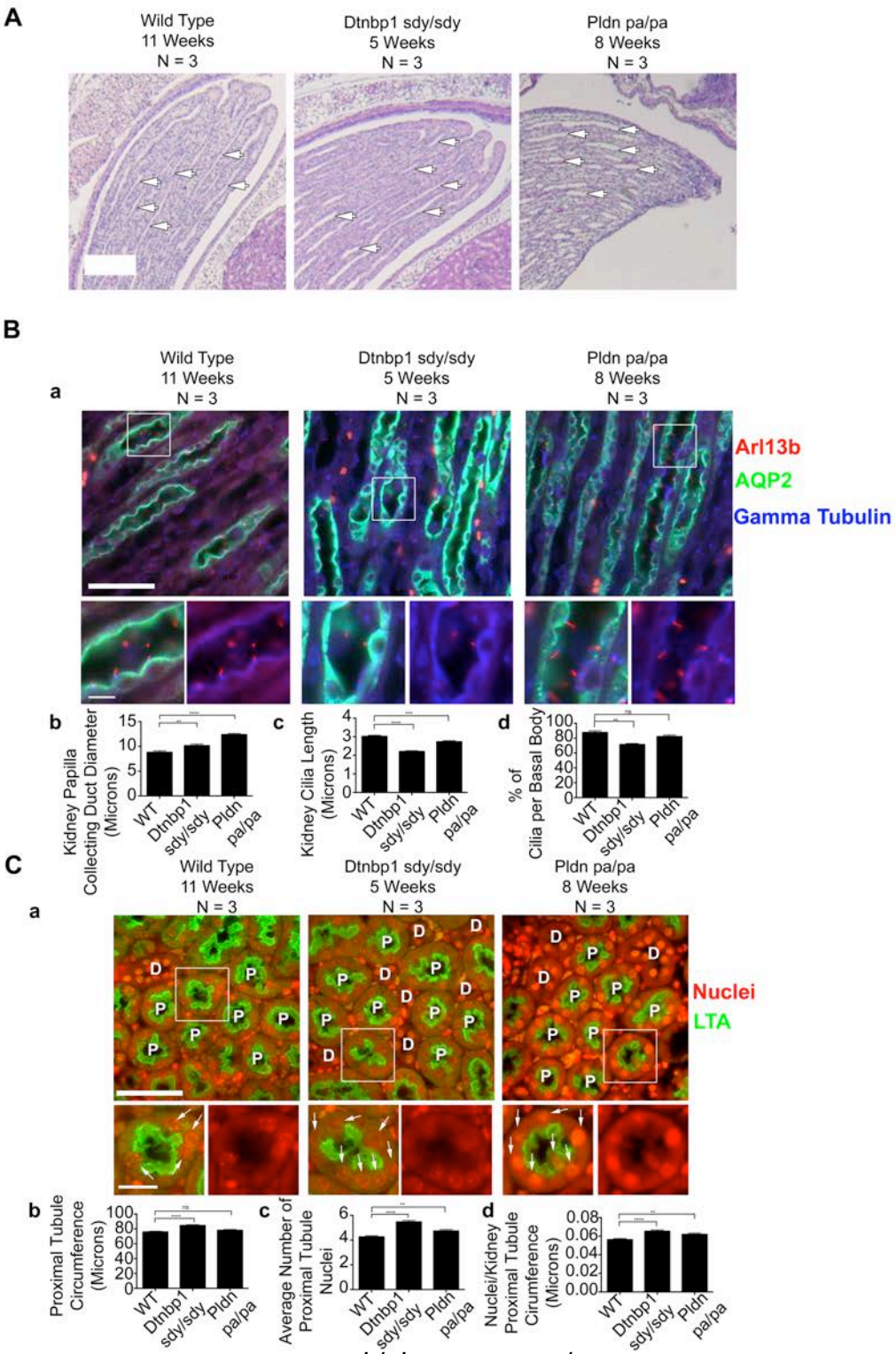

Figure II-14: Young *Dtnbp1*$^{sdy/sdy}$ and *Pldn*$^{pa/pa}$ mice have mildly cystic kidneys.

Figure II-14. Young *Dtnbp1*$^{sdy/sdy}$ and *Pldn*$^{pa/pa}$ mice have mildly cystic kidneys.

(**A**) Hematoxylin and eosin staining of mouse kidney papillae of wild type (11 weeks of age), *Dtnbp1*$^{sdy/sdy}$ (5 weeks of age), and *Pldn*$^{pa/pa}$ (8 weeks of age). Scale bar is 200 μm. (**B**) Immuohistochemistry and diameter quantification of wild type, *Dtnbp1*$^{sdy/sdy}$ and *Pldn*$^{pa/pa}$ kidney collecting ducts. (**Ba**) Selected images of mouse kidney sections stained with cilia marker Arl13b antibody (red), collecting duct marker AQP2 antibody (green), and basal body marker gamma tubulin antibody (blue). Scale bar is 50 μm. Insets are 250% enlargements. (**Bb**) Mean collecting duct diameter is increased in *Dtnbp1*$^{sdy/sdy}$ and *Pldn*$^{pa/pa}$ kidneys (n = 198 collecting ducts per group). (**Bc**) Mean cilia assembly is reduced in the *Dtnbp1*$^{sdy/sdy}$ and *Pldn*$^{pa/pa}$ kidneys (n = 300 cilia per group) and (**Bd**) the percentage of cilia per basal body is reduced *Dtnbp1*$^{sdy/sdy}$ kidneys (n = 300 basal bodies per group). (**C**) Immuohistochemistry, tubule circumference quantification, average number of tubule nuclei, and nuclei per tubule circumference of wild type, *Dtnbp1*$^{sdy/sdy}$ and *Pldn*$^{pa/pa}$ kidney proximal tubules. (**Ca**) Selected images of mouse kidney sections stained with proximal tubule marker LTA (green) and nuclei Dapi (red). Most tubules are proximal and some are marked with “P.” The few distal convoluted tubules are marked with “D.” Arrows indicate proximal tubule nuclei. Scale bar is 50 μm. Insets are 175% enlargements. (**Cb**) Mean proximal tubule circumference is increased in *Dtnbp1*$^{sdy/sdy}$ kidneys, (**Cc**) the average number of proximal tubule nuclei in the *Dtnbp1*$^{sdy/sdy}$ and *Pldn*$^{pa/pa}$ kidneys is increased, and (**Cd**) the nuclei/kidney proximal tubule circumference in

the *Dtnbp1*$^{sdy/sdy}$ and *Pldn*$^{pa/pa}$ kidneys is increased (n = 96 proximal tubules per group). n = 3 mice per experimental group. Error bars are standard error of the mean. The data was analyzed with One-way ANOVA and Bonferroni multiple comparisons test. * $p < 0.05$, ** $p < 0.01$, *** $p < 0.001$, **** $p < 0.0001$ and ns = non-significant.

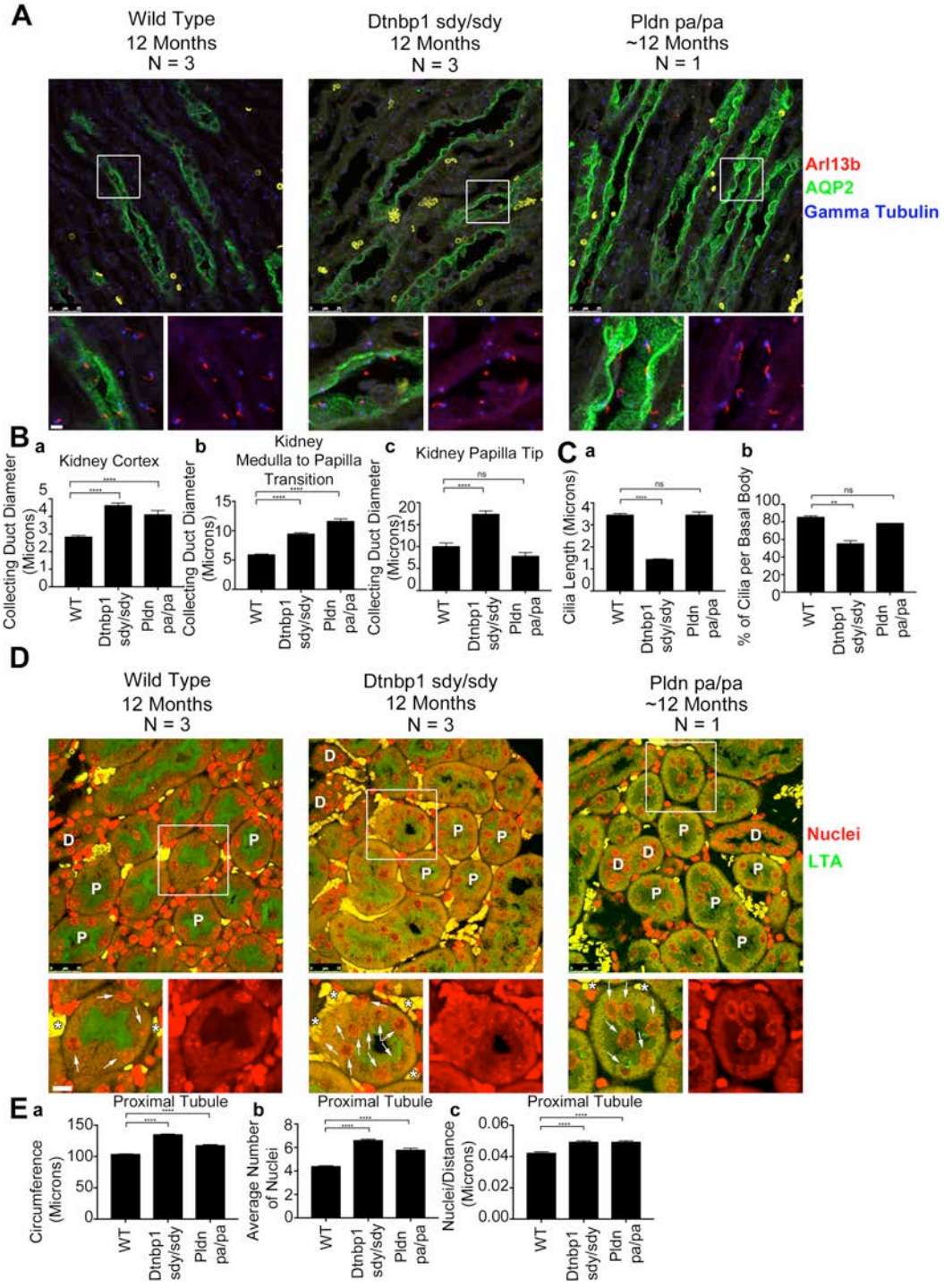

Figure II-15: *Dtnbp1*$^{sdy/sdy}$ and *Pldn*$^{pa/pa}$ mice have mildly cystic kidneys.

Figure II-15. *Dtnbp1*$^{sdy/sdy}$ and *Pldn*$^{pa/pa}$ mice have mildly cystic kidneys. (**A**) Selected confocal images of 12-month old wild type, *Dtnbp1*$^{sdy/sdy}$ and *Pldn*$^{pa/pa}$ mouse kidney sections stained with cilia marker Arl13b antibody (red), collecting duct marker AQP2 antibody (green), and basal body marker gamma tubulin antibody (blue). Scale bars are 25 μm. Insets are 285% enlargements. (**B**) Quantification of mean collecting duct diameters in three regions of the kidney; (**Ba**) cortex (wild type and *Dtnbp1*$^{sdy/sdy}$ n = 183 collecting ducts per group, *Pldn*$^{pa/pa}$ n = 61 collecting ducts), (**Bb**) medulla to papilla transition (wild type and *Dtnbp1*$^{sdy/sdy}$ n = 183 collecting ducts per group, *Pldn*$^{pa/pa}$ n = 61 collecting ducts), (**Bc**) tip of the papilla (wild type and *Dtnbp1*$^{sdy/sdy}$ n = 33 collecting ducts per group, *Pldn*$^{pa/pa}$ n = 11 collecting ducts). There is an increase in collecting duct diameter in the *Dtnbp1*$^{sdy/sdy}$ and *Pldn*$^{pa/pa}$ cortex and medulla to papilla transition. Additionally, the *Dtnbp1*$^{sdy/sdy}$ papilla tip collecting duct diameter is wider. (**C**) Quantification of mean kidney cilia length and the percentage of cilia per basal body. (**Ca**) Wild type and *Dtnbp1*$^{sdy/sdy}$ n = 300 cilia per group, *Pldn*$^{pa/pa}$ n = 100 cilia. Cilia in the *Dtnbp1*$^{sdy/sdy}$ kidneys are shorter compared to control. (**Cb**) Wild type and *Dtnbp1*$^{sdy/sd}$ n = 315 basal bodies per group, *Pldn*$^{pa/pa}$ n = 105 basal bodies. Percent cilia per basal body is reduced in the *Dtnbp1*$^{sdy/sdy}$ kidneys. (**D**) Selected confocal images of 12-month old wild type, *Dtnbp1*$^{sdy/sdy}$ and *Pldn*$^{pa/pa}$ kidney sections stained with proximal tubule marker LTA (green) and nuclei with Dapi (red). Most tubules are proximal and some are marked with “P.” The few distal convoluted tubules are marked with “D.” Arrows label proximal tubule

nuclei and asterisks indicate red blood cells. Scale bars are 25 μm. Insets are 172% enlargements. (**E**) Quantification of mean kidney proximal tubule nuclei circumference, mean number of proximal tubule nuclei, and nuclei number per proximal tubule circumference. Wild type and *Dtnbp1*$^{sdy/sdy}$ n = 225 proximal tubules per group, *Pldn*$^{pa/pa}$ n = 75 proximal tubules. (**Ea**) *Dtnbp1*$^{sdy/sdy}$ and *Pldn*$^{pa/pa}$ proximal tubules have an increased circumference. (**Eb**) *Dtnbp1*$^{sdy/sdy}$ and *Pldn*$^{pa/pa}$ proximal tubules have an increase in the mean number of nuclei. (**Ec**). Increase in nuclei number per proximal tubule circumference. n = 3 mice per Wild Type and *Dtnbp1*$^{sdy/sdy}$ groups, n = 1 mouse per *Pldn*$^{pa/pa}$ group. Tissue from the wild type and *Dtnbp1*$^{sdy/sdy}$ mice was harvested at precisely 12 months of age. Two of the three *Pldn*$^{pa/pa}$ mice died of a known lung fibrosis phenotype during the aging process. Tissue from the remaining *Pldn*$^{pa/pa}$ mouse was harvested at 11 months and 19 days of age. Error bars are standard error of the mean. The data was analyzed with One-way ANOVA and Bonferroni multiple comparisons test. ** $p < 0.01$, *** $p < 0.001$, **** $p < 0.0001$ and ns = non-significant.

In addition, we noted abnormal position of the proximal tubule nuclei in the two models. Proximal tubule cells typically have well-separated nuclei located near the basal surface. In the mutants, nuclei distribute throughout the cell including at the apical surface and often are found next to each other (Fig. II-15, D).

There is no difference in cilia assembly and the percentage of cilia per basal body in the *Pldn*$^{pa/pa}$ mice (Fig. II-15, C). However, the *Dtnbp1*$^{sdy/sdy}$ mice have a decrease in both cilia length and the percentage of cilia per basal body (Fig. II-15, C). The *Dtnbp1*$^{sdy/sdy}$ and *Pldn*$^{pa/pa}$ mouse phenotype strongly correlates with the biochemical and cell biology data and supports the conclusion that BLOC-1 is involved in trafficking polycystin-2 to primary cilia.

Polycystin-2 but not fibrocystin or smoothened is retained in the recycling endosome when the C-terminal tail of MyoVb is overexpressed.

The BLOC-1 complex is thought to function at the recycling endosome tubules that extend from sorting endosomes to direct cargos into the recycling endosome and lysosome (Delevoye et al., 2016; Dennis et al., 2016; Di Pietro et al., 2006; Ryder et al., 2013; Salazar et al., 2006; Setty et al., 2007). Because the recycling endosome is localized at the base of the cilium (Westlake et al., 2011), we questioned whether the function of BLOC-1 in trafficking polycystin-2 to cilia might involve its trafficking to or through the recycling endosome. To disrupt trafficking through the recycling endosome, we expressed a fragment of MyoVb that acts as a dominant negative on trafficking through this compartment (Lapierre et al., 2001; Volpicelli et al., 2002). The MyoVb dominant negative

fragment contains the C-terminal Rab11-binding domain but lacks the motor domain, allowing the fragment to bind Rab11-containing vesicles and interfere with their transport. GFP-MyoVb C-terminal tail colocalizes with the recycling endosome marker Rab11 (Fig. II-16, A) but not with the Golgi markers IFT20 (Fig. II-16, B) and GMAP210 (Fig. II-16, C). Expression of the MyoVb fragment induces compaction of the Golgi complex (Fig. II-16, B and C) but had only a small effect on cilia length (Fig. II-17, Ad and Bd).

We were unable to package the MyoVb expression vector into lentivirus, as it appears to interfere with some step of the process, and had to rely on electroporation to deliver the construct. MEK cells are difficult to transfect and so we used normal rat kidney (NRK) cells, which also have high levels of ciliary polycystin-2 and are easy to transfect. NRK cells transfected with GFP-MyoVb accumulated polycystin-2 at the recycling endosome (Figs. II-17, Aa; and II-18, A and B) and had a significant decrease in the steady-state levels of ciliary polycystin-2 (Fig. II-17, Ab and Ac). Additionally, we observed a moderate accumulation of endogenous Arl13b at the recycling endosome upon GFP-MyoVb overexpression (Fig. II-17 Aa).

To examine the effect of the MyoVb construct on trafficking of smoothened to the cilium, we used *Ift27*$^{-/-}$ NIH 3T3 cells as the lack of IFT27 causes smoothened to accumulate to high levels in cilia (Eguether et al., 2014).

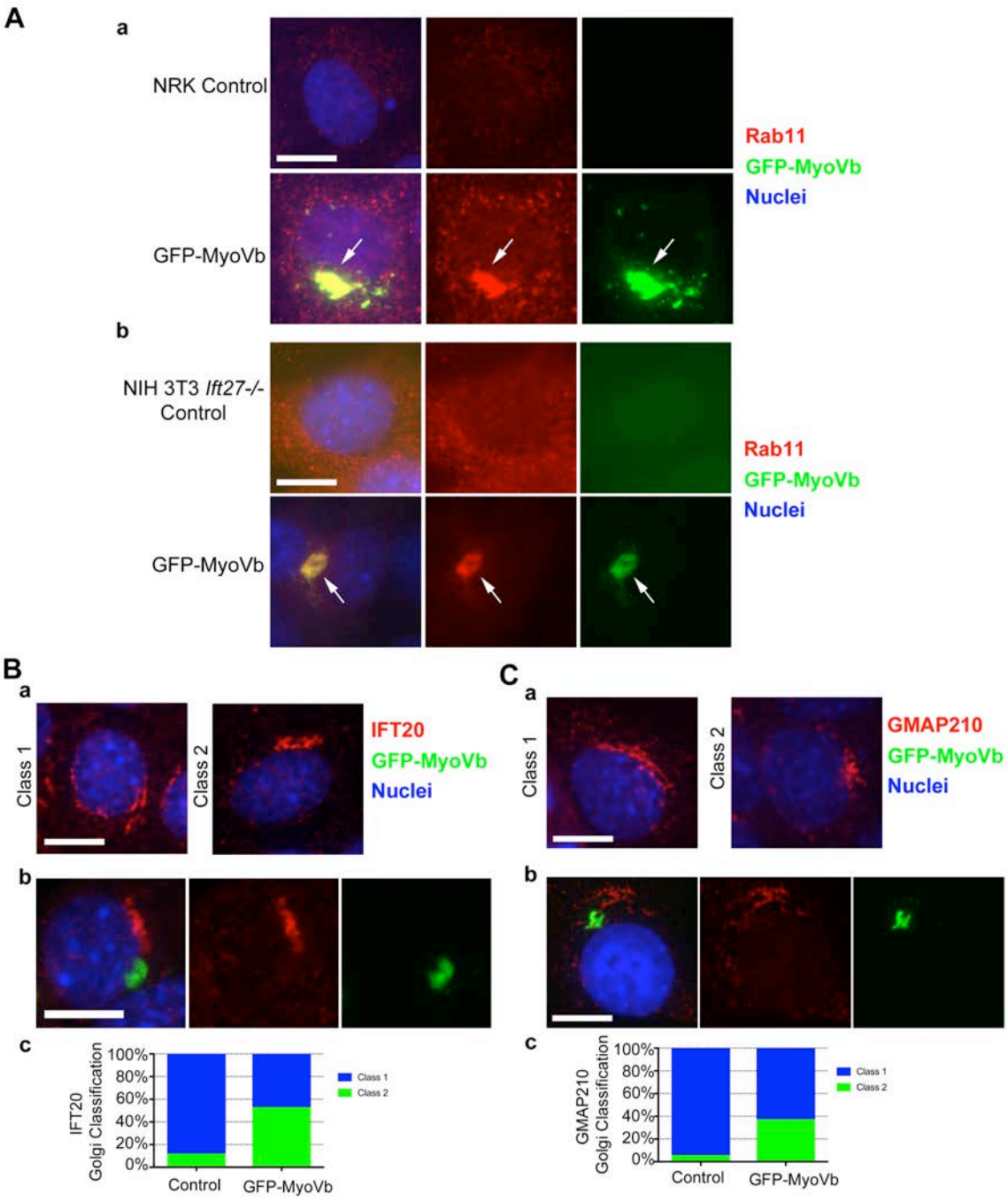

Figure II-16: GFP-MyoVb colocalizes with the recycling endosome marker Rab11 and induces compaction of the Golgi complex.

Figure II-16. GFP-MyoVb colocalizes with the recycling endosome marker Rab11 and induces compaction of the Golgi complex.

(**A**) NRK and NIH 3T3 *Ift27*$^{-/-}$ cells expressing GFP-MyoVb C-terminal tail. (**Aa**) Selected images of NRK control and GFP-MyoVb expressing cells stained with Rab11 antibody (red), GFP-MyoVb (green), and nuclei detected with DAPI (blue). Scale bar is 10 μm. (**Ab**) Selected images of NIH 3T3 *Ift27*$^{-/-}$ control and GFP-MyoVb expressing cells stained with Rab11 antibody (red), GFP-MyoVb (green), and nuclei detected with DAPI (blue). Scale bar is 10 μm. GFP-MyoVb colocalizes with the recycling endosome marker Rab11 (arrows). (**B and C**) Golgi classification and GFP-MyoVb expression induces Golgi compaction. (**Ba**) Selected images of IMCD3 cells stained with IFT20 antibody (red) and nuclei detected with DAPI (blue) or (**Ca**) GMAP210 antibody (red) and nuclei detected with DAPI (blue). Class 1: cells with noncompact Golgi around the nucleus. Class 2: cells with compact Golgi. Scale bars are 10 μm. (**Bb**) Selected images of IMCD3 cells stained with IFT20 antibody (red), GFP-MyoVb (green), and nuclei detected with DAPI (blue). GFP-MyoVb does not colocalize with IFT20 at the Golgi. Scale bar is 10 μm. (**Cb**) Selected images of IMCD3 cells stained with GMAP210 antibody (red), GFP-MyoVb (green), and nuclei detected with DAPI (blue). GFP-MyoVb does not colocalize with GMAP210 at the Golgi. Scale bar is 10 μm. (**Bc** and **Cc**) GFP-MyoVb expression induces compaction of the Golgi complex. n = 95 cells per experimental group.

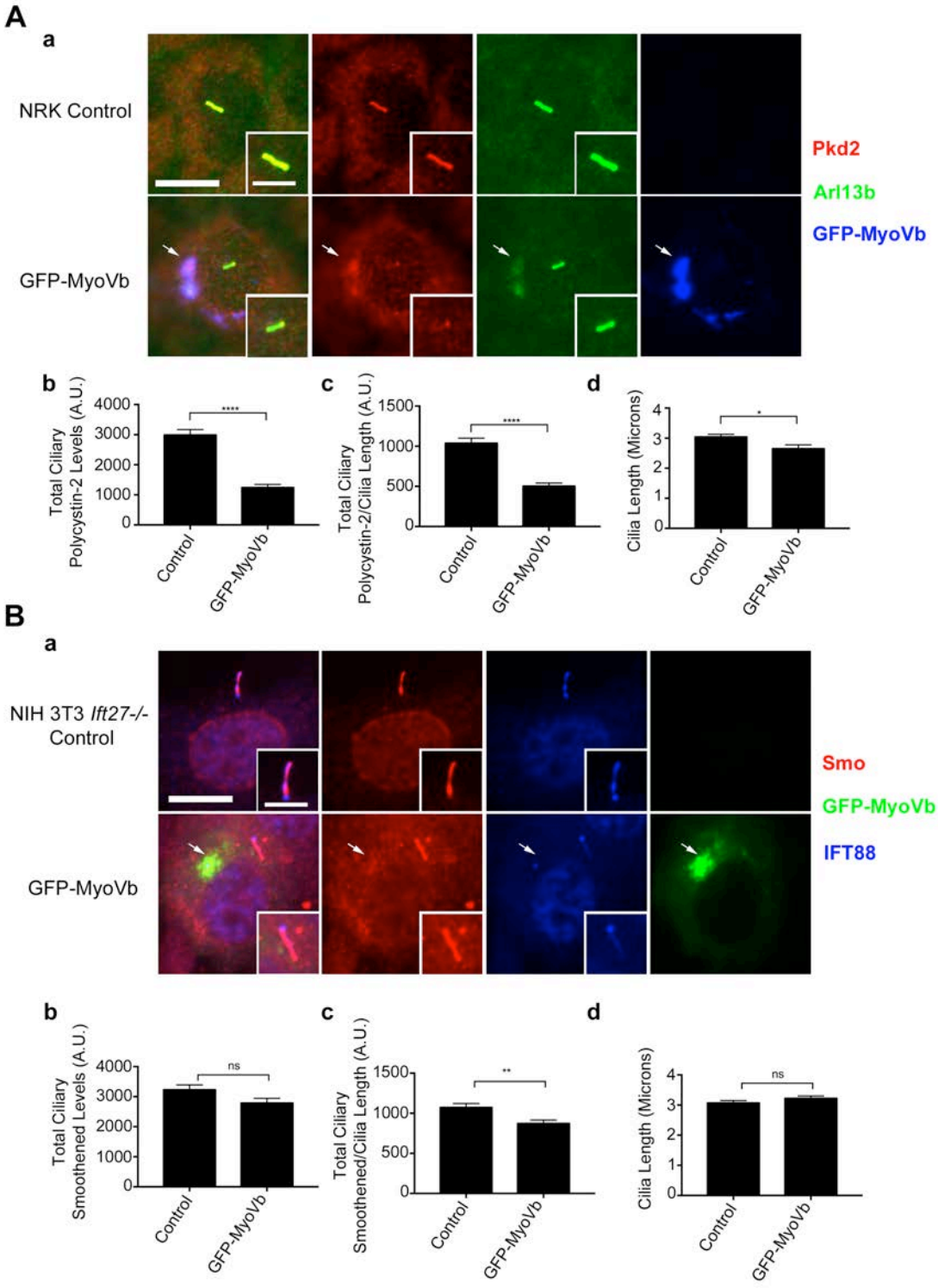

Figure II-17: Ciliary levels of polycystin-2 but not smoothened are reduced in GFP-MyoVb overexpressing cells.

Figure II-17. Ciliary levels of polycystin-2 but not smoothened are reduced in GFP-MyoVb overexpressing cells.

(**A**) NRK cells expressing GFP-MyoVb C-terminal tail. (**Aa**) Polycystin-2 (Pkd2) antibody staining (red), Arl13b antibody staining (green), and GFP-MyoVb (blue). Polycystin-2 and Arl13b co-localize with GFP-MyoVb at the recycling endosome (arrows). Scale bar is 10 μm. Insets are 150% enlargements of the cilia. (**Ab**) Mean steady-state ciliary polycystin-2 is decreased (**Ac**) ciliary polycystin-2/cilia is reduced, and (**Ad**) no difference in mean cilia length in NRK cells expressing GFP-MyoVb. (**B**) NIH 3T3 *Ift27-/-* cells expressing GFP-MyoVb C-terminal tail. (**Ba**) Smoothened (Smo) antibody staining (red), GFP-MyoVb (green), and IFT88 antibody staining (blue). Modest levels of smoothened co-localizes with GFP-MyoVb at the recycling endosome (arrows). Scale bar is 10 μm. Insets are 150% enlargements of the cilia. (**Bb**) No difference in mean steady-state ciliary smoothened, (**Bc**) total ciliary smoothened/length is decreased, and (**Bd**) no difference in mean ciliary length in GFP-MyoVb expressing cells. n = 102 cilia per experimental group. Error bars are standard error of the mean. The data was analyzed with unpaired student t-test. * $p < 0.05$, ** $p < 0.01$, **** $p < 0.0001$ and ns = non-significant.

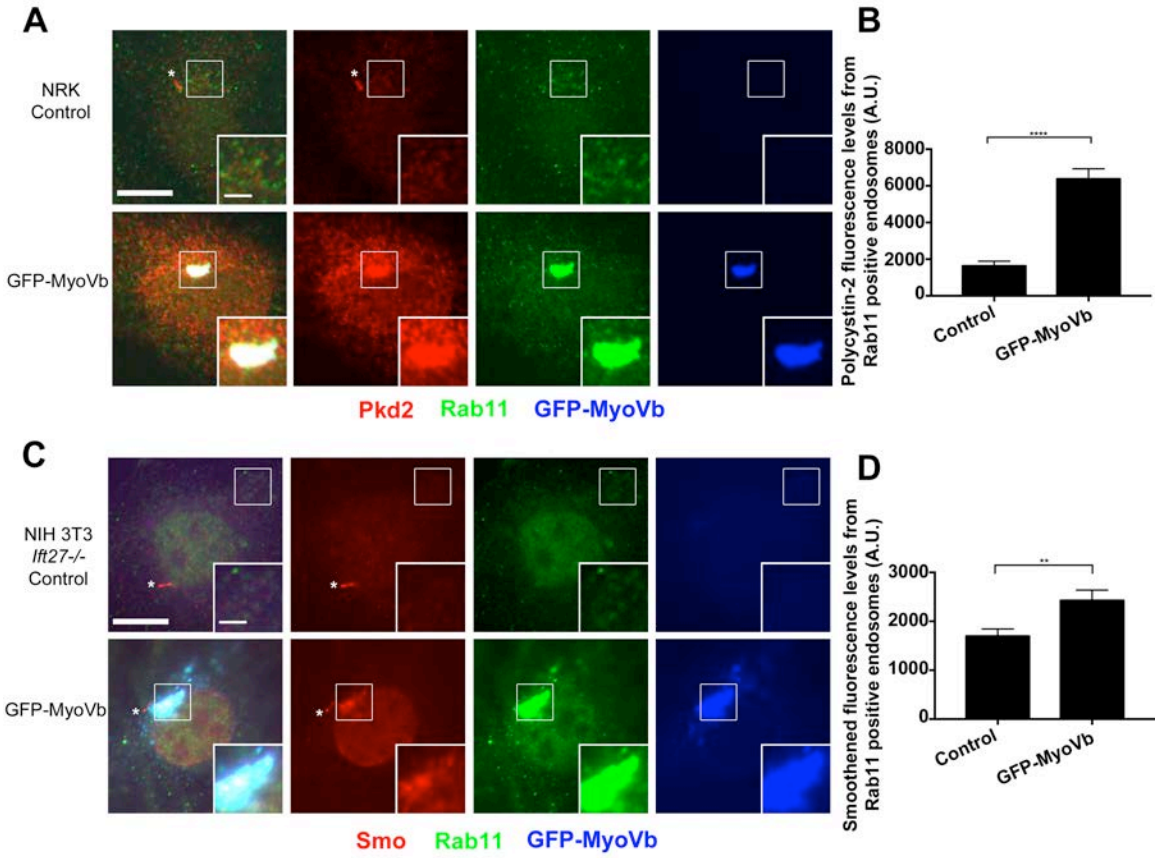

Figure II-18: Polycystin-2 and smoothened accumulate in Rab11 positive endosomes when GFP-MyoVb is expressed.

Figure II-18. Polycystin-2 and smoothened accumulate in Rab11 positive endosomes when GFP-MyoVb is expressed.

(**A**) Selected images of NRK control and GFP-MyoVb expressing cells stained with polycystin-2 (Pkd2) antibody (red), Rab11 antibody (green), and GFP-MyoVb (blue). A cilium positive for polycystin-2 is marked by an asterisk in the NRK control. Note the bolus accumulation of polycystin-2 in Rab11 positive endosomes and the lack of ciliary polycystin-2 staining when GFP-MyoVb is expressed. Insets are 200% enlargements of Rab11 positive endosomes. Scale bar is 10 μm. (**B**) Quantification of mean polycystin-2 fluorescence levels from Rab11 positive endosomes. There is a significant accumulation of polycystin-2 in Rab11 positive endosomes when GFP-MyoVb is expressed. n = 55 Rab11 positive endosome puncta groups. (**C**) Selected images of NIH 3T3 *Ift27 -/-* and GFP-MyoVb expressing cells stained with smoothened (Smo) antibody (red), Rab11 antibody (green), and GFP-MyoVb (blue). Cilia positive for smoothened are marked by asterisks in the NIH 3T3 *Ift27 -/-* control and GFP-MyoVb expressing cells. Note the minimal accumulation of smoothened in Rab11 positive endosomes and the presence of ciliary smoothened staining in the GFP-MyoVb expressing cells. Insets are 200% enlargements of Rab11 positive endosomes. Scale bar is 10 μm. (**D**) Quantification of mean smoothened fluorescence levels from Rab11 positive endosomes. There is a minimal yet significant accumulation of smoothened in Rab11 positive endosomes when GFP-MyoVb is expressed. n = 55 Rab11 positive endosome puncta groups. Error

bars are standard error of the mean. The data was analyzed with unpaired student t-test. ** $p < 0.01$ and **** $p < 0.0001$.

Expression of GFP-MyoVb C-terminal tail in these cells resulted in a moderate accumulation of smoothened in the recycling endosome (Figs. II-17 Ba; and II-18, C and D), but there was no difference in ciliary smoothened levels (Fig. II-17, Bb and Bc).

We went on to use a Flag-MyoVb construct in our pulse-chase trafficking assays for fibrocystin, polycystin-2, and smoothened. We observed a bolus of polycystin-2 co-localizing with the Flag-MyoVb in the recycling endosome after Golgi release (Fig. II-19, A). There is a decrease in both the ciliary length (Fig. II-19, B) and ciliary trafficking of polycystin-2 (Fig. II-19, C and D) in the Flag-MyoVb overexpressing cells. However, trafficking of fibrocystin and smoothened were not affected by the expression of the MyoVb dominant negative construct (Fig. II-20).

To determine whether knockdown of the exocyst or BLOC-1 components results in accumulation of endogenous polycystin-2 in endosome cellular compartments, we stained our shRNA MEK cell lines with the recycling endosome marker Rab11 (Fig. II-21). We did not detect accumulation of polycystin-2 in Rab11 positive endosomes in our exocyst or BLOC-1 knockdowns (Fig. II-21, B).

Ciliary Polycystin-2 is reduced by overexpression of dominant negative Rab11a.

To obtain more evidence that polycystin-2 is utilizing the recycling endosome for trafficking to the primary cilium, we measured ciliary polycystin-2 levels in cells

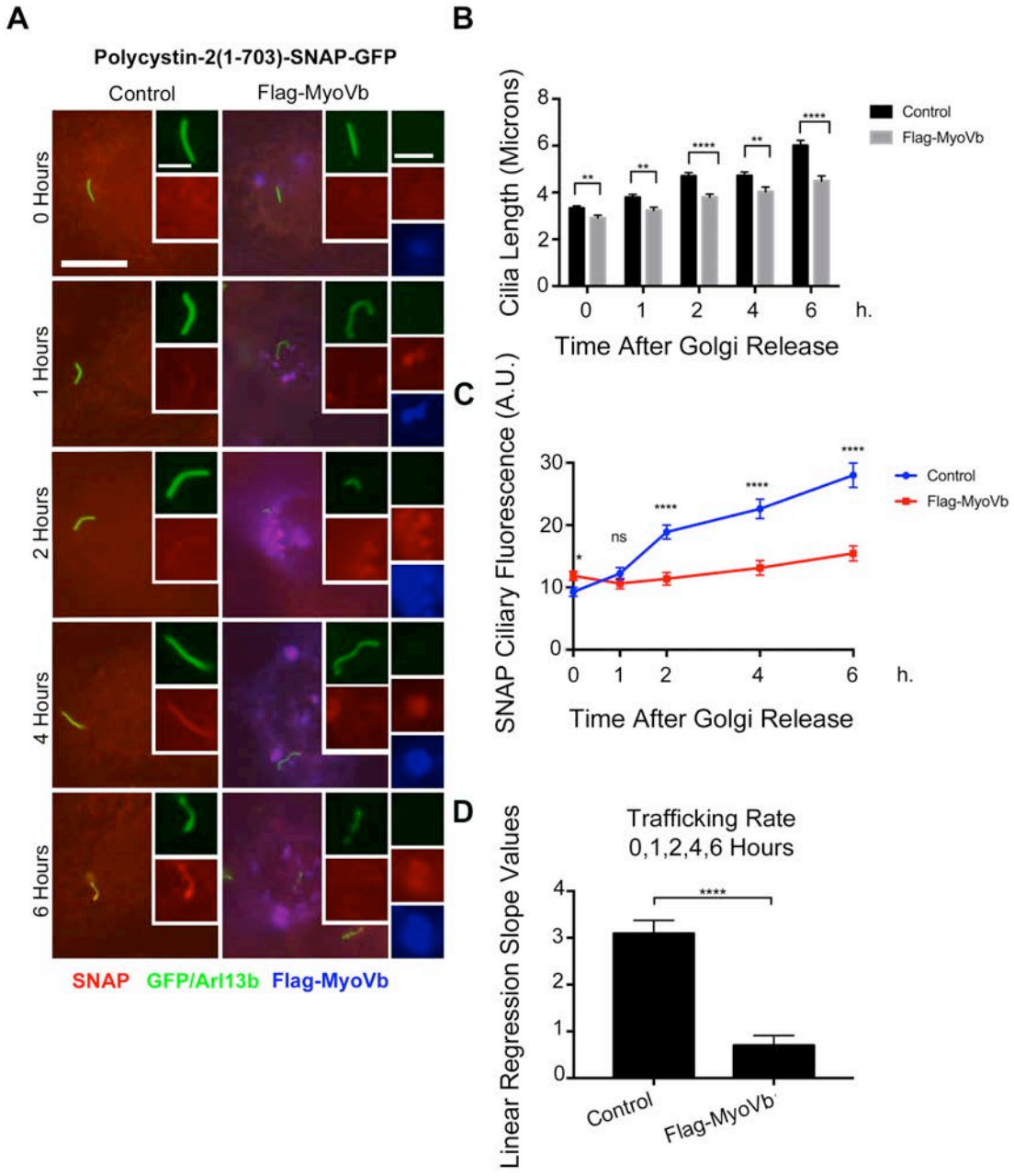

Figure II-19: Overexpression of MyoVb perturbs polycytin-2 trafficking to the primary cilium.

Figure 11-19. Overexpression of MyoVb perturbs polycytin-2 trafficking to the primary cilium.

(**A**) Selected trafficking images of Polycystin-2-GFP-SNAP IMCD Flp-In cells overexpressing Flag-MyoVb C-terminal tail. GFP and Arl13b antibody staining (green), SNAP TMR STAR (red), and Flag-MyoVb (blue). Insets depict newly synthesized Polycystin-2-GFP-SNAP trafficking to the cilium in control or Flag-MyoVb overexpressing cells. Insets also show accumulation of newly synthesized Polycystin-2-GFP-SNAP in the recycling endosome in the Flag-MyoVb overexpressing cells. Insets are 200% enlargements of the cilia and 170% enlargements of the recycling endosome. Scale bar is 10 μm. (**B**) Mean cilia length of Polycystin-2-GFP-SNAP IMCD Flp-In control and Flag-MyoVb overexpressing cells after the Golgi release. Cilia are shorter in Flag-MyoVb overexpressing cells. (**C**) Mean SNAP ciliary fluorescence of Polycystin-2-GFP-SNAP delivery to the cilium after Golgi release. Polycystin-2 ciliary trafficking decreased in Flag-MyoVb overexpressing cells. (**D**) Linear regression slope values of newly synthesized Polycystin-2-GFP-SNAP in IMCD Flp-In control and Flag-MyoVb overexpressing cells after the Golgi release utilizing data points taken at 0,1, 2, 4, 6 hrs. Mean SNAP ciliary fluorescence and mean ciliary length were plotted from three independent experiments in which 30 cilia were quantified for each condition (Control and Flag-MyoVb) at each time point (n = 90 total cilia per time point). Error bars represent standard error of the mean. The data was analyzed with unpaired student t-test. * $p < 0.05$, ** $p < 0.01$, **** $p < 0.0001$ and ns = non-significant.

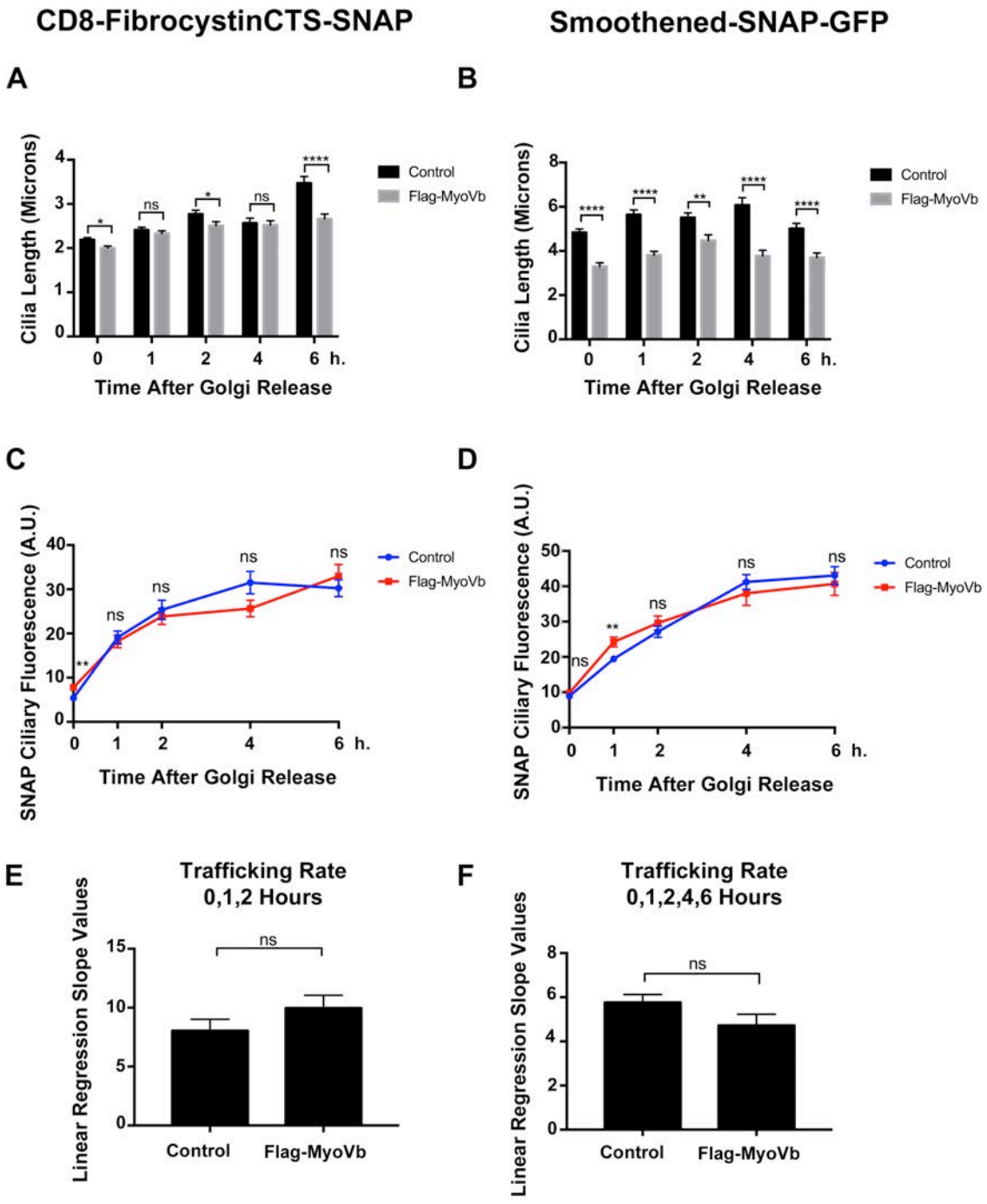

Figure II-20: Overexpression of MyoVb-GFP does not perturb fibrocystin or smoothened trafficking to the primary cilium.

Figure II-20. Overexpression of MyoVb-GFP does not perturb fibrocystin or smoothened trafficking to the primary cilium.

(**A**) Mean cilia length of CD8-FibrocystinCTS-SNAP and (**B**) Smoothened-SNAP-GFP IMCD Flp-In control and Flag-MyoVb expressing cells after Golgi release. (**C**) Mean SNAP ciliary fluorescence of CD8-FibrocystinCTS-SNAP and (**D**) Smoothened-SNAP-GFP delivery to the cilium in IMCD Flp-In control and Flag-MyoVb expressing cells after Golgi release. The mean SNAP ciliary fluorescence and ciliary length were plotted from three independent experiments in which 30 cilia were quantified for each condition (Control and Flag-MyoVb) at each time point (n = 90 total cilia per time point). (**E**) Linear regression slope values of newly synthesized CD8-FibrocystinCTS-SNAP and (**F**) Smoothened-SNAP-GFP in IMCD Flp-In control and Flag-MyoVb expressing cells after Golgi release at either 0, 1, 2 hrs or 0, 1, 2, 4, 6 hrs. Slope values between control and Flag-MyoVb groups were compared to one another to determine statistical significance. Error bars represent standard error of the mean. The data was analyzed with unpaired student t-test. * $p < 0.05$, ** $p < 0.01$, **** $p < 0.0001$ and ns = non-significant.

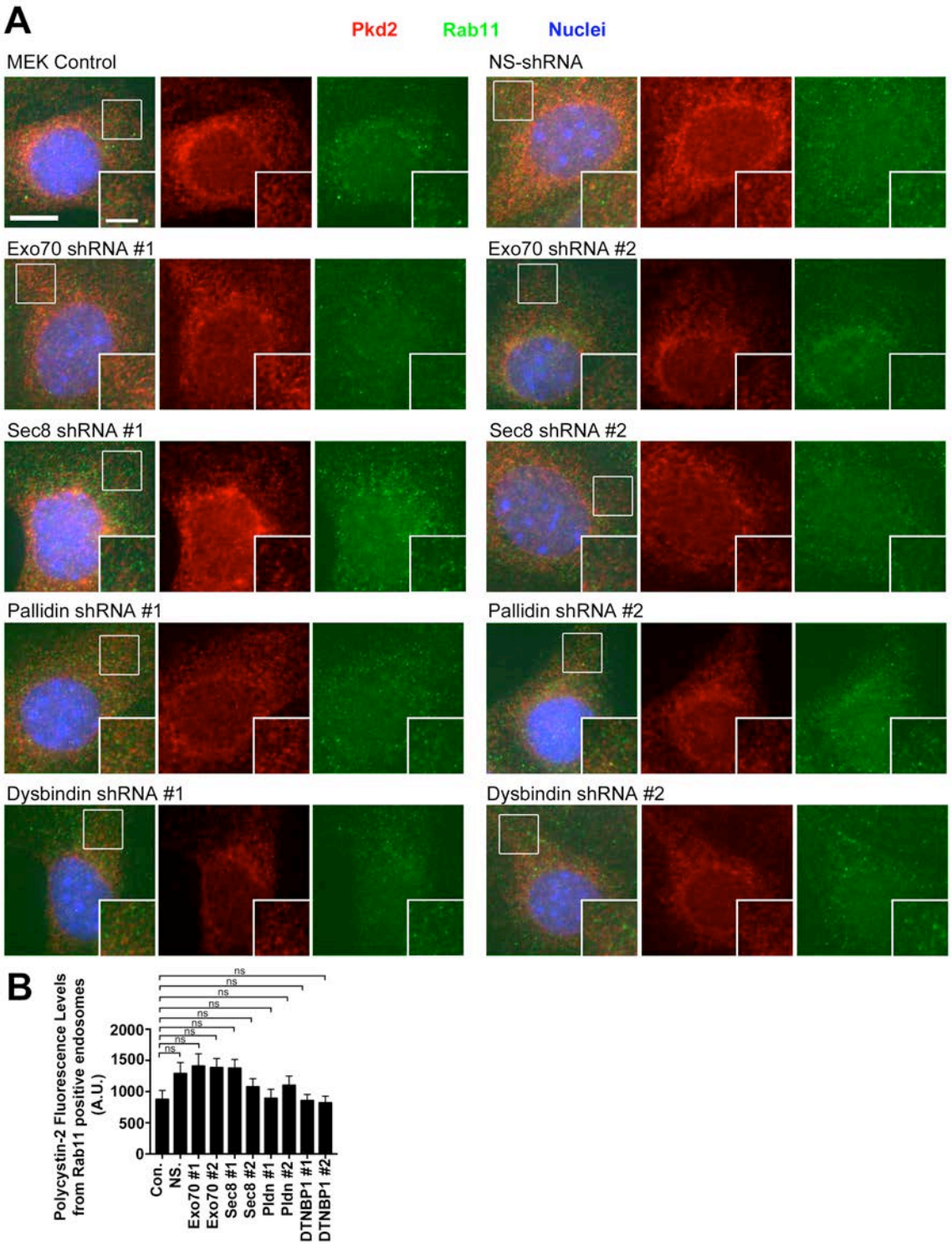

Figure II-21: Polycystin-2 is not detected in Rab11 positive endosomes when either the Exocyst or BLOC-1 is knocked down.

Figure II-21. Polycystin-2 is not detected in Rab11 positive endosomes when either the Exocyst or BLOC-1 is knocked down.

(**A**) Selected images of MEK control, NS-shRNA, Exo70 shRNA #1, Exo70 shRNA #2, Sec8 shRNA #1, Sec8 shRNA #2, Pallidin shRNA #1, Pallidin shRNA #2, Dysbindin shRNA #1, and Dysbindin shRNA #2 cells stained with polycystin-2 (Pkd2) antibody (red), Rab11 antibody (green), and nuclei detected with DAPI (blue). Scale bar is 10 μm. Insets are 150% enlargements of Rab11 positive endosomes. (**B**) Quantification of mean polycystin-2 fluorescence levels from Rab11 positive endosomes. There is no statistical difference between the control and experimental groups. n = 50 Rab11 positive endosome puncta groups. Error bars are standard error of the mean. The data was analyzed with One-way ANOVA and Bonferroni multiple comparisons test. ns = non-significant.

expressing wild type or mutant forms of Rab11a that are thought to disrupt the recycling endosome (Hehnly and Doxsey, 2014). Overexpressing wild type Rab11a, or Rab11aQ70L, which is thought to block GTP hydrolysis and keep the protein in a constitutively active GTP-bound form had no effect on ciliary levels of polycystin-2. However, overexpressing Rab11aS25N, which is thought to act as a dominant negative by binding guanine exchange factors, reduced ciliary polycystin-2 levels (Fig. II-22, A, B, C). None of these constructs affected ciliary length (Fig. II-22, D). Our finding that ciliary polycystin-2 levels are reduced in cells expressing Rab11aS25N is consistent with dominant negative forms of Rab11 disrupting the recycling endosome (Hehnly and Doxsey, 2014; Westlake et al., 2011) and further supports our model that polycystin-2 is trafficked to cilia through the recycling endosome.

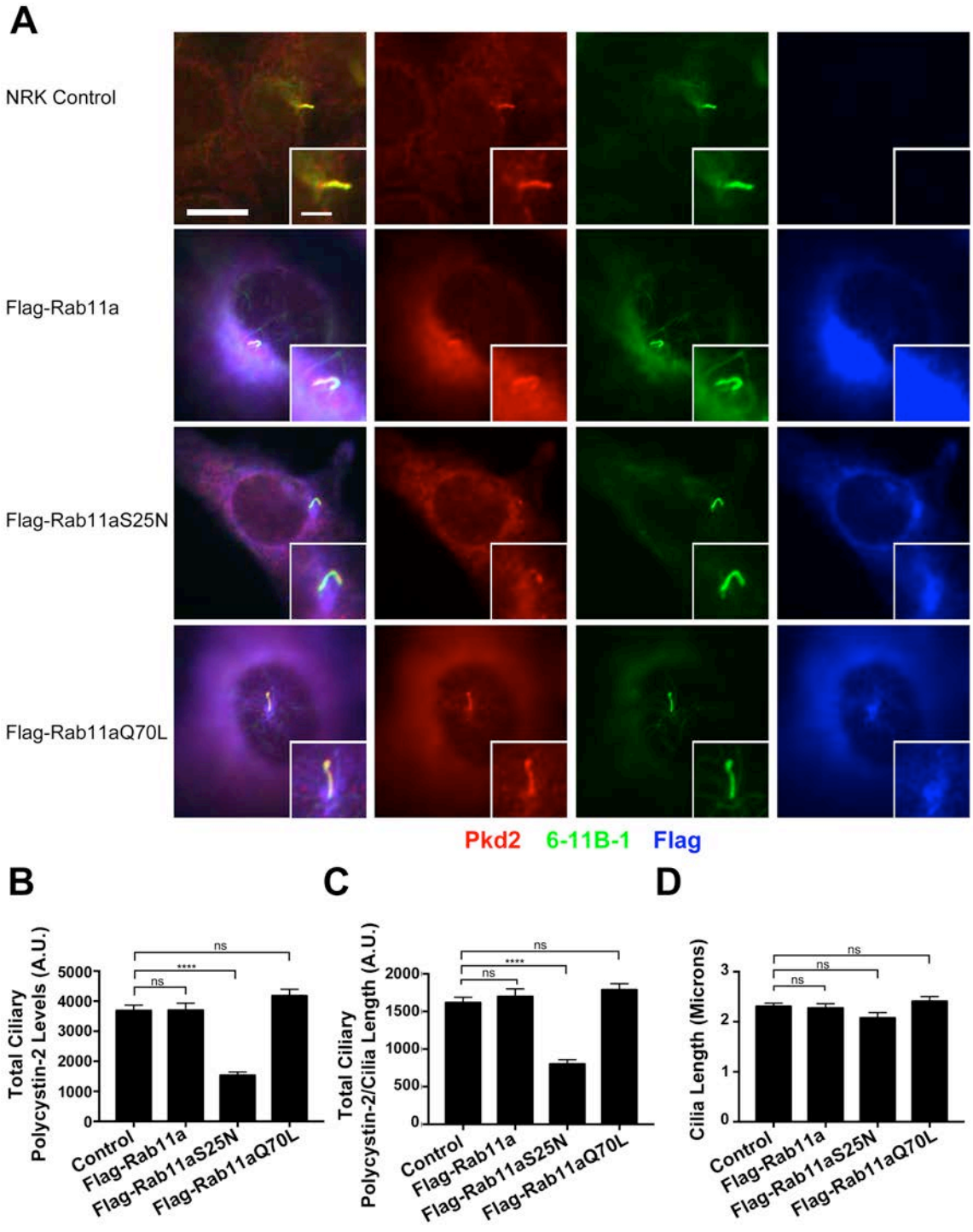

Figure II-22: Rab11aS25N expression perturbs polycystin-2 trafficking to the primary cilium.

Figure II-22. Rab11aS25N expression perturbs polycystin-2 trafficking to the primary cilium.

(**A**) Selected images of NRK cells expressing Flag-Rab11a, Flag-Rab11aS25N, or Flag-Rab11aQ70L stained for polycystin-2 (Pkd2) antibody (red), acetylated tubulin (6-11B-1) antibody (green), and Flag antibody (blue). Scale bar is 10 μm. Insets are 200% enlargements of the cilia. (**B**) Quantification of mean total ciliary polycystin-2 levels. Ciliary polycystin-2 is reduced in Flag-Rab11aS25N expressing cells. (**C**) Quantification of mean total ciliary polycystin-2/cilia length. Ciliary polycystin-2 per cilium length is reduced in Flag-Rab11aS25N expressing cells. (**D**) Quantification of mean cilia length. There is no difference in ciliary assembly when the Rab11a constructs are expressed. n = 85 cilia per experimental group. Error bars are standard error of the mean. The data was analyzed with One-way ANOVA and Bonferroni multiple comparisons test. **** $p < 0.0001$ and ns = non-significant.

Chapter III : Discussion

Cilia monitor the extracellular environment through specific receptors concentrated in their membranes, but we know little about how membrane proteins reach this organelle. Our prior work showed that IFT20 was required for delivery of polycystin-2 to primary cilia and rhodopsin to photoreceptor outer segments. IFT20 localizes to the Golgi complex by interaction with the golgin protein GMAP210 and is part of the IFT complex localized at cilia. This dual localization suggests that IFT20 could sort or traffic vesicles destined for the cilium, but details of how it accomplishes this are lacking. In our present work, we find that IFT20 interacts with the exocyst and the BLOC-1 complexes and we find that polycystin-2, fibrocystin, and smoothened each have unique requirements for delivery to cilia. Fibrocystin requires IFT20-GMAP210 and the exocyst. Polycystin-2 requires IFT20-GMAP210, the exocyst, and BLOC-1. However, smoothened delivery is largely independent of all of these proteins.

The exocyst was required for the delivery of polycystin-2 and fibrocystin to cilia. This complex consists of eight proteins (Sec3/Exoc1, Sec5/Exoc2, Sec6/Exoc3, Sec8/Exoc4, Sec10/Exoc5, Sec15/Exoc6, Exo70/Exoc7, and Exo84/Exoc8) conserved from yeast to mammals (Heider et al., 2016; Kee et al., 1997; TerBush et al., 1996). The exocyst tethers vesicles at target sites prior to membrane fusion (Heider and Munson, 2012; Luo et al., 2014). In polarized cells, the exocyst localizes along sites of secretion on the lateral membrane and at the base of the cilium (Grindstaff et al., 1998; Mazelova et al., 2009b; Rogers et al.,

2004). Knockdown of Sec10 disrupts ciliogenesis in MDCK cells and targeted deletion of Sec10 in the mouse kidney causes ciliary defects and cyst formation (Fogelgren et al., 2015; Seixas et al., 2016; Zuo et al., 2009). We found that IFT20 interacted with the Exo70 and Sec8 subunits. However, it is likely that IFT20 interacts with the entire exocyst complex as the Sec10 subunit also interacts with IFT20 and a large-scale proteomic study found IFT20 binding to multiple components (Exoc3, Exoc7, Exoc5, Exoc6B) (Fogelgren et al., 2011; Huttlin et al., 2015). We found that the localization of the exocyst at the base of the cilium is independent of IFT20, indicating that the exocyst is not delivered by IFT. This suggests the exocyst may capture or anchor vesicles containing ciliary cargos at the base of the cilium before membrane fusion. Because the exocyst can interact with IFT proteins, it may facilitate connections between ciliary membrane proteins and the IFT complex before entry into the cilium. However, the exocyst also interacts with BLOC-1 proteins, so it may have roles in capturing ciliary cargos from the endosome (Fig. III-1).

The BLOC-1 complex, which was required for trafficking of polycystin-2 to cilia contains eight proteins (pallidin, dysbindin, muted, snapin, cappuccino, BLOS1, BLOS2, and BLOS3) (Ciciotte et al., 2003; Falcon-Perez et al., 2002; Li et al., 2003; Moriyama and Bonifacino, 2002; Mullin et al., 2011; Starcevic and Dell'Angelica, 2004). This complex is best known for trafficking of proteins from the endosome system to the lysosome and lysosome-related organelles such as

A

Summary of the membrane protein trafficking rates from the Golgi apparatus to the cilium.

	Fibrocystin	Polycystin-2	Smoothened
IFT20 shRNA	↓	↓	↓
GMAP210 shRNA	↓	↓	↓
Exo70 shRNA	↓	↓	=
Sec8 shRNA	↓	↓	=
Pallidin shRNA	=	↓	=
Dysbindin shRNA	=	↓	=
MyoVb C-terminal tail	=	↓	=

Large arrow: > 40% decrease in the trafficking rates compared to the control
Small arrow: < 40% decrease in the trafficking rates compared to the control
Equal sign: < 30% decrease in the trafficking rates compared to the control

B

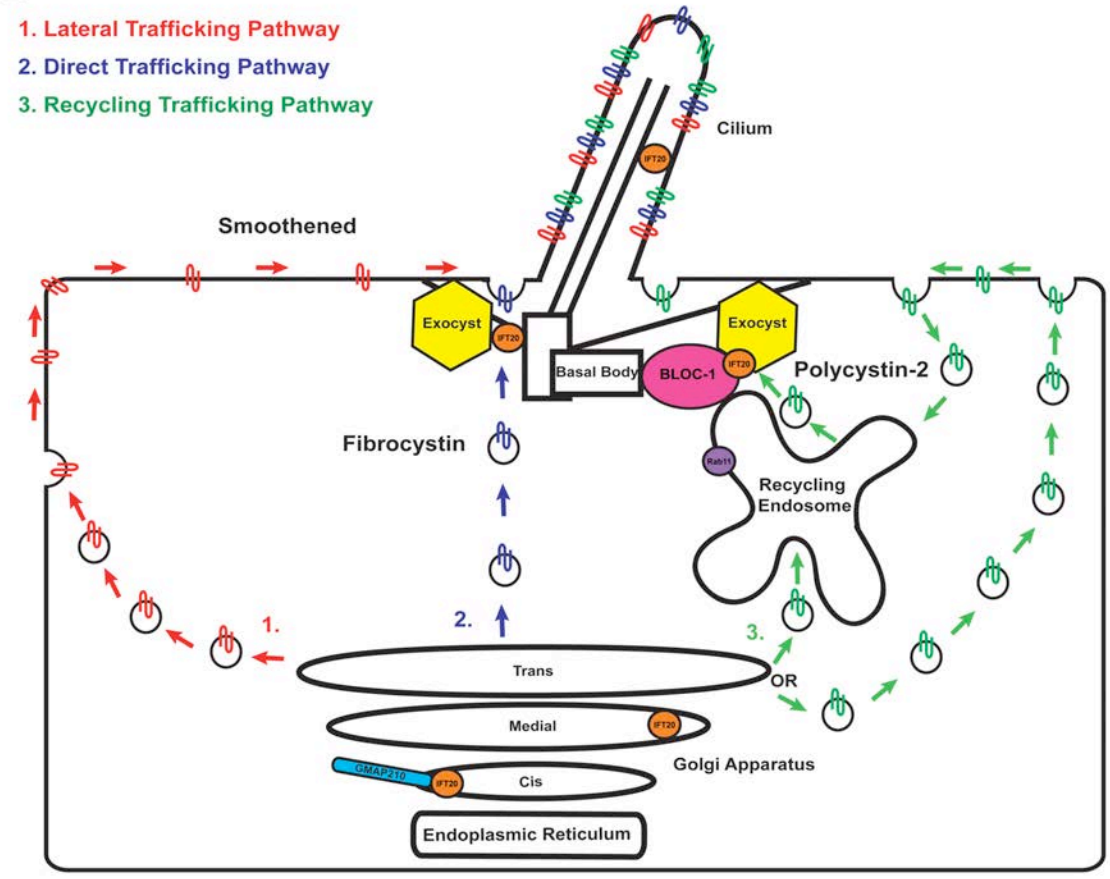

Figure III-1: Fibrocystin, polycystin-2 and smoothened take different trafficking routes to the primary cilium.

Figure III-1. Fibrocystin, polycystin-2, and smoothened take different trafficking routes to the primary cilium.

(**A**) Summary of the trafficking rates of membrane protein delivery from the Golgi apparatus to the cilium. Membrane proteins are listed horizontally. shRNAs and MyoVb C-terminal tail expression are listed on the left side. Large arrow: > 40% decrease in the trafficking rate compared to the control, small arrow: < 40% decrease in the trafficking rate compared to the control, and equal sign: < 30% decrease in the trafficking rate compared to the control. (**B**) IFT20 localizes at the *cis* Golgi compartment where it interacts with the vesicle tethering golgin GMAP210. IFT20 also localizes to the *medial* Golgi compartment, the cilium, and the basal body. Subunits of the exocyst localize to the basal body. Exocyst subunits Exo70 and Sec8 interact with IFT20. BLOC-1 also interacts with the exocyst. The exocyst tethers vesicles containing ciliary membrane protein cargo to the base of the cilium prior to SNARE-mediated fusion. We propose that fibrocystin is utilizing the direct trafficking pathway because it is affected only by knockdown of the IFT20-GMAP210 complex and the exocyst. Smoothened is likely using the lateral trafficking pathway because its delivery to cilia is not greatly affected by the knockdown of the IFT20-GMAP210 complex, and it is not affected by the knockdown of the exocyst or BLOC-1. The BLOC-1 subunit pallidin localizes to the basal body and its localization is partially dependent on IFT20. Pallidin interacts with IFT20 and polycystin-2. Knockdown of the BLOC-1 subunits pallidin and dysbindin affects the trafficking of polycystin-2 but not fibrocystin or smoothened. MyoVb C-terminal tail overexpression reduced ciliary

polycystin-2 levels and caused its accumulation at the recycling endosome. Additionally, expression of dominant negative Rab11aS25N perturbs polycystin-2 ciliary trafficking. This suggests that polycystin-2 is trafficked to the cilium through the recycling endosome. IFT20, BLOC-1, and the exocyst are acting together to deliver polycystin-2 cargo from the recycling endosome to the primary cilium.

melanosomes and platelet dense-granules (Di Pietro et al., 2006; Setty et al., 2008; Setty et al., 2007; Sitaram et al., 2012). BLOC-1 defects cause Hermansky-Pudlak syndrome, in which patients exhibit severe hypopigmentation and defects in platelet aggregation (Morgan et al., 2006). Recently BLOC-1 has been connected to schizophrenia, as a leading susceptibility gene encodes the dysbindin subunit, and brain tissue from schizophrenia patients have reduced dysbindin mRNA and protein levels (Mullin et al., 2011; Talbot et al., 2004; Weickert et al., 2008). The involvement of BLOC-1 in schizophrenia is not clear, however BLOC-1 is involved in dopamine and glutamate release (Kumamoto et al., 2006; Numakawa et al., 2004). Additionally, BLOC-1 regulates membrane protein targeting to synaptic vesicles and delivery of dopamine receptors to the cell surface (Iizuka et al., 2007; Ji et al., 2009; Larimore et al., 2011; Marley and von Zastrow, 2010b; Newell-Litwa et al., 2009).

Before our work, the BLOC-1 complex had no ciliary connections. However, we found interactions of BLOC-1 components with IFT20 and polycystin-2 and a requirement for this complex in the transport of polycystin-2 to cilia. Our finding that BLOC-1 is required for ciliary trafficking of polycystin-2 to cilia suggests that defects in BLOC-1-encoding genes should cause cystic kidneys. Previous studies showed that BLOC-1 mouse models have lower rates of lysosomal enzyme secretion into urine but no other analysis of kidney structure or function has been done (Novak and Swank, 1979). We found that young *Dtnbp1*$^{sdy/sdy}$ and *Pldn*$^{pa/pa}$ mice had dilations of the collecting ducts,

suggesting that they may become cystic with age. A second cohort of mice was aged twelve months. The animals have lung fibrosis, and most did not survive the year (McGarry et al., 2002). The survivors did not have prominent cystic disease, unlike the phenotype of *Pkd2* and *Ift20* mutant animals (Jonassen et al., 2008; Wu et al., 1998). However, both *Dtnbp1*$^{sdy/sdy}$ and *Pldn*$^{pa/pa}$ animal models showed significant dilation of the collecting ducts and proximal tubules. Additionally, *Dtnbp1*$^{sdy/sdy}$ mice have reduced ciliation and shortened cilia, which is similar to what we observed in cell culture after knockdown. This suggests that that BLOC-1 defects trigger increased proliferation of tubule cells, but compensatory mechanisms keep the tubules from greatly expanding. We also noted increased numbers of abnormally positioned nuclei in the *Dtnbp1*$^{sdy/sdy}$ and *Pldn*$^{pa/pa}$ proximal tubules. The disrupted nuclei positioning in the *Dtnbp1*$^{sdy/sdy}$ and *Pldn*$^{pa/pa}$ animals may be indicative of a loss of cell polarization within the kidney tubule. Little is known about this phenotype but aberrant nuclei positioning is associated with pathology in muscular dystrophy and hearing loss (Gundersen and Worman, 2013; Horn et al., 2013; Lei et al., 2009; Sullivan et al., 1999; Zhang et al., 2007).

BLOC-1 localizes to recycling endosome tubules that extend from sorting endosomes, where it controls tubule formation and trafficking of membrane proteins to melanosomes (Delevoye et al., 2016; Dennis et al., 2016; Di Pietro et al., 2006; Ryder et al., 2013; Salazar et al., 2006; Setty et al., 2007). Given that BLOC-1 is involved in polycystin-2 trafficking, we hypothesized that polycystin-2

is traversing the recycling endosome compartment before delivery to the cilium. To perturb trafficking through the recycling endosome we expressed the C-terminal tail of the myosin motor MyoVb (Lapierre et al., 2001; Volpicelli et al., 2002). This MyoVb fragment interacts with Rab11 but lacks motor activity (Lapierre et al., 2001). This construct caused polycystin-2 to accumulate in the recycling endosome and reduced the amount on cilia. In addition, expression of the Rab11aS25N dominant negative form of Rab11a perturbs ciliary polycystin-2 trafficking. While this is the first demonstration of a protein traveling through the recycling endosome to reach the cilium, the recycling endosome is involved in the early steps of cilia formation and the recycling endosome remains at the centrosome after ciliary assembly (Hehnly et al., 2012; Hehnly and Doxsey, 2014; Westlake et al., 2011). In addition to our data, other connections between the endosome system and trafficking of polycystin-2 to cilia are beginning to emerge. The lipid kinase PI3K-C2α localizes to the pericentriolar-recycling endosome at the base of the cilium and knockdown of this kinase reduced ciliary polycystin-2 (Franco et al., 2016). Similarly, knockdown of the endosome protein SDCCAG3 reduces ciliary polycystin-2 (Yu et al., 2016).

Summary

Our work uncovered previously unappreciated complexity in membrane protein trafficking pathways to cilia (Fig. III-1). These pathways include an IFT20-independent pathway where proteins travel to the plasma membrane before lateral diffusion into the cilium. A second, IFT20- and exocyst-dependent

pathway from the Golgi complex to the ciliary base and a third endosomal pathway whereby proteins traverse the recycling endosome on the way to the cilium. This complexity suggests that through evolution, the cell customized preexisting cellular trafficking pathways and machineries to generate distinct ciliary membrane protein trafficking routes.

Chapter IV : Materials and Methods

Cell Culture

NRK, IMCD3 (Rauchman et al., 1993), and IMCD3 Flp-In (Mukhopadhyay et al., 2010) cells were grown in 47.5% DMEM (4.5 g/L glucose) 47.5% F12, 5% fetal bovine serum (FBS), 100 U/ml penicillin, and 100 g/ml streptomycin (all from Gibco-Invitrogen) at 37°C in 5% CO_2. MEK cells were grown in the same culture medium described above but with 10% FBS. NIH 3T3 cells were cultured in 90% DMEM (4.5 g/L glucose), 10% FBS, 100 U/ml penicillin, and 100 g/ml streptomycin (Gibco-Invitrogen). Cells were serum-starved for 48 hrs to induce ciliation in their described culture medium but with 0.25% FBS.

DNA Constructs

The open reading frames of MmKXD1 (NM_029366.2), MmPallidin (NM_019788.3) and MmExo70 (AF014461.1) were amplified from mouse kidney cDNA using primers that placed them in frame with the Flag epitope pJAF113 (Follit et al., 2009) to generate constructs WJM1, WJM2, and FX70 respectively. Flag-GFP (JAF146), Flag-MmIFT54 (FX34), Flag-MmIFT25 (JAF143) and Flag-MmIFT20 (JAF134) were previously described (Follit et al., 2009). The OcMyoVb (AF176517.1) C-terminal tail was amplified from GFP-OcMyoVb C-terminus (Lapierre et al., 2001; Volpicelli et al., 2002) and cloned into pJAF113 to generate WJM30. Flag-MmRab11a (NM_017382.5) was amplified and Gibson assembled into a lenti-viral pHAGE vector to generate GP730. Gibson assembly

mutagenesis was utilized to generate Flag-MmRab11aS25N (GP731) and Flag-MmRab11aQ70L (GP733). The coding sequences of HsCD8-MmFibrocystinCTS-SNAP (JAF271), HsPolycystin-2(1-703)-GFP-SNAP (pJag689) (a gift from J. Shah, Harvard Medical School, Boston, MA), and MmSmoothened-SNAP-GFP (JAF250) were amplified and TA-cloned into pCR8-GW-Topo vector (Invitrogen) to make entry clones. The entry clones were gateway-cloned into the destination vector pEF5B-FRT-DEST using Gateway LR Clonase II Enzyme Mix (Invitrogen) to generate the respective Flp-In expression clones WJM8, WJM15 and WJM6. All DNA constructs were verified by sequencing.

Flp-In System

The Flp-In system comprises of a construct encoding the Flp recombinase pCAGGS-FlpE (Addgene) and the Flp-In expression clone in the pEF5B-FRT-DEST backbone, a gift from M. Nachury (Stanford University School of Medicine, Stanford, CA). pCAGGS-FlpE and the expression clone were electroporated (BioRad) into IMCD3 Flp-In cells (a gift from P. Jackson, Stanford University School of Medicine, Stanford, CA), in the following proportions: pCAGGS-FlpE, 9; expression clone: 1. Starting 48 hrs after electroporation, cells were drug selected with 4 µg/ml of blasticidin for 72 hrs. Colonies were recovered after 1 – 2 weeks in culture and screened by immunofluorescence.

Lenti-shRNA Production

All lenti-shRNAs are in the pGIPZ vector backbone (Open Biosystems/GE Dharmacon). The lenti-shRNA system comprises of two packaging vectors (psPAX2 and pMD2.G; Addgene). The virus was packaged by cotransfecting 1.2 x 10^6 human embryonic kidney (HEK) 293T cells per well of a six-well cell culture plate with the lenti-shRNA pGIPZ vector and the two packaging vectors in the following proportions: pGIPZ, 2; psPAX2, 2; pMD2.G, 1. Effectene (Qiagen) transfection reagent was used. After 48 hrs, the virus was harvested and filtered through a 0.45 µm filter. Virus was concentrated using Lenti-x concentrator (Clontech) and the pellet was resuspended in 80% DMEM (4.5 g/L glucose), 20% FBS, 100 U/ml penicillin, 100 g/ml streptomycin, and 5 µg/ml polybrene (Sigma). Virus was finally added to cells plated at 1.25 x 10^5 cells per well of a six-well cell culture plate. Cells were infected for 72 hrs before being drug selected with 1 µg/ml of puromycin for 72 hrs.

Full hairpin sequence (mature antisense sequences are bold-face type):

IFT20 shRNA #1: 5’ –

TGCTGTTGACAGTGAGCGCGGTCTAATTGAGCTTGTTGATTAGTGAAGCCA

CAGATGTAA**TCAACAAGCTCAATTAGAC**CATGCCTACTGCCTCGGA – 3’

IFT20 shRNA #2: 5’ –

TGCTGTTGACAGTGAGCGAAAGGACTTTGTGGACAAAATTTAGTGAAGCCA

CAGATGTAA**ATTTTGTCCACAAAGTCCT**TGTGCCTACTGCCTCGGA – 3’

GMAP shRNA #1: 5’ –

TGCTGTTGACAGTGAGCGCCGGTTGACAGTGATAACAATTTAGTGAAGCCA

CAGATGTAA**ATTGTTATCACTGTCAACC**GATGCCTACTGCCTCGGA – 3’

GMAP shRNA #2: 5’ –

TGCTGTTGACAGTGAGCGACAGCTGTTTGCAGAAGATCAATAGTGAAGCCA

CAGATGTAT**TGATCTTCTGCAAACAGCT**GCTGCCTACTGCCTCGGA – 3’

Exo70 shRNA #1: 5’ –

TGCTGTTGACAGTGAGCGACTGGCTAAAGGTGACTGACTATAGTGAAGCCA

CAGATGTAT**AGTCAGTCACCTTTAGCCA**GCTGCCTACTGCCTCGGA – 3’

Exo70 shRNA #2: 5’ –

TGCTGTTGACAGTGAGCGACGCCATCTTCCTACACAACAATAGTGAAGCCA

CAGATGTAT**TGTTGTGTAGGAAGATGGC**GCTGCCTACTGCCTCGGA – 3’

Sec8 shRNA #1: 5’ –

TGCTGTTGACAGTGAGCGAATCGTGGAGAAGACAGTACAATAGTGAAGCCA

CAGATGTAT**TGTACTGTCTTCTCCACGA**TGTGCCTACTGCCTCGGA – 3’

Sec8 shRNA #2: 5’ –

TGCTGTTGACAGTGAGCGAATCGTTCAGCACTACACAGAATAGTGAAGCCA

CAGATGTAT**TCTGTGTAGTGCTGAACGA**TCTGCCTACTGCCTCGGA – 3’

Pallidin shRNA #1: 5’ –

TGCTGTTGACAGTGAGCGCACCAAGTTGTGTTACTAGATATAGTGAAGCCA

CAGATGTAT**ATCTAGTAACACAACTTGG**TTTGCCTACTGCCTCGGA – 3’

Pallidin shRNA #2: 5’ –

TGCTGTTGACAGTGAGCGAGGCGATAGAGAGATCGATAAATAGTGAAGCCA

CAGATGTAT**TTATCGATCTCTCTATCGC**CCTGCCTACTGCCTCGGA – 3’

Dysbindin shRNA #1: 5’ –

TGCTGTTGACAGTGAGCGACAGGTGCTTAGAGGTTTTCAATAGTGAAGCCA

CAGATGTAT**TGAAAACCTCTAAGCACCT**GGTGCCTACTGCCTCGGA – 3’

Dysbindin shRNA #2: 5’ –

TGCTGTTGACAGTGAGCGCCCGAAGTACTCTGCTGGACTATAGTGAAGCCA

CAGATGTAT**AGTCCAGCAGAGTACTTCG**GTTGCCTACTGCCTCGGA – 3’

pHAGE Lentivirus Production

Lentivirus production using the pHAGE system was previously described (Eguether et al., 2014). In brief, the pHAGE system utilizes four packaging vectors (Tat, Rev, Gag/Pol, and VSV-G). The virus was packaged by co-transfecting 1.2 x 10^6 HEK 293T cells per well of a six-well cell culture plate with the backbone vector and the four packaging vectors in the following proportions (Backbone: 5, Tat: 0.5, Rev: 0.5, Gag/Pol: 0.5, VSV-G: 1) using Effectene (Qiagen) transfection reagent. After 48 hrs, the virus was harvested and filtered through a 0.45 µm filter. Virus was concentrated using Lenti-x concentrator (Clontech) and resuspended in 47.5% DMEM (4.5 g/L glucose) 47.5% F12, 10% FBS, 100 U/ml penicillin, and 100 g/ml streptomycin and 5 µg/ml polybrene (Sigma). Virus was added to cells plated at 1.25 x 10^5 cells per well of a six-well cell culture plate. After 48 hrs, the medium was changed and the cells drug

selected with 50 µg/ml of Nourseothricin N-acetyl transferase (Kochupurakkal and Iglehart, 2013) (Sigma) for 72 hrs.

Fluorescence Pulse-Chase Trafficking Assay

The fluorescence pulse-chase assay was previously described (Follit and Pazour, 2013; Follit et al., 2014). In brief, cells expressing DNA constructs fused to the SNAP tag were incubated with 0.04 µM cell permeable nonfluorescent benzylguanine block (SNAP-Cell Block; New England Biolabs) for 20 minutes to block all binding sites on the SNAP tag. The cells were then washed three times with complete growth media and were allowed to synthesize new protein for 1.5 hrs. Next, a final concentration of 20 mM HEPES, pH 7.4 and 150 µg/ml cycloheximide was added. The temperature was shifted to 19˚C for 2 hrs to allow accumulation of newly synthesized protein at the Golgi apparatus. The cells were shifted back to 37˚C, allowing newly synthesized protein to be released from the Golgi. Cells were fixed at the indicated time points and labeled with 0.3 µM fluorescent SNAP-TMR STAR (New England Biolabs).

Immunofluorescence

Immunofluorescence microscopy was described previously (Follit et al., 2006). Cells were grown on coverslips and fixed for 15 minutes with 2% paraformaldehyde in PHEM (0.05 M Pipes, 0.025 M HEPES, 0.01 M EGTA, 0.01 M $MgCl_2$, pH 7.2) followed by membrane permeabilization with 0.1% Triton X-100 in PHEM with 2% paraformaldehyde for 2 minutes. In some instances, cells were

treated with 0.05% SDS in PBS for 5 min to recover antigens. To visualize basal bodies, cells were pre-extracted with 0.1% Triton X-100 in PHEM for 1 minute, followed by fixation in cold 100% methanol for 10 minutes. Cells were washed with 1X phosphate buffered saline (PBS) and blocked in 1% bovine serum albumin in 1X TBST (150 mM NaCl, 1% Tween 20, 50 mM Tris pH 7.5) for 1 hr. Primary antibodies were diluted in blocking solution and incubated for 2 hrs at room temperature. Cells were washed four times with blocking solution over 20 minutes. Next, they were incubated with 1:2000 dilutions of either Alexa -488, -568, -594, -647, and 680-conjugated IgG anti-mouse or IgG anti-rabbit (Thermo Fisher), SNAP TMR STAR (New England Bio Labs) for 1 hr. Cells were then washed again with blocking solution followed by three washes with 1X PBS. Coverslips were mounted onto slides with prolong medium (Molecular Probes).

Immunoprecipitations and Immunoblotting

Immunoprecipitation assays were previously described (Follit et al., 2009). Cells were washed once with cold 1X PBS + 1mM PMSF. They were lysed with Cell lytic buffer (Sigma) supplemented with 0.1 % NP-40 (Sigma), 0.1% CHAPSO (BioRad) and 1X Complete Protease Inhibitors (Roche) then rotated at 4˚C for 10 minutes. After centrifugation, the supernatant was incubated with pre-washed Anti-Flag M2 affinity gel beads (Sigma) for 90 minutes at 4˚C. The beads were washed three times with TBST (300 mM NaCl, 1% Tween 20, 50 mM Tris pH 7.5), followed by three washes with TBS (150 mM NaCl, 50 mM Tris pH 7.5).

Flag tagged proteins were eluted from the beads using 200 µg/ml 3X Flag peptide (Sigma).

Immunoblotting was performed as previously described (Pazour et al., 1998). Total-cell lysates were harvested by washing the cells once with cold 1X PBS then scraping the cells into protein denaturing buffer and passing it through a 22-gauge needle. Samples were run on SDS-PAGE and transferred to polyvinylidene difluoride membrane at 4˚C overnight. Polyvinylidene difluoride was equilibrated with 1X TBST (150 mM NaCl, 1% Tween 20, 50 mM Tris pH 7.5) for 10 minutes, and membranes were blocked with 5% nonfat dry milk in 1X TBST supplemented with 1% fish gelatin (Sigma) for 30 minutes. Primary antibodies were diluted in the blocking solution as recommended by the manufacturer and incubated with the membrane for 2 hrs at room temperature. Goat anti-rabbit-IgG, (H+L) or Goat anti-mouse-IgG, (H+L) Horseradish peroxidase-conjugated secondary antibodies (Thermo Fisher) and Dura Western Substrate (Pierce) were used to detect the primary antibodies. Immunoblot images were acquired using either a LAS-3000 imaging system (Fujifilm, Tokyo, Japan) or a Molecular Imager Chemi Doc^{TM} XRS+ imaging system (BioRad).

Primary antibodies used include anti-MmPallidin (a gift from E. Dell'Angelica, University of California, Los Angeles School of Medicine, Los Angeles, CA) (Nazarian et al., 2006), anti-MmDTNBP1 (11132-1-AP, Proteintech), anti-MmExo70 (70X13F3, Sigma), anti-MmSec8 (14G1, Stressgen), anti-gamma tubulin (GTU88, Sigma), anti-gamma tubulin (a gift from S. Doxsey,

University of Massachusetts Medical School, Worcester, MA) (Zheng et al., 1995), anti-SpAcetylated tubulin (6-11B-1, Sigma), anti-Flag (F1804, Sigma), anti-MmArl13b (N295B/66, Davis/NIH NeuroMab Facility), anti-MmSmoothened (E-5, Santa Cruz), anti-MmAQP2 (SAB5200110, Sigma), anti-MmRab11 (47, BD Transduction Laboratories), anti-MmRab11 (20229-1-AP, Proteintech), anti-MmIFT20 (Pazour et al., 2002a), anti-MmGMAP210 (Follit et al., 2008), anti-MmPkd2 (Pazour et al., 2002b), anti-MmIFT27 (Follit et al., 2009), and anti-MmIFT88 (Pazour et al., 2002a).

Mouse Breeding

All mouse work was approved by the Institutional Animal Care and Use Committee (IACUC) at Emory University. All mice were in C57BL/6 background and are described in (Larimore et al., 2014).

Histology

Harvesting and Fixing Tissues

Wild type and *Dtnbp1*$^{sdy/sdy}$ and *Pldn*$^{pa/pa}$ mice were sacrificed with CO_2 narcosis followed by cervical dislocation. Kidneys were harvested and fixed in 4% paraformaldehyde in 1X PBS overnight at 4˚C, followed by paraffin embedding (Jonassen et al., 2008).

Hematoxylin and Eosin staining

Paraffin tissue sections were dewaxed using SafeClear (Fisher Diagnostics) and rehydrated with graded aqueous solutions of ethanol. The

sections were stained in CAT Hematoxylin solution (Biocare Medical) for 8 minutes followed by washing in running tap water for 5 minutes and differentiation in 2% hydrochloric acid in 70% ethanol for 30 seconds. The sections were washed in running tap water for 1 minute before Bluing in Tacha's Bluing Solution (Biocare Medical) for 1 minute followed by washing in running tap water for 5 minutes. Next, the samples were dipped ten times in 95% ethanol, counterstained in Edgar Degas Eosin solution (Biocare Medical) for 1 minute and washed three times in 100% ethanol for 1 minute. Last, the sections were cleared in two changes of xylene for 5 minutes and mounted with Permount (Fisher Scientific) (San Agustin et al., 2016).

Immunohistochemistry

Paraffin sections were dewaxed and rehydrated as described above. Antigen retrieval was performed in 10 mM sodium citrate, pH 6.0, in the autoclave for 40 minutes at 121˚C. Samples were cooled to ambient temperature and equilibrated in 1X TBS (50 mM Tris-buffered saline, pH 7.4) for 5 minutes, followed by blocking in 4% non-immune goat serum, 0.1% cold water fish skin gelatin (Sigma), 0.1% Triton X-100, in 1X TBST (150 mM NaCl, 1% Tween 20, 50 mM Tris pH 7.5) for 30 minutes. Sections were washed in 1X TBST and incubated with primary antibodies or 488-conjugated *Lotus tetragonolobus* agglutinin (LTA) (Vector Laboratories) diluted in 0.1% cold water fish skin gelatin in 1X TBST overnight at 4˚C. Next, samples were washed with 1X TBST and incubated with 1:1000 dilutions of secondary antibodies diluted in 0.1% cold water fish skin

gelatin in 1X TBST for 1 hr. Last, the sections were washed with 1X TBST, rinsed with 1X TBS, dipped in 1X TBS supplemented with 1 mg/ml DAPI for 5 seconds, and mounted with Prolong Gold (Life Technologies) (San Agustin et al., 2016).

Microscopy

Wide-field images were captured using an Orca ER camera on a Zeiss Axiovert 200M microscope equipped with either a EC plan-Neofluar 40X/1.3 NA oil or Plan-Apochromat 100X/1.4 NA oil Zeiss objective (Thornwood, NY) using Openlab software (Improvision, Lexington, MA). Immunohistochemistry images were captured using a DFC365 FX camera (Leica) on a LEICA TCS SPE DM 500 Q confocal microscope (Leica) equipped with an ACS Apo 40X/1.15 NA oil Leica objective. Z-stacks were acquired using Leica Application Suite Advanced Fluorescence software and converted to single planes by maximum projection with ImageJ software. Bright field images were acquired with a Zeiss Axioskop 2 Plus using a N-Achroplan 2.5X/0.07 NA air Zeiss objective equipped with an Axiocam HRC color digital camera and Axiovision acquisition software. All images were acquired at room temperature.

Data Analysis

Quantification of fluorescent pixel intensity, immunoblot pixel intensity, and length was measured using the measurement tools of ImageJ. Linear regression and statistical analysis was determined using Graph Pad Prism software. Linear regression analysis of newly synthesized membrane protein delivery to the cilium

was performed on selected time points: 0, 1, 2 Hours for CD8-FibrocystinCTS-SNAP; 0, 1, 2, 4, 6 Hours for Polycystin-2-GFP-SNAP; and 0, 1, 2, 4, 6 Hours for Smoothened-SNAP-GFP. The time points were chosen by determining which data points remained linear before (or if) reaching a plateau in the control groups. The slope values obtained from this analysis represent the trafficking rates of newly synthesized membrane protein delivery to the cilium. Slope values between control and experimental groups were compared with one another to determine statistical significance. Data was subjected to either unpaired Student's t test or One-way ANOVA and Bonferroni or Tukey's multiple comparisons test where * $p < 0.05$, ** $p < 0.01$, *** $p < 0.001$, **** $p < 0.0001$ and ns = non-significant.

Chapter V : Conclusion

My thesis work supports the hypothesis that membrane protein receptors use distinct molecular machineries and trafficking routes for delivery to the primary cilium. This chapter will summarize my findings, discuss future inquiries, and provide experimental approaches that can be used to address these questions. This conclusion will guide the next group of researchers who are investigating the targeting of membrane proteins to cilia.

Golgi-IFT Complex

Polycystin-2 and fibrocystin trafficking to cilia is dependent on IFT20 and GMAP210, which is consistent with loss of function IFT20 animals having a cystic kidney phenotype (Jonassen et al., 2008). I hypothesize that loss of function GMAP210 animals will also have cystic kidneys. Because GMAP210 null animals die after birth due to heart and lung defects, a Cre-Lox recombination system will need to be used to delete GMAP210 in the kidneys of adult animals (Follit et al., 2008). If the GMAP210 loss of function animals have cystic kidneys then this result would further support the involvement of GMAP210 in trafficking cystoproteins to cilia.

Smoothened trafficking to cilia is independent of IFT20 and GMAP210 suggesting that smoothened ciliary transport might be independent of IFT. To address this question, the IFT machinery has to be removed or disrupted in pre-existing cilia and then examined for ciliary receptor localization. This method is

widely used in *Chlamydomonas reinhardtii* IFT temperature sensitive mutants that have fully formed cilia before being shifted to a non-permissive temperature to disrupt the function of a protein of interest (Kozminski et al., 1995). However, *Chlamydomonas reinhardtii* do not express smoothened and there is currently no method to do these types of temperature sensitive mutant experiments in mammalian cells. An auxin-inducible degron (AID) system can be used in mammalian cells to test whether IFT is required for receptor trafficking to cilia. Auxin is a plant hormone that promotes the interaction of a specific E3 ubiquitin ligase with an AID allowing for its degradation by the proteasome (Nishimura et al., 2009). The AID can be fused to any protein of interest and can be co-expressed with the specific E3 ubiquitin ligase, allowing for rapid depletion of a protein of interest (within thirty minutes) in the presence of auxin (Nishimura et al., 2009). An IFT20 null mammalian cell line will express both exogenous IFT20 fused to the AID and the E3 ubiquitin ligase, then the cells will be treated with auxin to rapidly target the exogenous IFT20 for degradation which will disrupt the IFT system. Time points can be taken to analyze receptor localization at the cilium in the absence of IFT. This method is certainly feasible but the main concern would be how long the cilium would still be present after addition of auxin to the cells.

IFT20 interacts with both the exocyst and BLOC-1 and these complexes are involved in membrane protein trafficking to cilia. The BirA proximal biotinylation system can be used to identify new proteins that potentially interact

with IFT20 and may be required for ciliary receptor targeting. BirA is a biotin protein ligase that can be fused to any protein of interest and when BirA is in the presence of biotin it can biotinylate proteins that are within an estimated proximity of 20 – 30nm of the bait protein (Roux et al., 2012). A streptavidin pull down can then be used to recover the biotinylated proteins for mass spectrometry analysis. The advantage of the BirA proximal biotinylation system is that it allows for the identification of weak or transient protein interactions that may not be detectable through conventional pull down methods. IFT20 null mammalian cells expressing IFT20 fused to the BirA will be treated with biotin, then pull down and mass spectrometry analysis will be performed on the cell lysates. Cloning and immunoprecipitation methods can be used to validate the potential interactions with IFT20. A possible concern is that the BirA tag may interfere with the cellular localization of IFT20 and fluorescence microscopy will need to be performed to ensure the proper localization of the fusion protein.

Exocyst

Fibrocystin and polycystin-2 trafficking to cilia is dependent on the exocyst complex. It would be exciting to identify the target membrane location at the base of the cilium where the exocyst is tethering newly delivered receptor-carrying vesicles. To test this question, SNAP tag pulse-chase trafficking assays can be performed using either total internal reflection fluorescence microscopy (TIRFM) or superresolution structured illumination microscopy (SIM). TIRFM uses near field excitation close to the cell surface to identify vesicle-tethering events in

living cells and this method can utilize three different colors to detect proteins of interest (Axelrod, 2008; Toomre and Bewersdorf, 2010). For example, mammalian cells will express both the polycystin-2(1-703)-GFP-SNAP construct and the exocyst subunit Sec8 fused to a fluorescent tag. The GFP tag will label the cilium, the SNAP tag will mark the newly delivered receptor, and Sec8 will label the exocyst at the base of the cilium. The cells will be imaged after temperature shift from 19˚C to 37˚C when membrane proteins are released from the Golgi apparatus and an increase in the co-localization of newly delivered receptors with the exocyst at the base of the cilium over time would be expected. The caveat with the TIRFM method is that it will require a lot of optimization in regards to microscope settings and the choice of fluorescent molecules.

SIM can be used to identify membrane protein tethering at the base of cilia in fixed cells. SIM excites the sample with patterned light and uses data processing to yield the super-resolved image at an *x*-*y*-resolution of ~100nm (Toomre and Bewersdorf, 2010). Unlike other superresolution microscopy techniques, SIM is highly compatible with fluorophores used in standard wide-field imaging. The same experimental method described for TIRFM will be used except the cells will be fixed and stained at different time points. I would expect to see an increase in the co-localization of newly delivered protein with the exocyst at the base of the cilium over time. The SIM method will also require experimental optimization and storage space for the large data files.

Smoothened trafficking to cilia is independent of the exocyst which was surprising because the exocyst complexes located on the basolateral membrane of epithelial cells were thought to tether smoothened carrying vesicles due to its proposed use of the lateral trafficking pathway (Grindstaff et al., 1998; Milenkovic et al., 2009). Other protein complexes could be tethering smoothened at target membranes during the process of ciliary transport. The BirA proximal biotinylation system can be used to identify new proteins that potentially interact with smoothened and these proteins may be involved in receptor trafficking. Once these protein interactions are validated, they can then be tested for their involvement in smoothened delivery to cilia using the SNAP tag fluorescence based pulse-chase assay.

Knockdown of the exocyst in mammalian cells reduces the steady-state levels of the peripheral membrane protein Arl13b at the cilium implying that the exocyst is involved in its trafficking to cilia. To address this question, the SNAP tag fluorescence based pulse-chase trafficking assay can be performed on exocyst knockdown cells expressing an Arl13b-SNAP-GFP construct and a reduction in Arl13b ciliary trafficking would be expected. A possible concern is that the SNAP and GFP tags may interfere with the cellular localization of Arl13b and fluorescence microscopy will need to be performed to ensure that the fusion protein localizes at the cilium.

BLOC-1

Polycystin-2 but not fibrocystin or smoothened trafficking to cilia is dependent on BLOC-1, which supports the involvement of the BLOC-1 complex in trafficking specific receptors to the cilium. It would be interesting to find other membrane proteins that are dependent on BLOC-1 for their delivery to cilia. The BLOC-1 subunit dysbindin is a schizophrenia susceptibility gene and patients diagnosed with schizophrenia are treated with antipsychotic drugs that target dopamine receptors (Hartwig et al., 2017; Seeman, 2013; Talbot et al., 2004; Weickert et al., 2008). Dopamine receptors-1, -2, and -5 localize at the cilium and dysbindin is involved in the trafficking of dopamine receptor-2 to the cell surface (Iizuka et al., 2007; Ji et al., 2009; Marley and von Zastrow, 2010a). I hypothesize that dysbindin regulates the transport of dopamine receptors to cilia and this question can be tested by performing the fluorescence based pulse-chase trafficking assay on dysbindin knockdown cells expressing dopamine receptors fused to both a SNAP and GFP tag. I expect that the dysbindin knockdown cells will show a reduction in the trafficking of specific dopamine receptors to cilia. A possible concern is that ciliary targeting of the dopamine receptors is independent of dysbindin but this result will still be informative because it indicates that dopamine receptors use a different trafficking mechanism for delivery to the cell surface and cilia.

The scaffolding protein disrupted in schizophrenia-1 (DISC-1) is also a schizophrenia susceptibility gene and it localizes at the base of the cilium (Marley and von Zastrow, 2010a; Millar et al., 2000). Yeast-II hybrid screen analysis

suggests that DISC-1 potentially interacts with IFT20, which implies that it may be involved in receptor trafficking to cilia (Camargo et al., 2007). To determine if DISC-1 interacts with IFT20, immunoprecipitation experiments will be performed on mammalian cells expressing DISC-1 fused to a Flag tag. The caveat to this experiment is that there may not be an interaction and new IFT20 interacting proteins will be identified using the previously described BirA proximal biotinylation system. If DISC-1 interacts with IFT20, than it would be interesting to test whether it is involved in selective dopamine receptor trafficking to cilia by performing the fluorescence based pulse-chase trafficking assay on DISC-1 knockdown cells. A possible concern is that DISC-1 is not involved in dopamine receptor trafficking and then other neuronal receptors such as SSTR3 and MCHR1 can be examined to determine if they are dependent on DISC-1 for ciliary transport (Berbari et al., 2008b).

DISC-1 loss of function animals display schizophrenia associated behavioral phenotypes and it would be intriguing to perform behavioral experiments on mice with IFT20 deleted from their brain tissue to ascertain if they exhibit a similar phenotype (Clapcote et al., 2007). Examples of behavioral tests include an acoustic startle response that examines information selection processing which is reduced in patients diagnosed with schizophrenia (Geyer and Ellenbroek, 2003). Maze tests can also be used to investigate memory loss and increased anxiety which are characteristics that are observed in schizophrenia patients (Arguello and Gogos, 2006).

The heterotetrameric adaptor protein-3 (AP-3) complex interacts with BLOC-1 and is involved in trafficking proteins from endosomes to lysosomes and lysosome related organelles, indicating that AP-3 may play a role in receptor targeting to cilia (Gokhale et al., 2016; Gokhale et al., 2012; Sitaram et al., 2012). To answer this question, fluorescence based pulse-chase trafficking assays can be performed on AP-3 knockdown cells expressing polycystin-2(1-703)-GFP-SNAP and a reduction in receptor ciliary trafficking would be expected because polycystin-2 delivery to cilia is dependent on BLOC-1. The caveat to this experiment is that AP-3 may not be involved in polycystin-2 targeting to cilia and this result will still be informative because it implies that BLOC-1 targeting of polycystin-2 to cilia is independent of AP-3.

Loss of function BLOC-1 animals have cystic kidneys, indicating that AP-3 loss of function animals may also have a cystic kidney phenotype. To test this hypothesis, hematoxylin and eosin staining and immunohistochemistry can be performed on kidneys from AP-3 animals. BLOC-1 and AP-3 loss of function animals both have severe pigmentation and platelet aggregation phenotypes which strongly suggests that the AP-3 animals will also have cystic kidneys (Feng et al., 1999; Huang et al., 1999). The presence of a cystic kidney phenotype in the AP-3 animals will further support its involvement in receptor trafficking to cilia.

Recycling Trafficking Pathway

The peripheral membrane protein Arl13b was observed accumulating at Rab11 positive endosomes in mammalian cells expressing the dominant negative MyoVb C-terminal tail construct, which perturbs trafficking through endosomes, inferring that Arl13b may be utilizing the recycling trafficking pathway for ciliary delivery. To address this question, the total steady-state levels of endogenous Arl13b at the cilium can be measured in cells expressing the dominant negative MyoVb motor. Fluorescence based pulse-chase trafficking assays can also be performed on cells expressing both the dominant negative MyoVb motor and Arl13b fused to the SNAP and GFP tag. Additionally, the same Arl13b experiments described above can be performed in cells expressing dominant negative Rab11a, which is another method to disrupt the endosome system (Hehnly and Doxsey, 2014). I would expect the steady-state levels of Arl13b at the cilium and the trafficking rate of Arl13b to cilia to be reduced in these experiments if it is using the recycling pathway. If Arl13b is not traversing through endosomes to localize at cilia than this will still be an informative result that supports the use of distinct membrane protein trafficking pathways to cilia.

Closing Remarks

The membrane proteins receptors fibrocystin, polycystin-2, and smoothened are most likely taking different trafficking pathways to the primary cilium. It is still unclear why these receptors are using different trafficking pathways and it might be due to the cell customizing preexisting intracellular transport routes through the process of evolution. Continued investigation is required to identify the

trafficking pathways that are used by specific ciliary membrane proteins and the molecular machineries required for their targeting to the cilium.

Chapter VI : Bibliography

Alcedo, J., M. Ayzenzon, T. Von Ohlen, M. Noll, and J.E. Hooper. 1996. The Drosophila smoothened gene encodes a seven-pass membrane protein, a putative receptor for the hedgehog signal. *Cell*. 86:221-232.

Alessandri, J.L., N. Dagoneau, J.M. Laville, J. Baruteau, J.C. Hebert, and V. Cormier-Daire. 2010. RAB23 mutation in a large family from Comoros Islands with Carpenter syndrome. *Am J Med Genet A*. 152A:982-986.

Anderson, R.G. 1972. The three-dimensional structure of the basal body from the rhesus monkey oviduct. *J Cell Biol*. 54:246-265.

Ang, A.L., T. Taguchi, S. Francis, H. Folsch, L.J. Murrells, M. Pypaert, G. Warren, and I. Mellman. 2004. Recycling endosomes can serve as intermediates during transport from the Golgi to the plasma membrane of MDCK cells. *J Cell Biol*. 167:531-543.

Arguello, P.A., and J.A. Gogos. 2006. Modeling madness in mice: one piece at a time. *Neuron*. 52:179-196.

Awata, J., S. Takada, C. Standley, K.F. Lechtreck, K.D. Bellve, G.J. Pazour, K.E. Fogarty, and G.B. Witman. 2014. NPHP4 controls ciliary trafficking of membrane proteins and large soluble proteins at the transition zone. *J Cell Sci*. 127:4714-4727.

Axelrod, D. 2008. Chapter 7: Total internal reflection fluorescence microscopy. *Methods Cell Biol*. 89:169-221.

Badgandi, H.B., S.H. Hwang, I.S. Shimada, E. Loriot, and S. Mukhopadhyay. 2017. Tubby family proteins are adapters for ciliary trafficking of integral membrane proteins. *J Cell Biol*. 216:743-760.

Barnes, N.M., and T. Sharp. 1999. A review of central 5-HT receptors and their function. *Neuropharmacology*. 38:1083-1152.

Berbari, N.F., A.D. Johnson, J.S. Lewis, C.C. Askwith, and K. Mykytyn. 2008a. Identification of ciliary localization sequences within the third intracellular loop of G protein-coupled receptors. *Mol Biol Cell*. 19:1540-1547.

Berbari, N.F., N.W. Kin, N. Sharma, E.J. Michaud, R.A. Kesterson, and B.K. Yoder. 2011. Mutations in Traf3ip1 reveal defects in ciliogenesis, embryonic development, and altered cell size regulation. *Dev Biol*. 360:66-76.

Berbari, N.F., J.S. Lewis, G.A. Bishop, C.C. Askwith, and K. Mykytyn. 2008b. Bardet-Biedl syndrome proteins are required for the localization of G protein-coupled receptors to primary cilia. *Proc Natl Acad Sci U S A*. 105:4242-4246.

Berbari, N.F., A.K. O'Connor, C.J. Haycraft, and B.K. Yoder. 2009. The primary cilium as a complex signaling center. *Curr Biol*. 19:R526-535.

Besharse, J.C., J.G. Hollyfield, and M.E. Rayborn. 1977. Turnover of rod photoreceptor outer segments. II. Membrane addition and loss in relationship to light. *J Cell Biol*. 75:507-527.

Besharse, J.C., and C.J. Horst. 1990. The photoreceptor connecting cilium: a model for the transition zone. pp 389–417 pp.

Besharse, J.C., and K.H. Pfenninger. 1980. Membrane assembly in retinal photoreceptors I. Freeze-fracture analysis of cytoplasmic vesicles in relationship to disc assembly. *J Cell Biol*. 87:451-463.

Bijlmakers, M.J., and M. Marsh. 2003. The on-off story of protein palmitoylation. *Trends Cell Biol*. 13:32-42.

Boehlke, C., M. Bashkurov, A. Buescher, T. Krick, A.K. John, R. Nitschke, G. Walz, and E.W. Kuehn. 2010. Differential role of Rab proteins in ciliary trafficking: Rab23 regulates smoothened levels. *J Cell Sci*. 123:1460-1467.

Bouck, G.B. 1971. The structure, origin, isolation, and composition of the tubular mastigonemes of the Ochromas flagellum. *J Cell Biol*. 50:362-384.

Brailov, I., M. Bancila, M.J. Brisorgueil, M.C. Miquel, M. Hamon, and D. Verge. 2000. Localization of 5-HT(6) receptors at the plasma membrane of neuronal cilia in the rat brain. *Brain Res*. 872:271-275.

Burns, M.E., and V.Y. Arshavsky. 2005. Beyond counting photons: trials and trends in vertebrate visual transduction. *Neuron*. 48:387-401.

Cai, Y., Y. Maeda, A. Cedzich, V.E. Torres, G. Wu, T. Hayashi, T. Mochizuki, J.H. Park, R. Witzgall, and S. Somlo. 1999. Identification and characterization of polycystin-2, the PKD2 gene product. *J Biol Chem*. 274:28557-28565.

Camargo, L.M., V. Collura, J.C. Rain, K. Mizuguchi, H. Hermjakob, S. Kerrien, T.P. Bonnert, P.J. Whiting, and N.J. Brandon. 2007. Disrupted in Schizophrenia 1 Interactome: evidence for the close connectivity of risk genes and a potential synaptic basis for schizophrenia. *Mol Psychiatry*. 12:74-86.

Cantagrel, V., J.L. Silhavy, S.L. Bielas, D. Swistun, S.E. Marsh, J.Y. Bertrand, S. Audollent, T. Attie-Bitach, K.R. Holden, W.B. Dobyns, D. Traver, L. Al-Gazali, B.R. Ali, T.H. Lindner, T. Caspary, E.A. Otto, F. Hildebrandt, I.A. Glass, C.V. Logan, C.A. Johnson, C. Bennett, F. Brancati, G. International Joubert Syndrome Related Disorders Study, E.M. Valente, C.G. Woods, and J.G. Gleeson. 2008. Mutations in the cilia gene ARL13B lead to the classical form of Joubert syndrome. *Am J Hum Genet*. 83:170-179.

Cao, M., J. Ning, C.I. Hernandez-Lara, O. Belzile, Q. Wang, S.K. Dutcher, Y. Liu, and W.J. Snell. 2015. Uni-directional ciliary membrane protein trafficking by a cytoplasmic retrograde IFT motor and ciliary ectosome shedding. *Elife*. 4.

Caparros-Martin, J.A., A. De Luca, F. Cartault, M. Aglan, S. Temtamy, G.A. Otaify, M. Mehrez, M. Valencia, L. Vazquez, J.L. Alessandri, J. Nevado, I. Rueda-Arenas, K.E. Heath, M.C. Digilio, B. Dallapiccola, J.A. Goodship, P. Mill, P. Lapunzina, and V.L. Ruiz-Perez. 2015. Specific variants in WDR35 cause a distinctive form of Ellis-van Creveld syndrome by disrupting the recruitment of the EvC complex and SMO into the cilium. *Hum Mol Genet*. 24:4126-4137.

Caspary, T., C.E. Larkins, and K.V. Anderson. 2007. The graded response to Sonic Hedgehog depends on cilia architecture. *Dev Cell*. 12:767-778.

Cevik, S., Y. Hori, O.I. Kaplan, K. Kida, T. Toivenon, C. Foley-Fisher, D. Cottell, T. Katada, K. Kontani, and O.E. Blacque. 2010. Joubert syndrome Arl13b functions at ciliary membranes and stabilizes protein transport in Caenorhabditis elegans. *J Cell Biol*. 188:953-969.

Chih, B., P. Liu, Y. Chinn, C. Chalouni, L.G. Komuves, P.E. Hass, W. Sandoval, and A.S. Peterson. 2011. A ciliopathy complex at the transition zone protects the cilia as a privileged membrane domain. *Nat Cell Biol*. 14:61-72.

Ciciotte, S.L., B. Gwynn, K. Moriyama, M. Huizing, W.A. Gahl, J.S. Bonifacino, and L.L. Peters. 2003. Cappuccino, a mouse model of Hermansky-Pudlak syndrome, encodes a novel protein that is part of the pallidin-muted complex (BLOC-1). *Blood*. 101:4402-4407.

Clapcote, S.J., T.V. Lipina, J.K. Millar, S. Mackie, S. Christie, F. Ogawa, J.P. Lerch, K. Trimble, M. Uchiyama, Y. Sakuraba, H. Kaneda, T. Shiroishi, M.D. Houslay, R.M. Henkelman, J.G. Sled, Y. Gondo, D.J. Porteous, and J.C. Roder. 2007. Behavioral phenotypes of Disc1 missense mutations in mice. *Neuron*. 54:387-402.

Corbit, K.C., P. Aanstad, V. Singla, A.R. Norman, D.Y. Stainier, and J.F. Reiter. 2005. Vertebrate Smoothened functions at the primary cilium. *Nature*. 437:1018-1021.

Craige, B., C.C. Tsao, D.R. Diener, Y. Hou, K.F. Lechtreck, J.L. Rosenbaum, and G.B. Witman. 2010. CEP290 tethers flagellar transition zone microtubules to the membrane and regulates flagellar protein content. *J Cell Biol*. 190:927-940.

Crouse, J.A., V.S. Lopes, J.T. Sanagustin, B.T. Keady, D.S. Williams, and G.J. Pazour. 2014. Distinct functions for IFT140 and IFT20 in opsin transport. *Cytoskeleton (Hoboken)*. 71:302-310.

Cuvillier, A., F. Redon, J.C. Antoine, P. Chardin, T. DeVos, and G. Merlin. 2000. LdARL-3A, a Leishmania promastigote-specific ADP-ribosylation factor-like protein, is essential for flagellum integrity. *J Cell Sci*. 113 (Pt 11):2065-2074.

Czarnecki, P.G., and J.V. Shah. 2012. The ciliary transition zone: from morphology and molecules to medicine. *Trends Cell Biol*. 22:201-210.

D'Souza-Schorey, C., and P. Chavrier. 2006. ARF proteins: roles in membrane traffic and beyond. *Nat Rev Mol Cell Biol*. 7:347-358.

Delevoye, C., X. Heiligenstein, L. Ripoll, F. Gilles-Marsens, M.K. Dennis, R.A. Linares, L. Derman, A. Gokhale, E. Morel, V. Faundez, M.S. Marks, and G. Raposo. 2016. BLOC-1 Brings Together the Actin and Microtubule Cytoskeletons to Generate Recycling Endosomes. *Curr Biol*. 26:1-13.

Dennis, M.K., C. Delevoye, A. Acosta-Ruiz, I. Hurbain, M. Romao, G.G. Hesketh, P.S. Goff, E.V. Sviderskaya, D.C. Bennett, J.P. Luzio, T. Galli, D.J. Owen, G. Raposo, and M.S. Marks. 2016. BLOC-1 and BLOC-3 regulate VAMP7 cycling to and from melanosomes via distinct tubular transport carriers. *J Cell Biol*. 214:293-308.

Deretic, D., L.A. Huber, N. Ransom, M. Mancini, K. Simons, and D.S. Papermaster. 1995. rab8 in retinal photoreceptors may participate in rhodopsin transport and in rod outer segment disk morphogenesis. *J Cell Sci*. 108 (Pt 1):215-224.

Deretic, D., and D.S. Papermaster. 1991. Polarized sorting of rhodopsin on post-Golgi membranes in frog retinal photoreceptor cells. *J Cell Biol*. 113:1281-1293.

Deretic, D., A.H. Williams, N. Ransom, V. Morel, P.A. Hargrave, and A. Arendt. 2005. Rhodopsin C terminus, the site of mutations causing retinal disease, regulates trafficking by binding to ADP-ribosylation factor 4 (ARF4). *Proc Natl Acad Sci U S A*. 102:3301-3306.

Di Pietro, S.M., J.M. Falcon-Perez, D. Tenza, S.R. Setty, M.S. Marks, G. Raposo, and E.C. Dell'Angelica. 2006. BLOC-1 interacts with BLOC-2 and the AP-3 complex to facilitate protein trafficking on endosomes. *Mol Biol Cell*. 17:4027-4038.

Dixon-Salazar, T.J., J.L. Silhavy, N. Udpa, J. Schroth, S. Bielas, A.E. Schaffer, J. Olvera, V. Bafna, M.S. Zaki, G.H. Abdel-Salam, L.A. Mansour, L. Selim, S. Abdel-Hadi, N. Marzouki, T. Ben-Omran, N.A. Al-Saana, F.M. Sonmez, F. Celep, M. Azam, K.J. Hill, A. Collazo, A.G. Fenstermaker, G. Novarino, N. Akizu, K.V. Garimella, C. Sougnez, C. Russ, S.B. Gabriel, and J.G. Gleeson. 2012. Exome sequencing can improve diagnosis and alter patient management. *Sci Transl Med*. 4:138ra178.

Domire, J.S., J.A. Green, K.G. Lee, A.D. Johnson, C.C. Askwith, and K. Mykytyn. 2011. Dopamine receptor 1 localizes to neuronal cilia in a dynamic process that requires the Bardet-Biedl syndrome proteins. *Cell Mol Life Sci*. 68:2951-2960.

Donaldson, J.G., and C.L. Jackson. 2011. ARF family G proteins and their regulators: roles in membrane transport, development and disease. *Nat Rev Mol Cell Biol*. 12:362-375.

Drin, G., J.F. Casella, R. Gautier, T. Boehmer, T.U. Schwartz, and B. Antonny. 2007. A general amphipathic alpha-helical motif for sensing membrane curvature. *Nat Struct Mol Biol*. 14:138-146.

Drin, G., V. Morello, J.F. Casella, P. Gounon, and B. Antonny. 2008. Asymmetric tethering of flat and curved lipid membranes by a golgin. *Science*. 320:670-673.

Dryja, T.P., T.L. McGee, E. Reichel, L.B. Hahn, G.S. Cowley, D.W. Yandell, M.A. Sandberg, and E.L. Berson. 1990. A point mutation of the rhodopsin gene in one form of retinitis pigmentosa. *Nature*. 343:364-366.

Duldulao, N.A., S. Lee, and Z. Sun. 2009. Cilia localization is essential for in vivo functions of the Joubert syndrome protein Arl13b/Scorpion. *Development*. 136:4033-4042.

Dunbar, L.A., P. Aronson, and M.J. Caplan. 2000. A transmembrane segment determines the steady-state localization of an ion-transporting adenosine triphosphatase. *J Cell Biol*. 148:769-778.

Dutcher, S.K., and E.T. O'Toole. 2016. The basal bodies of Chlamydomonas reinhardtii. *Cilia*. 5:18.

Eggenschwiler, J.T., O.V. Bulgakov, J. Qin, T. Li, and K.V. Anderson. 2006. Mouse Rab23 regulates hedgehog signaling from smoothened to Gli proteins. *Dev Biol*. 290:1-12.

Eggenschwiler, J.T., E. Espinoza, and K.V. Anderson. 2001. Rab23 is an essential negative regulator of the mouse Sonic hedgehog signalling pathway. *Nature*. 412:194-198.

Eguether, T., J.T. San Agustin, B.T. Keady, J.A. Jonassen, Y. Liang, R. Francis, K. Tobita, C.A. Johnson, Z.A. Abdelhamed, C.W. Lo, and G.J. Pazour. 2014. IFT27 links the BBSome to IFT for maintenance of the ciliary signaling compartment. *Dev Cell*. 31:279-290.

Evans, R.J., N. Schwarz, K. Nagel-Wolfrum, U. Wolfrum, A.J. Hardcastle, and M.E. Cheetham. 2010. The retinitis pigmentosa protein RP2 links pericentriolar vesicle transport between the Golgi and the primary cilium. *Hum Mol Genet*. 19:1358-1367.

Falcon-Perez, J.M., M. Starcevic, R. Gautam, and E.C. Dell'Angelica. 2002. BLOC-1, a novel complex containing the pallidin and muted proteins involved in the biogenesis of melanosomes and platelet-dense granules. *J Biol Chem*. 277:28191-28199.

Feng, L., A.B. Seymour, S. Jiang, A. To, A.A. Peden, E.K. Novak, L. Zhen, M.E. Rusiniak, E.M. Eicher, M.S. Robinson, M.B. Gorin, and R.T. Swank. 1999. The beta3A subunit gene (Ap3b1) of the AP-3 adaptor complex is altered in the mouse hypopigmentation mutant pearl, a model for Hermansky-Pudlak syndrome and night blindness. *Hum Mol Genet*. 8:323-330.

Finetti, F., L. Patrussi, D. Galgano, C. Cassioli, G. Perinetti, G.J. Pazour, and C.T. Baldari. 2015. The small GTPase Rab8 interacts with VAMP-3 to regulate the delivery of recycling T-cell receptors to the immune synapse. *J Cell Sci*. 128:2541-2552.

Fogelgren, B., S.Y. Lin, X. Zuo, K.M. Jaffe, K.M. Park, R.J. Reichert, P.D. Bell, R.D. Burdine, and J.H. Lipschutz. 2011. The exocyst protein Sec10 interacts with Polycystin-2 and knockdown causes PKD-phenotypes. *PLoS Genet*. 7:e1001361.

Fogelgren, B., N. Polgar, V.H. Lui, A.J. Lee, K.K. Tamashiro, J.A. Napoli, C.B. Walton, X. Zuo, and J.H. Lipschutz. 2015. Urothelial Defects from Targeted Inactivation of Exocyst Sec10 in Mice Cause Ureteropelvic Junction Obstructions. *PLoS One*. 10:e0129346.

Follit, J.A., L. Li, Y. Vucica, and G.J. Pazour. 2010. The cytoplasmic tail of fibrocystin contains a ciliary targeting sequence. *J Cell Biol*. 188:21-28.

Follit, J.A., and G.J. Pazour. 2013. Analysis of ciliary membrane protein dynamics using SNAP technology. *Methods Enzymol*. 524:195-204.

Follit, J.A., J.T. San Agustin, J.A. Jonassen, T. Huang, J.A. Rivera-Perez, K.D. Tremblay, and G.J. Pazour. 2014. Arf4 is required for Mammalian development but dispensable for ciliary assembly. *PLoS Genet*. 10:e1004170.

Follit, J.A., J.T. San Agustin, F. Xu, J.A. Jonassen, R. Samtani, C.W. Lo, and G.J. Pazour. 2008. The Golgin GMAP210/TRIP11 anchors IFT20 to the Golgi complex. *PLoS Genet*. 4:e1000315.

Follit, J.A., R.A. Tuft, K.E. Fogarty, and G.J. Pazour. 2006. The intraflagellar transport protein IFT20 is associated with the Golgi complex and is required for cilia assembly. *Mol Biol Cell*. 17:3781-3792.

Follit, J.A., F. Xu, B.T. Keady, and G.J. Pazour. 2009. Characterization of mouse IFT complex B. *Cell Motil Cytoskeleton*. 66:457-468.

Francis, S.S., J. Sfakianos, B. Lo, and I. Mellman. 2011. A hierarchy of signals regulates entry of membrane proteins into the ciliary membrane domain in epithelial cells. *J Cell Biol*. 193:219-233.

Franco, I., J.P. Margaria, M.C. De Santis, A. Ranghino, D. Monteyne, M. Chiaravalli, M. Pema, C.C. Campa, E. Ratto, F. Gulluni, D. Perez-Morga, S. Somlo, G.R. Merlo, A. Boletta, and E. Hirsch. 2016. Phosphoinositide 3-Kinase-C2alpha Regulates Polycystin-2 Ciliary Entry and Protects against Kidney Cyst Formation. *J Am Soc Nephrol*. 27:1135-1144.

Friedrich, G.A., J.D. Hildebrand, and P. Soriano. 1997. The secretory protein Sec8 is required for paraxial mesoderm formation in the mouse. *Dev Biol*. 192:364-374.

Fu, W., L. Wang, S. Kim, J. Li, and B.D. Dynlacht. 2016. Role for the IFT-A Complex in Selective Transport to the Primary Cilium. *Cell Rep*. 17:1505-1517.

Garcia-Gonzalo, F.R., K.C. Corbit, M.S. Sirerol-Piquer, G. Ramaswami, E.A. Otto, T.R. Noriega, A.D. Seol, J.F. Robinson, C.L. Bennett, D.J. Josifova, J.M. Garcia-Verdugo, N. Katsanis, F. Hildebrandt, and J.F. Reiter. 2011. A transition zone complex regulates mammalian ciliogenesis and ciliary membrane composition. *Nat Genet*. 43:776-784.

Geng, L., D. Okuhara, Z. Yu, X. Tian, Y. Cai, S. Shibazaki, and S. Somlo. 2006. Polycystin-2 traffics to cilia independently of polycystin-1 by using an N-terminal RVxP motif. *J Cell Sci*. 119:1383-1395.

Geng, L., Y. Segal, B. Peissel, N. Deng, Y. Pei, F. Carone, H.G. Rennke, A.M. Glucksmann-Kuis, M.C. Schneider, M. Ericsson, S.T. Reeders, and J. Zhou. 1996. Identification and localization of polycystin, the PKD1 gene product. *J Clin Invest*. 98:2674-2682.

Geyer, M.A., and B. Ellenbroek. 2003. Animal behavior models of the mechanisms underlying antipsychotic atypicality. *Prog Neuropsychopharmacol Biol Psychiatry*. 27:1071-1079.

Gillingham, A.K., and S. Munro. 2007. The small G proteins of the Arf family and their regulators. *Annu Rev Cell Dev Biol*. 23:579-611.

Gilula, N.B., and P. Satir. 1972. The ciliary necklace. A ciliary membrane specialization. *J Cell Biol*. 53:494-509.

Gokhale, A., C. Hartwig, A.H. Freeman, R. Das, S.A. Zlatic, R. Vistein, A. Burch, G. Carrot, A.F. Lewis, S. Nelms, D.K. Dickman, M.A. Puthenveedu, D.N. Cox, and V. Faundez. 2016. The Proteome of BLOC-1 Genetic Defects Identifies the

Arp2/3 Actin Polymerization Complex to Function Downstream of the Schizophrenia Susceptibility Factor Dysbindin at the Synapse. *J Neurosci*. 36:12393-12411.

Gokhale, A., J. Larimore, E. Werner, L. So, A. Moreno-De-Luca, C. Lese-Martin, V.V. Lupashin, Y. Smith, and V. Faundez. 2012. Quantitative proteomic and genetic analyses of the schizophrenia susceptibility factor dysbindin identify novel roles of the biogenesis of lysosome-related organelles complex 1. *J Neurosci*. 32:3697-3711.

Gotthardt, K., M. Lokaj, C. Koerner, N. Falk, A. Giessl, and A. Wittinghofer. 2015. A G-protein activation cascade from Arl13B to Arl3 and implications for ciliary targeting of lipidated proteins. *Elife*. 4.

Grayson, C., F. Bartolini, J.P. Chapple, K.R. Willison, A. Bhamidipati, S.A. Lewis, P.J. Luthert, A.J. Hardcastle, N.J. Cowan, and M.E. Cheetham. 2002. Localization in the human retina of the X-linked retinitis pigmentosa protein RP2, its homologue cofactor C and the RP2 interacting protein Arl3. *Hum Mol Genet*. 11:3065-3074.

Green, E.S., M.D. Menz, M.M. LaVail, and J.G. Flannery. 2000. Characterization of rhodopsin mis-sorting and constitutive activation in a transgenic rat model of retinitis pigmentosa. *Invest Ophthalmol Vis Sci*. 41:1546-1553.

Grindstaff, K.K., C. Yeaman, N. Anandasabapathy, S.C. Hsu, E. Rodriguez-Boulan, R.H. Scheller, and W.J. Nelson. 1998. Sec6/8 complex is recruited to cell-cell contacts and specifies transport vesicle delivery to the basal-lateral membrane in epithelial cells. *Cell*. 93:731-740.

Gundersen, G.G., and H.J. Worman. 2013. Nuclear positioning. *Cell*. 152:1376-1389.

Hamon, M., E. Doucet, K. Lefevre, M.C. Miquel, L. Lanfumey, R. Insausti, D. Frechilla, J. Del Rio, and D. Verge. 1999. Antibodies and antisense oligonucleotide for probing the distribution and putative functions of central 5-HT6 receptors. *Neuropsychopharmacology*. 21:68S-76S.

Handel, M., S. Schulz, A. Stanarius, M. Schreff, M. Erdtmann-Vourliotis, H. Schmidt, G. Wolf, and V. Hollt. 1999. Selective targeting of somatostatin receptor 3 to neuronal cilia. *Neuroscience*. 89:909-926.

Hanke-Gogokhia, C., Z. Wu, C.D. Gerstner, J.M. Frederick, H. Zhang, and W. Baehr. 2016. Arf-like Protein 3 (ARL3) Regulates Protein Trafficking and Ciliogenesis in Mouse Photoreceptors. *J Biol Chem*. 291:7142-7155.

Harris, P.C., and V.E. Torres. 2009. Polycystic kidney disease. *Annu Rev Med*. 60:321-337.

Hartman, M.A., and J.A. Spudich. 2012. The myosin superfamily at a glance. *J Cell Sci*. 125:1627-1632.

Hartwig, C., W.J. Monis, X. Chen, D.K. Dickman, G.J. Pazour, and V. Faundez. 2017. Neurodevelopmental Disease Mechanisms, Primary Cilia, and Endosomes Converge on the BLOC-1 and BORC Complexes. *Dev Neurobiol*.

Hayes, M.J., K. Bryon, J. Satkurunathan, and T.P. Levine. 2011. Yeast homologues of three BLOC-1 subunits highlight KxDL proteins as conserved interactors of BLOC-1. *Traffic*. 12:260-268.

He, B., F. Xi, X. Zhang, J. Zhang, and W. Guo. 2007. Exo70 interacts with phospholipids and mediates the targeting of the exocyst to the plasma membrane. *EMBO J*. 26:4053-4065.

Hehnly, H., C.T. Chen, C.M. Powers, H.L. Liu, and S. Doxsey. 2012. The centrosome regulates the Rab11- dependent recycling endosome pathway at appendages of the mother centriole. *Curr Biol*. 22:1944-1950.

Hehnly, H., and S. Doxsey. 2014. Rab11 endosomes contribute to mitotic spindle organization and orientation. *Dev Cell*. 28:497-507.

Heider, M.R., M. Gu, C.M. Duffy, A.M. Mirza, L.L. Marcotte, A.C. Walls, N. Farrall, Z. Hakhverdyan, M.C. Field, M.P. Rout, A. Frost, and M. Munson. 2016. Subunit connectivity, assembly determinants and architecture of the yeast exocyst complex. *Nat Struct Mol Biol*. 23:59-66.

Heider, M.R., and M. Munson. 2012. Exorcising the exocyst complex. *Traffic*. 13:898-907.

Hildebrandt, F., T. Benzing, and N. Katsanis. 2011. Ciliopathies. *N Engl J Med*. 364:1533-1543.

Hilgendorf, K.I., C.T. Johnson, and P.K. Jackson. 2016. The primary cilium as a cellular receiver: organizing ciliary GPCR signaling. *Curr Opin Cell Biol*. 39:84-92.

Hirano, T., Y. Katoh, and K. Nakayama. 2017. Intraflagellar transport-A complex mediates ciliary entry and retrograde trafficking of ciliary G protein-coupled receptors. *Mol Biol Cell*. 28:429-439.

Horn, H.F., Z. Brownstein, D.R. Lenz, S. Shivatzki, A.A. Dror, O. Dagan-Rosenfeld, L.M. Friedman, K.J. Roux, S. Kozlov, K.T. Jeang, M. Frydman, B. Burke, C.L. Stewart, and K.B. Avraham. 2013. The LINC complex is essential for hearing. *J Clin Invest*. 123:740-750.

Huang, L., Y.M. Kuo, and J. Gitschier. 1999. The pallid gene encodes a novel, syntaxin 13-interacting protein involved in platelet storage pool deficiency. *Nat Genet*. 23:329-332.

Hughes, J., C.J. Ward, B. Peral, R. Aspinwall, K. Clark, J.L. San Millan, V. Gamble, and P.C. Harris. 1995. The polycystic kidney disease 1 (PKD1) gene encodes a novel protein with multiple cell recognition domains. *Nat Genet*. 10:151-160.

Hunnicutt, G.R., M.G. Kosfiszer, and W.J. Snell. 1990. Cell body and flagellar agglutinins in Chlamydomonas reinhardtii: the cell body plasma membrane is a reservoir for agglutinins whose migration to the flagella is regulated by a functional barrier. *J Cell Biol*. 111:1605-1616.

Hunziker, W., and C. Fumey. 1994. A di-leucine motif mediates endocytosis and basolateral sorting of macrophage IgG Fc receptors in MDCK cells. *EMBO J*. 13:2963-2969.

Hurd, T.W., S. Fan, and B.L. Margolis. 2011. Localization of retinitis pigmentosa 2 to cilia is regulated by Importin beta2. *J Cell Sci*. 124:718-726.

Huttlin, E.L., L. Ting, R.J. Bruckner, F. Gebreab, M.P. Gygi, J. Szpyt, S. Tam, G. Zarraga, G. Colby, K. Baltier, R. Dong, V. Guarani, L.P. Vaites, A. Ordureau, R. Rad, B.K. Erickson, M. Wuhr, J. Chick, B. Zhai, D. Kolippakkam, J. Mintseris, R.A. Obar, T. Harris, S. Artavanis-Tsakonas, M.E. Sowa, P. De Camilli, J.A. Paulo, J.W. Harper, and S.P. Gygi. 2015. The BioPlex Network: A Systematic Exploration of the Human Interactome. *Cell*. 162:425-440.

Iizuka, Y., Y. Sei, D.R. Weinberger, and R.E. Straub. 2007. Evidence that the BLOC-1 protein dysbindin modulates dopamine D2 receptor internalization and signaling but not D1 internalization. *J Neurosci*. 27:12390-12395.

Jahn, R., and R.H. Scheller. 2006. SNAREs--engines for membrane fusion. *Nat Rev Mol Cell Biol*. 7:631-643.

Jenkins, D., D. Seelow, F.S. Jehee, C.A. Perlyn, L.G. Alonso, D.F. Bueno, D. Donnai, D. Josifova, I.M. Mathijssen, J.E. Morton, K.H. Orstavik, E. Sweeney, S.A. Wall, J.L. Marsh, P. Nurnberg, M.R. Passos-Bueno, and A.O. Wilkie. 2007. RAB23 mutations in Carpenter syndrome imply an unexpected role for hedgehog signaling in cranial-suture development and obesity. *Am J Hum Genet*. 80:1162-1170.

Jenkins, P.M., T.W. Hurd, L. Zhang, D.P. McEwen, R.L. Brown, B. Margolis, K.J. Verhey, and J.R. Martens. 2006. Ciliary targeting of olfactory CNG channels requires the CNGB1b subunit and the kinesin-2 motor protein, KIF17. *Curr Biol*. 16:1211-1216.

Ji, Y., F. Yang, F. Papaleo, H.X. Wang, W.J. Gao, D.R. Weinberger, and B. Lu. 2009. Role of dysbindin in dopamine receptor trafficking and cortical GABA function. *Proc Natl Acad Sci U S A*. 106:19593-19598.

Jin, H., S.R. White, T. Shida, S. Schulz, M. Aguiar, S.P. Gygi, J.F. Bazan, and M.V. Nachury. 2010. The conserved Bardet-Biedl syndrome proteins assemble a coat that traffics membrane proteins to cilia. *Cell*. 141:1208-1219.

Jonassen, J.A., J. San Agustin, J.A. Follit, and G.J. Pazour. 2008. Deletion of IFT20 in the mouse kidney causes misorientation of the mitotic spindle and cystic kidney disease. *J Cell Biol*. 183:377-384.

Jonassen, J.A., J. SanAgustin, S.P. Baker, and G.J. Pazour. 2012. Disruption of IFT complex A causes cystic kidneys without mitotic spindle misorientation. *J Am Soc Nephrol*. 23:641-651.

Keady, B.T., Y.Z. Le, and G.J. Pazour. 2011. IFT20 is required for opsin trafficking and photoreceptor outer segment development. *Mol Biol Cell*. 22:921-930.

Keady, B.T., R. Samtani, K. Tobita, M. Tsuchya, J.T. San Agustin, J.A. Follit, J.A. Jonassen, R. Subramanian, C.W. Lo, and G.J. Pazour. 2012. IFT25 links the signal-dependent movement of Hedgehog components to intraflagellar transport. *Dev Cell*. 22:940-951.

Kee, Y., J.S. Yoo, C.D. Hazuka, K.E. Peterson, S.C. Hsu, and R.H. Scheller. 1997. Subunit structure of the mammalian exocyst complex. *Proc Natl Acad Sci U S A*. 94:14438-14443.

Khan, S., I. Ullah, Irfanullah, M. Touseef, S. Basit, M.N. Khan, and W. Ahmad. 2013. Novel homozygous mutations in the genes ARL6 and BBS10 underlying Bardet-Biedl syndrome. *Gene*. 515:84-88.

Kim, H., H. Xu, Q. Yao, W. Li, Q. Huang, P. Outeda, V. Cebotaru, M. Chiaravalli, A. Boletta, K. Piontek, G.G. Germino, E.J. Weinman, T. Watnick, and F. Qian. 2014. Ciliary membrane proteins traffic through the Golgi via a Rabep1/GGA1/Arl3-dependent mechanism. *Nat Commun*. 5:5482.

Kinney, M.S., and S.K. Fisher. 1978. The photoreceptors and pigment epithelium of the larval Xenopus retina: morphogenesis and outer segment renewal. *Proc R Soc Lond B Biol Sci*. 201:149-167.

Kochupurakkal, B.S., and J.D. Iglehart. 2013. Nourseothricin N-acetyl transferase: a positive selection marker for mammalian cells. *PLoS One*. 8:e68509.

Kozminski, K.G., P.L. Beech, and J.L. Rosenbaum. 1995. The Chlamydomonas kinesin-like protein FLA10 is involved in motility associated with the flagellar membrane. *J Cell Biol*. 131:1517-1527.

Kumamoto, N., S. Matsuzaki, K. Inoue, T. Hattori, S. Shimizu, R. Hashimoto, A. Yamatodani, T. Katayama, and M. Tohyama. 2006. Hyperactivation of midbrain dopaminergic system in schizophrenia could be attributed to the down-regulation of dysbindin. *Biochem Biophys Res Commun*. 345:904-909.

Lahlou, H., J. Guillermet, M. Hortala, F. Vernejoul, S. Pyronnet, C. Bousquet, and C. Susini. 2004. Molecular signaling of somatostatin receptors. *Ann N Y Acad Sci*. 1014:121-131.

Lapierre, L.A., R. Kumar, C.M. Hales, J. Navarre, S.G. Bhartur, J.O. Burnette, D.W. Provance, Jr., J.A. Mercer, M. Bahler, and J.R. Goldenring. 2001. Myosin vb is associated with plasma membrane recycling systems. *Mol Biol Cell*. 12:1843-1857.

Larimore, J., K. Tornieri, P.V. Ryder, A. Gokhale, S.A. Zlatic, B. Craige, J.D. Lee, K. Talbot, J.F. Pare, Y. Smith, and V. Faundez. 2011. The schizophrenia susceptibility factor dysbindin and its associated complex sort cargoes from cell bodies to the synapse. *Mol Biol Cell*. 22:4854-4867.

Larimore, J., S.A. Zlatic, A. Gokhale, K. Tornieri, K.S. Singleton, A.P. Mullin, J. Tang, K. Talbot, and V. Faundez. 2014. Mutations in the BLOC-1 subunits dysbindin and muted generate divergent and dosage-dependent phenotypes. *J Biol Chem*. 289:14291-14300.

Leaf, A., and M. Von Zastrow. 2015. Dopamine receptors reveal an essential role of IFT-B, KIF17, and Rab23 in delivering specific receptors to primary cilia. *Elife*. 4.

Lechtreck, K.F., J.M. Brown, J.L. Sampaio, J.M. Craft, A. Shevchenko, J.E. Evans, and G.B. Witman. 2013. Cycling of the signaling protein phospholipase D through cilia requires the BBSome only for the export phase. *J Cell Biol*. 201:249-261.

Lechtreck, K.F., E.C. Johnson, T. Sakai, D. Cochran, B.A. Ballif, J. Rush, G.J. Pazour, M. Ikebe, and G.B. Witman. 2009. The Chlamydomonas reinhardtii BBSome is an

IFT cargo required for export of specific signaling proteins from flagella. *J Cell Biol*. 187:1117-1132.

Lei, K., X. Zhang, X. Ding, X. Guo, M. Chen, B. Zhu, T. Xu, Y. Zhuang, R. Xu, and M. Han. 2009. SUN1 and SUN2 play critical but partially redundant roles in anchoring nuclei in skeletal muscle cells in mice. *Proc Natl Acad Sci U S A*. 106:10207-10212.

Li, W., Q. Zhang, N. Oiso, E.K. Novak, R. Gautam, E.P. O'Brien, C.L. Tinsley, D.J. Blake, R.A. Spritz, N.G. Copeland, N.A. Jenkins, D. Amato, B.A. Roe, M. Starcevic, E.C. Dell'Angelica, R.W. Elliott, V. Mishra, S.F. Kingsmore, R.E. Paylor, and R.T. Swank. 2003. Hermansky-Pudlak syndrome type 7 (HPS-7) results from mutant dysbindin, a member of the biogenesis of lysosome-related organelles complex 1 (BLOC-1). *Nat Genet*. 35:84-89.

Li, Y., Q. Wei, Y. Zhang, K. Ling, and J. Hu. 2010. The small GTPases ARL-13 and ARL-3 coordinate intraflagellar transport and ciliogenesis. *J Cell Biol*. 189:1039-1051.

Li, Z.Y., F. Wong, J.H. Chang, D.E. Possin, Y. Hao, R.M. Petters, and A.H. Milam. 1998. Rhodopsin transgenic pigs as a model for human retinitis pigmentosa. *Invest Ophthalmol Vis Sci*. 39:808-819.

Liem, K.F., Jr., A. Ashe, M. He, P. Satir, J. Moran, D. Beier, C. Wicking, and K.V. Anderson. 2012. The IFT-A complex regulates Shh signaling through cilia structure and membrane protein trafficking. *J Cell Biol*. 197:789-800.

Liew, G.M., F. Ye, A.R. Nager, J.P. Murphy, J.S. Lee, M. Aguiar, D.K. Breslow, S.P. Gygi, and M.V. Nachury. 2014. The intraflagellar transport protein IFT27 promotes BBSome exit from cilia through the GTPase ARL6/BBS3. *Dev Cell*. 31:265-278.

Lisanti, M.P., I.W. Caras, M.A. Davitz, and E. Rodriguez-Boulan. 1989. A glycophospholipid membrane anchor acts as an apical targeting signal in polarized epithelial cells. *J Cell Biol*. 109:2145-2156.

Lobo, G.P., D. Fulmer, L. Guo, X. Zuo, Y. Dang, S.H. Kim, Y. Su, K. George, E. Obert, B. Fogelgren, D. Nihalani, R.A. Norris, B. Rohrer, and J.H. Lipschutz. 2017. The exocyst is required for photoreceptor ciliogenesis and retinal development. *J Biol Chem*.

Lu, Q., C. Insinna, C. Ott, J. Stauffer, P.A. Pintado, J. Rahajeng, U. Baxa, V. Walia, A. Cuenca, Y.S. Hwang, I.O. Daar, S. Lopes, J. Lippincott-Schwartz, P.K. Jackson, S. Caplan, and C.J. Westlake. 2015. Early steps in primary cilium assembly require EHD1/EHD3-dependent ciliary vesicle formation. *Nat Cell Biol*. 17:531.

Luo, G., J. Zhang, and W. Guo. 2014. The role of Sec3p in secretory vesicle targeting and exocyst complex assembly. *Mol Biol Cell*. 25:3813-3822.

Maerker, T., E. van Wijk, N. Overlack, F.F. Kersten, J. McGee, T. Goldmann, E. Sehn, R. Roepman, E.J. Walsh, H. Kremer, and U. Wolfrum. 2008. A novel Usher protein network at the periciliary reloading point between molecular

transport machineries in vertebrate photoreceptor cells. *Hum Mol Genet*. 17:71-86.
Marley, A., and M. von Zastrow. 2010a. DISC1 regulates primary cilia that display specific dopamine receptors. *PLoS One*. 5:e10902.
Marley, A., and M. von Zastrow. 2010b. Dysbindin promotes the post-endocytic sorting of G protein-coupled receptors to lysosomes. *PLoS One*. 5:e9325.
Matter, K., W. Hunziker, and I. Mellman. 1992. Basolateral sorting of LDL receptor in MDCK cells: the cytoplasmic domain contains two tyrosine-dependent targeting determinants. *Cell*. 71:741-753.
Mazelova, J., L. Astuto-Gribble, H. Inoue, B.M. Tam, E. Schonteich, R. Prekeris, O.L. Moritz, P.A. Randazzo, and D. Deretic. 2009a. Ciliary targeting motif VxPx directs assembly of a trafficking module through Arf4. *EMBO J*. 28:183-192.
Mazelova, J., N. Ransom, L. Astuto-Gribble, M.C. Wilson, and D. Deretic. 2009b. Syntaxin 3 and SNAP-25 pairing, regulated by omega-3 docosahexaenoic acid, controls the delivery of rhodopsin for the biogenesis of cilia-derived sensory organelles, the rod outer segments. *J Cell Sci*. 122:2003-2013.
McGarry, M.P., M. Borchers, E.K. Novak, N.A. Lee, P.J. Ohtake, J.J. Lee, and R.T. Swank. 2002. Pulmonary pathologies in pallid mice result from nonhematopoietic defects. *Exp Mol Pathol*. 72:213-220.
McIntyre, J.C., M.M. Hege, and N.F. Berbari. 2016. Trafficking of ciliary G protein-coupled receptors. *Methods Cell Biol*. 132:35-54.
Mellman, I., and W.J. Nelson. 2008. Coordinated protein sorting, targeting and distribution in polarized cells. *Nat Rev Mol Cell Biol*. 9:833-845.
Menezes, L.F., Y. Cai, Y. Nagasawa, A.M. Silva, M.L. Watkins, A.M. Da Silva, S. Somlo, L.M. Guay-Woodford, G.G. Germino, and L.F. Onuchic. 2004. Polyductin, the PKHD1 gene product, comprises isoforms expressed in plasma membrane, primary cilium, and cytoplasm. *Kidney Int*. 66:1345-1355.
Mick, D.U., R.B. Rodrigues, R.D. Leib, C.M. Adams, A.S. Chien, S.P. Gygi, and M.V. Nachury. 2015. Proteomics of Primary Cilia by Proximity Labeling. *Dev Cell*. 35:497-512.
Milenkovic, L., M.P. Scott, and R. Rohatgi. 2009. Lateral transport of Smoothened from the plasma membrane to the membrane of the cilium. *J Cell Biol*. 187:365-374.
Millar, J.K., J.C. Wilson-Annan, S. Anderson, S. Christie, M.S. Taylor, C.A. Semple, R.S. Devon, D.M. St Clair, W.J. Muir, D.H. Blackwood, and D.J. Porteous. 2000. Disruption of two novel genes by a translocation co-segregating with schizophrenia. *Hum Mol Genet*. 9:1415-1423.
Mochizuki, T., G. Wu, T. Hayashi, S.L. Xenophontos, B. Veldhuisen, J.J. Saris, D.M. Reynolds, Y. Cai, P.A. Gabow, A. Pierides, W.J. Kimberling, M.H. Breuning, C.C. Deltas, D.J. Peters, and S. Somlo. 1996. PKD2, a gene for polycystic kidney disease that encodes an integral membrane protein. *Science*. 272:1339-1342.

Moench, S.J., J. Moreland, D.H. Stewart, and T.G. Dewey. 1994. Fluorescence studies of the location and membrane accessibility of the palmitoylation sites of rhodopsin. *Biochemistry*. 33:5791-5796.

Monis, W.J., V. Faundez, and G.J. Pazour. 2017. BLOC-1 is required for selective membrane protein trafficking from endosomes to primary cilia. *J Cell Biol*.

Morgan, N.V., S. Pasha, C.A. Johnson, J.R. Ainsworth, R.A. Eady, B. Dawood, C. McKeown, R.C. Trembath, J. Wilde, S.P. Watson, and E.R. Maher. 2006. A germline mutation in BLOC1S3/reduced pigmentation causes a novel variant of Hermansky-Pudlak syndrome (HPS8). *Am J Hum Genet*. 78:160-166.

Moritz, O.L., B.M. Tam, L.L. Hurd, J. Peranen, D. Deretic, and D.S. Papermaster. 2001. Mutant rab8 Impairs docking and fusion of rhodopsin-bearing post-Golgi membranes and causes cell death of transgenic Xenopus rods. *Mol Biol Cell*. 12:2341-2351.

Moriyama, K., and J.S. Bonifacino. 2002. Pallidin is a component of a multi-protein complex involved in the biogenesis of lysosome-related organelles. *Traffic*. 3:666-677.

Mukhopadhyay, S., X. Wen, B. Chih, C.D. Nelson, W.S. Lane, S.J. Scales, and P.K. Jackson. 2010. TULP3 bridges the IFT-A complex and membrane phosphoinositides to promote trafficking of G protein-coupled receptors into primary cilia. *Genes Dev*. 24:2180-2193.

Mukhopadhyay, S., X. Wen, N. Ratti, A. Loktev, L. Rangell, S.J. Scales, and P.K. Jackson. 2013. The ciliary G-protein-coupled receptor Gpr161 negatively regulates the Sonic hedgehog pathway via cAMP signaling. *Cell*. 152:210-223.

Mullin, A.P., A. Gokhale, J. Larimore, and V. Faundez. 2011. Cell biology of the BLOC-1 complex subunit dysbindin, a schizophrenia susceptibility gene. *Mol Neurobiol*. 44:53-64.

Nachury, M.V., A.V. Loktev, Q. Zhang, C.J. Westlake, J. Peranen, A. Merdes, D.C. Slusarski, R.H. Scheller, J.F. Bazan, V.C. Sheffield, and P.K. Jackson. 2007. A core complex of BBS proteins cooperates with the GTPase Rab8 to promote ciliary membrane biogenesis. *Cell*. 129:1201-1213.

Nachury, M.V., E.S. Seeley, and H. Jin. 2010. Trafficking to the ciliary membrane: how to get across the periciliary diffusion barrier? *Annu Rev Cell Dev Biol*. 26:59-87.

Nager, A.R., J.S. Goldstein, V. Herranz-Perez, D. Portran, F. Ye, J.M. Garcia-Verdugo, and M.V. Nachury. 2017. An Actin Network Dispatches Ciliary GPCRs into Extracellular Vesicles to Modulate Signaling. *Cell*. 168:252-263 e214.

Nazarian, R., M. Starcevic, M.J. Spencer, and E.C. Dell'Angelica. 2006. Reinvestigation of the dysbindin subunit of BLOC-1 (biogenesis of lysosome-related organelles complex-1) as a dystrobrevin-binding protein. *Biochem J*. 395:587-598.

Newell-Litwa, K., G. Salazar, Y. Smith, and V. Faundez. 2009. Roles of BLOC-1 and adaptor protein-3 complexes in cargo sorting to synaptic vesicles. *Mol Biol Cell*. 20:1441-1453.

Nishimura, K., T. Fukagawa, H. Takisawa, T. Kakimoto, and M. Kanemaki. 2009. An auxin-based degron system for the rapid depletion of proteins in nonplant cells. *Nat Methods*. 6:917-922.

Novak, E.K., and R.T. Swank. 1979. Lysosomal dysfunctions associated with mutations at mouse pigment genes. *Genetics*. 92:189-204.

Numakawa, T., Y. Yagasaki, T. Ishimoto, T. Okada, T. Suzuki, N. Iwata, N. Ozaki, T. Taguchi, M. Tatsumi, K. Kamijima, R.E. Straub, D.R. Weinberger, H. Kunugi, and R. Hashimoto. 2004. Evidence of novel neuronal functions of dysbindin, a susceptibility gene for schizophrenia. *Hum Mol Genet*. 13:2699-2708.

Ohba, T., E.C. Schirmer, T. Nishimoto, and L. Gerace. 2004. Energy- and temperature-dependent transport of integral proteins to the inner nuclear membrane via the nuclear pore. *J Cell Biol*. 167:1051-1062.

Onnis, A., F. Finetti, L. Patrussi, M. Gottardo, C. Cassioli, S. Spano, and C.T. Baldari. 2015. The small GTPase Rab29 is a common regulator of immune synapse assembly and ciliogenesis. *Cell Death Differ*. 22:1687-1699.

Onuchic, L.F., L. Furu, Y. Nagasawa, X. Hou, T. Eggermann, Z. Ren, C. Bergmann, J. Senderek, E. Esquivel, R. Zeltner, S. Rudnik-Schoneborn, M. Mrug, W. Sweeney, E.D. Avner, K. Zerres, L.M. Guay-Woodford, S. Somlo, and G.G. Germino. 2002. PKHD1, the polycystic kidney and hepatic disease 1 gene, encodes a novel large protein containing multiple immunoglobulin-like plexin-transcription-factor domains and parallel beta-helix 1 repeats. *Am J Hum Genet*. 70:1305-1317.

Oprins, A., R. Duden, T.E. Kreis, H.J. Geuze, and J.W. Slot. 1993. Beta-COP localizes mainly to the cis-Golgi side in exocrine pancreas. *J Cell Biol*. 121:49-59.

Papermaster, D.S., B.G. Schneider, and J.C. Besharse. 1985. Vesicular transport of newly synthesized opsin from the Golgi apparatus toward the rod outer segment. Ultrastructural immunocytochemical and autoradiographic evidence in Xenopus retinas. *Invest Ophthalmol Vis Sci*. 26:1386-1404.

Pazour, G.J., S.A. Baker, J.A. Deane, D.G. Cole, B.L. Dickert, J.L. Rosenbaum, G.B. Witman, and J.C. Besharse. 2002a. The intraflagellar transport protein, IFT88, is essential for vertebrate photoreceptor assembly and maintenance. *J Cell Biol*. 157:103-113.

Pazour, G.J., and R.A. Bloodgood. 2008. Targeting proteins to the ciliary membrane. *Curr Top Dev Biol*. 85:115-149.

Pazour, G.J., J.T. San Agustin, J.A. Follit, J.L. Rosenbaum, and G.B. Witman. 2002b. Polycystin-2 localizes to kidney cilia and the ciliary level is elevated in orpk mice with polycystic kidney disease. *Curr Biol*. 12:R378-380.

Pazour, G.J., C.G. Wilkerson, and G.B. Witman. 1998. A dynein light chain is essential for the retrograde particle movement of intraflagellar transport (IFT). *J Cell Biol*. 141:979-992.

Pearring, J.N., R.Y. Salinas, S.A. Baker, and V.Y. Arshavsky. 2013. Protein sorting, targeting and trafficking in photoreceptor cells. *Prog Retin Eye Res*. 36:24-51.

Pearring, J.N., J.T. San Agustin, E.S. Lobanova, C.J. Gabriel, E.C. Lieu, W.J. Monis, M.W. Stuck, L. Strittmatter, S.M. Jaber, V.Y. Arshavsky, and G.J. Pazour. 2017. Loss of Arf4 causes severe degeneration of the exocrine pancreas but not cystic kidney disease or retinal degeneration. *PLoS Genet*. 13:e1006740.

Pearse, B.M. 1976. Clathrin: a unique protein associated with intracellular transfer of membrane by coated vesicles. *Proc Natl Acad Sci U S A*. 73:1255-1259.

Peters, K.R., G.E. Palade, B.G. Schneider, and D.S. Papermaster. 1983. Fine structure of a periciliary ridge complex of frog retinal rod cells revealed by ultrahigh resolution scanning electron microscopy. *J Cell Biol*. 96:265-276.

Pissios, P., R.L. Bradley, and E. Maratos-Flier. 2006. Expanding the scales: The multiple roles of MCH in regulating energy balance and other biological functions. *Endocr Rev*. 27:606-620.

Qian, F., F.J. Germino, Y. Cai, X. Zhang, S. Somlo, and G.G. Germino. 1997. PKD1 interacts with PKD2 through a probable coiled-coil domain. *Nat Genet*. 16:179-183.

Rauchman, M.I., S.K. Nigam, E. Delpire, and S.R. Gullans. 1993. An osmotically tolerant inner medullary collecting duct cell line from an SV40 transgenic mouse. *Am J Physiol*. 265:F416-424.

Reiter, J.F., O.E. Blacque, and M.R. Leroux. 2012. The base of the cilium: roles for transition fibres and the transition zone in ciliary formation, maintenance and compartmentalization. *EMBO Rep*. 13:608-618.

Ringo, D.L. 1967. Flagellar motion and fine structure of the flagellar apparatus in Chlamydomonas. *J Cell Biol*. 33:543-571.

Rogers, K.K., P.D. Wilson, R.W. Snyder, X. Zhang, W. Guo, C.R. Burrow, and J.H. Lipschutz. 2004. The exocyst localizes to the primary cilium in MDCK cells. *Biochem Biophys Res Commun*. 319:138-143.

Rohatgi, R., L. Milenkovic, and M.P. Scott. 2007. Patched1 regulates hedgehog signaling at the primary cilium. *Science*. 317:372-376.

Rosenbaum, J.L., and G.B. Witman. 2002. Intraflagellar transport. *Nat Rev Mol Cell Biol*. 3:813-825.

Roux, K.J., D.I. Kim, M. Raida, and B. Burke. 2012. A promiscuous biotin ligase fusion protein identifies proximal and interacting proteins in mammalian cells. *J Cell Biol*. 196:801-810.

Rual, J.F., K. Venkatesan, T. Hao, T. Hirozane-Kishikawa, A. Dricot, N. Li, G.F. Berriz, F.D. Gibbons, M. Dreze, N. Ayivi-Guedehoussou, N. Klitgord, C. Simon, M. Boxem, S. Milstein, J. Rosenberg, D.S. Goldberg, L.V. Zhang, S.L. Wong, G. Franklin, S. Li, J.S. Albala, J. Lim, C. Fraughton, E. Llamosas, S. Cevik, C. Bex, P. Lamesch, R.S. Sikorski, J. Vandenhaute, H.Y. Zoghbi, A. Smolyar, S. Bosak, R. Sequerra, L. Doucette-Stamm, M.E. Cusick, D.E. Hill, F.P. Roth, and M. Vidal. 2005. Towards a proteome-scale map of the human protein-protein interaction network. *Nature*. 437:1173-1178.

Ryder, P.V., R. Vistein, A. Gokhale, M.N. Seaman, M.A. Puthenveedu, and V. Faundez. 2013. The WASH complex, an endosomal Arp2/3 activator, interacts with the

Hermansky-Pudlak syndrome complex BLOC-1 and its cargo phosphatidylinositol-4-kinase type IIalpha. *Mol Biol Cell*. 24:2269-2284.

Salazar, G., B. Craige, M.L. Styers, K.A. Newell-Litwa, M.M. Doucette, B.H. Wainer, J.M. Falcon-Perez, E.C. Dell'Angelica, A.A. Peden, E. Werner, and V. Faundez. 2006. BLOC-1 complex deficiency alters the targeting of adaptor protein complex-3 cargoes. *Mol Biol Cell*. 17:4014-4026.

San Agustin, J.T., N. Klena, K. Granath, A. Panigrahy, E. Stewart, W. Devine, L. Strittmatter, J.A. Jonassen, X. Liu, C.W. Lo, and G.J. Pazour. 2016. Genetic link between renal birth defects and congenital heart disease. *Nat Commun*. 7:11103.

Sandberg, M.A., C. Weigel-DiFranco, T.P. Dryja, and E.L. Berson. 1995. Clinical expression correlates with location of rhodopsin mutation in dominant retinitis pigmentosa. *Invest Ophthalmol Vis Sci*. 36:1934-1942.

Sato, T., T. Iwano, M. Kunii, S. Matsuda, R. Mizuguchi, Y. Jung, H. Hagiwara, Y. Yoshihara, M. Yuzaki, R. Harada, and A. Harada. 2014. Rab8a and Rab8b are essential for several apical transport pathways but insufficient for ciliogenesis. *J Cell Sci*. 127:422-431.

Sato, T., S. Mushiake, Y. Kato, K. Sato, M. Sato, N. Takeda, K. Ozono, K. Miki, Y. Kubo, A. Tsuji, R. Harada, and A. Harada. 2007. The Rab8 GTPase regulates apical protein localization in intestinal cells. *Nature*. 448:366-369.

Sattar, S., and J.G. Gleeson. 2011. The ciliopathies in neuronal development: a clinical approach to investigation of Joubert syndrome and Joubert syndrome-related disorders. *Dev Med Child Neurol*. 53:793-798.

Scheffers, M.S., P. van der Bent, F. Prins, L. Spruit, M.H. Breuning, S.V. Litvinov, E. de Heer, and D.J. Peters. 2000. Polycystin-1, the product of the polycystic kidney disease 1 gene, co-localizes with desmosomes in MDCK cells. *Hum Mol Genet*. 9:2743-2750.

Schou, K.B., S.K. Morthorst, S.T. Christensen, and L.B. Pedersen. 2014. Identification of conserved, centrosome-targeting ASH domains in TRAPPII complex subunits and TRAPPC8. *Cilia*. 3:6.

Schrick, J.J., P. Vogel, A. Abuin, B. Hampton, and D.S. Rice. 2006. ADP-ribosylation factor-like 3 is involved in kidney and photoreceptor development. *Am J Pathol*. 168:1288-1298.

Schulz, S., M. Handel, M. Schreff, H. Schmidt, and V. Hollt. 2000. Localization of five somatostatin receptors in the rat central nervous system using subtype-specific antibodies. *J Physiol Paris*. 94:259-264.

Seeman, P. 2013. Schizophrenia and dopamine receptors. *Eur Neuropsychopharmacol*. 23:999-1009.

Seixas, C., S.Y. Choi, N. Polgar, N.L. Umberger, M.P. East, X. Zuo, H. Moreiras, R. Ghossoub, A. Benmerah, R.A. Kahn, B. Fogelgren, T. Caspary, J.H. Lipschutz, and D.C. Barral. 2016. Arl13b and the exocyst interact synergistically in ciliogenesis. *Mol Biol Cell*. 27:308-320.

Seo, S., Q. Zhang, K. Bugge, D.K. Breslow, C.C. Searby, M.V. Nachury, and V.C. Sheffield. 2011. A novel protein LZTFL1 regulates ciliary trafficking of the BBSome and Smoothened. *PLoS Genet*. 7:e1002358.

Setou, M., T. Nakagawa, D.H. Seog, and N. Hirokawa. 2000. Kinesin superfamily motor protein KIF17 and mLin-10 in NMDA receptor-containing vesicle transport. *Science*. 288:1796-1802.

Setty, S.R., D. Tenza, E.V. Sviderskaya, D.C. Bennett, G. Raposo, and M.S. Marks. 2008. Cell-specific ATP7A transport sustains copper-dependent tyrosinase activity in melanosomes. *Nature*. 454:1142-1146.

Setty, S.R., D. Tenza, S.T. Truschel, E. Chou, E.V. Sviderskaya, A.C. Theos, M.L. Lamoreux, S.M. Di Pietro, M. Starcevic, D.C. Bennett, E.C. Dell'Angelica, G. Raposo, and M.S. Marks. 2007. BLOC-1 is required for cargo-specific sorting from vacuolar early endosomes toward lysosome-related organelles. *Mol Biol Cell*. 18:768-780.

Signor, D., K.P. Wedaman, L.S. Rose, and J.M. Scholey. 1999. Two heteromeric kinesin complexes in chemosensory neurons and sensory cilia of Caenorhabditis elegans. *Mol Biol Cell*. 10:345-360.

Sitaram, A., M.K. Dennis, R. Chaudhuri, W. De Jesus-Rojas, D. Tenza, S.R. Setty, C.S. Wood, E.V. Sviderskaya, D.C. Bennett, G. Raposo, J.S. Bonifacino, and M.S. Marks. 2012. Differential recognition of a dileucine-based sorting signal by AP-1 and AP-3 reveals a requirement for both BLOC-1 and AP-3 in delivery of OCA2 to melanosomes. *Mol Biol Cell*. 23:3178-3192.

Soullam, B., and H.J. Worman. 1995. Signals and structural features involved in integral membrane protein targeting to the inner nuclear membrane. *J Cell Biol*. 130:15-27.

Starcevic, M., and E.C. Dell'Angelica. 2004. Identification of snapin and three novel proteins (BLOS1, BLOS2, and BLOS3/reduced pigmentation) as subunits of biogenesis of lysosome-related organelles complex-1 (BLOC-1). *J Biol Chem*. 279:28393-28401.

Stenmark, H. 2009. Rab GTPases as coordinators of vesicle traffic. *Nat Rev Mol Cell Biol*. 10:513-525.

Stenmark, H., and V.M. Olkkonen. 2001. The Rab GTPase family. *Genome Biol*. 2:REVIEWS3007.

Stewart, M. 2007. Molecular mechanism of the nuclear protein import cycle. *Nat Rev Mol Cell Biol*. 8:195-208.

Stoops, E.H., and M.J. Caplan. 2014. Trafficking to the apical and basolateral membranes in polarized epithelial cells. *J Am Soc Nephrol*. 25:1375-1386.

Su, X., K. Driscoll, G. Yao, A. Raed, M. Wu, P.L. Beales, and J. Zhou. 2014. Bardet-Biedl syndrome proteins 1 and 3 regulate the ciliary trafficking of polycystic kidney disease 1 protein. *Hum Mol Genet*. 23:5441-5451.

Su, X., M. Wu, G. Yao, W. El-Jouni, C. Luo, A. Tabari, and J. Zhou. 2015. Regulation of polycystin-1 ciliary trafficking by motifs at its C-terminus and polycystin-2 but not by cleavage at the GPS site. *J Cell Sci*. 128:4063-4073.

Sullivan, T., D. Escalante-Alcalde, H. Bhatt, M. Anver, N. Bhat, K. Nagashima, C.L. Stewart, and B. Burke. 1999. Loss of A-type lamin expression compromises nuclear envelope integrity leading to muscular dystrophy. *J Cell Biol*. 147:913-920.

Sun, X., A. Zhang, B. Baker, L. Sun, A. Howard, J. Buswell, D. Maurel, A. Masharina, K. Johnsson, C.J. Noren, M.Q. Xu, and I.R. Correa, Jr. 2011. Development of SNAP-tag fluorogenic probes for wash-free fluorescence imaging. *Chembiochem*. 12:2217-2226.

Sun, Z., A. Amsterdam, G.J. Pazour, D.G. Cole, M.S. Miller, and N. Hopkins. 2004. A genetic screen in zebrafish identifies cilia genes as a principal cause of cystic kidney. *Development*. 131:4085-4093.

Sung, C.H., C. Makino, D. Baylor, and J. Nathans. 1994. A rhodopsin gene mutation responsible for autosomal dominant retinitis pigmentosa results in a protein that is defective in localization to the photoreceptor outer segment. *J Neurosci*. 14:5818-5833.

Talbot, K., W.L. Eidem, C.L. Tinsley, M.A. Benson, E.W. Thompson, R.J. Smith, C.G. Hahn, S.J. Siegel, J.Q. Trojanowski, R.E. Gur, D.J. Blake, and S.E. Arnold. 2004. Dysbindin-1 is reduced in intrinsic, glutamatergic terminals of the hippocampal formation in schizophrenia. *J Clin Invest*. 113:1353-1363.

Tam, B.M., O.L. Moritz, L.B. Hurd, and D.S. Papermaster. 2000. Identification of an outer segment targeting signal in the COOH terminus of rhodopsin using transgenic Xenopus laevis. *J Cell Biol*. 151:1369-1380.

TerBush, D.R., T. Maurice, D. Roth, and P. Novick. 1996. The Exocyst is a multiprotein complex required for exocytosis in Saccharomyces cerevisiae. *EMBO J*. 15:6483-6494.

TerBush, D.R., and P. Novick. 1995. Sec6, Sec8, and Sec15 are components of a multisubunit complex which localizes to small bud tips in Saccharomyces cerevisiae. *J Cell Biol*. 130:299-312.

Toomre, D., and J. Bewersdorf. 2010. A new wave of cellular imaging. *Annu Rev Cell Dev Biol*. 26:285-314.

Urban, J., K. Parczyk, A. Leutz, M. Kayne, and C. Kondor-Koch. 1987. Constitutive apical secretion of an 80-kD sulfated glycoprotein complex in the polarized epithelial Madin-Darby canine kidney cell line. *J Cell Biol*. 105:2735-2743.

Vale, R.D. 2003. The molecular motor toolbox for intracellular transport. *Cell*. 112:467-480.

van den Heuvel, M., and P.W. Ingham. 1996. smoothened encodes a receptor-like serpentine protein required for hedgehog signalling. *Nature*. 382:547-551.

Veltel, S., R. Gasper, E. Eisenacher, and A. Wittinghofer. 2008. The retinitis pigmentosa 2 gene product is a GTPase-activating protein for Arf-like 3. *Nat Struct Mol Biol*. 15:373-380.

Volpicelli, L.A., J.J. Lah, G. Fang, J.R. Goldenring, and A.I. Levey. 2002. Rab11a and myosin Vb regulate recycling of the M4 muscarinic acetylcholine receptor. *J Neurosci*. 22:9776-9784.

Wang, J., K. Huo, L. Ma, L. Tang, D. Li, X. Huang, Y. Yuan, C. Li, W. Wang, W. Guan, H. Chen, C. Jin, J. Wei, W. Zhang, Y. Yang, Q. Liu, Y. Zhou, C. Zhang, Z. Wu, W. Xu, Y. Zhang, T. Liu, D. Yu, Y. Zhang, L. Chen, D. Zhu, X. Zhong, L. Kang, X. Gan, X. Yu, Q. Ma, J. Yan, L. Zhou, Z. Liu, Y. Zhu, T. Zhou, F. He, and X. Yang. 2011. Toward an understanding of the protein interaction network of the human liver. *Mol Syst Biol*. 7:536.

Wang, J., M. Silva, L.A. Haas, N.S. Morsci, K.C. Nguyen, D.H. Hall, and M.M. Barr. 2014. C. elegans ciliated sensory neurons release extracellular vesicles that function in animal communication. *Curr Biol*. 24:519-525.

Wang, S., Y. Luo, P.D. Wilson, G.B. Witman, and J. Zhou. 2004a. The autosomal recessive polycystic kidney disease protein is localized to primary cilia, with concentration in the basal body area. *J Am Soc Nephrol*. 15:592-602.

Wang, S., J. Zhang, S.M. Nauli, X. Li, P.G. Starremans, Y. Luo, K.A. Roberts, and J. Zhou. 2007. Fibrocystin/polyductin, found in the same protein complex with polycystin-2, regulates calcium responses in kidney epithelia. *Mol Cell Biol*. 27:3241-3252.

Wang, Z., H. Wei, Y. Yu, J. Sun, Y. Yang, G. Xing, S. Wu, Y. Zhou, Y. Zhu, C. Zhang, T. Zhou, X. Zhao, Q. Sun, and F. He. 2004b. Characterization of Ceap-11 and Ceap-16, two novel splicing-variant-proteins, associated with centrosome, microtubule aggregation and cell proliferation. *J Mol Biol*. 343:71-82.

Ward, C.J., M.C. Hogan, S. Rossetti, D. Walker, T. Sneddon, X. Wang, V. Kubly, J.M. Cunningham, R. Bacallao, M. Ishibashi, D.S. Milliner, V.E. Torres, and P.C. Harris. 2002. The gene mutated in autosomal recessive polycystic kidney disease encodes a large, receptor-like protein. *Nat Genet*. 30:259-269.

Ward, C.J., D. Yuan, T.V. Masyuk, X. Wang, R. Punyashthiti, S. Whelan, R. Bacallao, R. Torra, N.F. LaRusso, V.E. Torres, and P.C. Harris. 2003. Cellular and subcellular localization of the ARPKD protein; fibrocystin is expressed on primary cilia. *Hum Mol Genet*. 12:2703-2710.

Ward, H.H., U. Brown-Glaberman, J. Wang, Y. Morita, S.L. Alper, E.J. Bedrick, V.H. Gattone, 2nd, D. Deretic, and A. Wandinger-Ness. 2011. A conserved signal and GTPase complex are required for the ciliary transport of polycystin-1. *Mol Biol Cell*. 22:3289-3305.

Weickert, C.S., D.A. Rothmond, T.M. Hyde, J.E. Kleinman, and R.E. Straub. 2008. Reduced DTNBP1 (dysbindin-1) mRNA in the hippocampal formation of schizophrenia patients. *Schizophr Res*. 98:105-110.

Weiss, R.L., D.A. Goodenough, and U.W. Goodenough. 1977. Membrane particle arrays associated with the basal body and with contractile vacuole secretion in Chlamydomonas. *J Cell Biol*. 72:133-143.

Weisz, O.A., and E. Rodriguez-Boulan. 2009. Apical trafficking in epithelial cells: signals, clusters and motors. *J Cell Sci*. 122:4253-4266.

Westlake, C.J., L.M. Baye, M.V. Nachury, K.J. Wright, K.E. Ervin, L. Phu, C. Chalouni, J.S. Beck, D.S. Kirkpatrick, D.C. Slusarski, V.C. Sheffield, R.H. Scheller, and P.K. Jackson. 2011. Primary cilia membrane assembly is initiated by Rab11 and

transport protein particle II (TRAPPII) complex-dependent trafficking of Rabin8 to the centrosome. *Proc Natl Acad Sci U S A*. 108:2759-2764.
Williams, D.S. 2002. Transport to the photoreceptor outer segment by myosin VIIa and kinesin II. *Vision Res*. 42:455-462.
Wong, M., and S. Munro. 2014. Membrane trafficking. The specificity of vesicle traffic to the Golgi is encoded in the golgin coiled-coil proteins. *Science*. 346:1256898.
Wood, C.R., K. Huang, D.R. Diener, and J.L. Rosenbaum. 2013. The cilium secretes bioactive ectosomes. *Curr Biol*. 23:906-911.
Wu, G., V. D'Agati, Y. Cai, G. Markowitz, J.H. Park, D.M. Reynolds, Y. Maeda, T.C. Le, H. Hou, Jr., R. Kucherlapati, W. Edelmann, and S. Somlo. 1998. Somatic inactivation of Pkd2 results in polycystic kidney disease. *Cell*. 93:177-188.
Wu, H., C. Turner, J. Gardner, B. Temple, and P. Brennwald. 2010. The Exo70 subunit of the exocyst is an effector for both Cdc42 and Rho3 function in polarized exocytosis. *Mol Biol Cell*. 21:430-442.
Wu, W., F. Lin, and H.J. Worman. 2002. Intracellular trafficking of MAN1, an integral protein of the nuclear envelope inner membrane. *J Cell Sci*. 115:1361-1371.
Xu, Q., Y. Zhang, Q. Wei, Y. Huang, Y. Li, K. Ling, and J. Hu. 2015. BBS4 and BBS5 show functional redundancy in the BBSome to regulate the degradative sorting of ciliary sensory receptors. *Sci Rep*. 5:11855.
Yang, Q., X. He, L. Yang, Z. Zhou, A.R. Cullinane, A. Wei, Z. Zhang, Z. Hao, A. Zhang, M. He, Y. Feng, X. Gao, W.A. Gahl, M. Huizing, and W. Li. 2012. The BLOS1-interacting protein KXD1 is involved in the biogenesis of lysosome-related organelles. *Traffic*. 13:1160-1169.
Yoder, B.K., X. Hou, and L.M. Guay-Woodford. 2002. The polycystic kidney disease proteins, polycystin-1, polycystin-2, polaris, and cystin, are co-localized in renal cilia. *J Am Soc Nephrol*. 13:2508-2516.
Yokoyama, T. 2017. Ciliary subcompartments and cysto-proteins. *Anat Sci Int*. 92:207-214.
Yoshimura, S., J. Egerer, E. Fuchs, A.K. Haas, and F.A. Barr. 2007. Functional dissection of Rab GTPases involved in primary cilium formation. *J Cell Biol*. 178:363-369.
Young, R.W. 1967. The renewal of photoreceptor cell outer segments. *J Cell Biol*. 33:61-72.
Yu, F., S. Sharma, A. Skowronek, and K.S. Erdmann. 2016. The serologically defined colon cancer antigen-3 (SDCCAG3) is involved in the regulation of ciliogenesis. *Sci Rep*. 6:35399.
Zerial, M., and H. McBride. 2001. Rab proteins as membrane organizers. *Nat Rev Mol Cell Biol*. 2:107-117.
Zhang, M.Z., W. Mai, C. Li, S.Y. Cho, C. Hao, G. Moeckel, R. Zhao, I. Kim, J. Wang, H. Xiong, H. Wang, Y. Sato, Y. Wu, Y. Nakanuma, M. Lilova, Y. Pei, R.C. Harris, S. Li, R.J. Coffey, L. Sun, D. Wu, X.Z. Chen, M.D. Breyer, Z.J. Zhao, J.A. McKanna, and G. Wu. 2004. PKHD1 protein encoded by the gene for autosomal recessive

polycystic kidney disease associates with basal bodies and primary cilia in renal epithelial cells. *Proc Natl Acad Sci U S A*. 101:2311-2316.

Zhang, Q., D. Nishimura, S. Seo, T. Vogel, D.A. Morgan, C. Searby, K. Bugge, E.M. Stone, K. Rahmouni, and V.C. Sheffield. 2011. Bardet-Biedl syndrome 3 (Bbs3) knockout mouse model reveals common BBS-associated phenotypes and Bbs3 unique phenotypes. *Proc Natl Acad Sci U S A*. 108:20678-20683.

Zhang, X., R. Xu, B. Zhu, X. Yang, X. Ding, S. Duan, T. Xu, Y. Zhuang, and M. Han. 2007. Syne-1 and Syne-2 play crucial roles in myonuclear anchorage and motor neuron innervation. *Development*. 134:901-908.

Zhao, C., Y. Omori, K. Brodowska, P. Kovach, and J. Malicki. 2012. Kinesin-2 family in vertebrate ciliogenesis. *Proc Natl Acad Sci U S A*. 109:2388-2393.

Zheng, Y., M.L. Wong, B. Alberts, and T. Mitchison. 1995. Nucleation of microtubule assembly by a gamma-tubulin-containing ring complex. *Nature*. 378:578-583.

Zhou, C., L. Cunningham, A.I. Marcus, Y. Li, and R.A. Kahn. 2006. Arl2 and Arl3 regulate different microtubule-dependent processes. *Mol Biol Cell*. 17:2476-2487.

Zhu, B., X. Zhu, L. Wang, Y. Liang, Q. Feng, and J. Pan. 2017. Functional exploration of the IFT-A complex in intraflagellar transport and ciliogenesis. *PLoS Genet*. 13:e1006627.

Zuleger, N., A.R. Kerr, and E.C. Schirmer. 2012. Many mechanisms, one entrance: membrane protein translocation into the nucleus. *Cell Mol Life Sci*. 69:2205-2216.

Zuo, X., W. Guo, and J.H. Lipschutz. 2009. The exocyst protein Sec10 is necessary for primary ciliogenesis and cystogenesis in vitro. *Mol Biol Cell*. 20:2522-2529.

Zuo, X., J. Zhang, Y. Zhang, S.C. Hsu, D. Zhou, and W. Guo. 2006. Exo70 interacts with the Arp2/3 complex and regulates cell migration. *Nat Cell Biol*. 8:1383-1388.